Spring 2018

Regional Stratigraphy and Distribution of the Coastal Group, St. Elizabeth Parish, Southwestern Jamaica

Brett M. Kenning
Missouri State University, Brett555@live.missouristate.edu

REGIONAL STRATIGRAPHY AND DISTRIBUTION OF THE COASTAL GROUP, ST. ELIZABETH PARISH, SOUTHWESTERN JAMAICA

A Masters Thesis

Presented to

The Graduate College of

Missouri State University

In Partial Fulfillment

Of the Requirements for the Degree

Masters of Science, Geospatial Sciences in Geography and Geology

By

Brett Michael Kenning

May 2018

REGIONAL STRATIGRAPHY AND DISTRIBUTION OF THE COASTAL GROUP, ST. ELIZABETH PARISH, SOUTHWESTERN JAMAICA

Geography, Geology, and Planning

Missouri State University, May 2018

Master of Science

Brett Michael Kenning

ABSTRACT

This contribution examines the characteristics and ages of sedimentary units in the Coastal Group located along the southwestern Jamaica coast between Great Pedro Bluff and Fort Charles Bay in southwestern St. Elizabeth Parish. The coastline is characterized by laterally discontinuous low cliff exposures, separated by modern beach deposits and tectonically raised shore platforms composed of the White Limestone Group (mid-Eocene to mid-Miocene) and coral rudstone to floatstone and calcareous sandstone of the Coastal Group (late Pleistocene). Electron-Spin Resonance spectroscopy conducted on corals collected from a coral rudstone to floatstone facies yielded an estimated age of 120 ka. The coral facies may represent the Falmouth Formation, and it has been confirmed to have been deposited within the MIS 5e (132 ka – 115 ka). However, the other units within the Coastal Group likely are diachronous. Significant amounts of sand and silt components are present throughout the Coastal Group exposures. These vertical exposures cannot be a standard for determining relative mean sea level (RMSL) as they have been tectonically disturbed and the upper surface of the coral facies may have been eroded below cross-bedded sandstones. Due to the widespread variability of sedimentary units both locally and longshore, assignment of existing stratigraphic nomenclature of the Coastal Group to these formations is difficult. The stacking patterns of these sedimentary units indicate changes in depositional environments and is suggestive of potential magnitudes of sea-level rise. This investigation presents the first detailed measured and described sections for this interval in southwestern Jamaica.

KEYWORDS: Jamaica, Coastal Group, stratigraphy, MIS 5e, sea-level change.

This abstract is approved as to form and content

_____

Kevin Ray Evans, PhD
Chairperson, Advisory Committee
Missouri State University

REGIONAL STRATIGRAPHY AND DISTRIBUTION OF THE COASTAL GROUP, ST. ELIZABETH PARISH, SOUTHWESTERN JAMAICA

By

Brett Michael Kenning

A Masters Thesis
Submitted to the Graduate College
Of Missouri State University
In Partial Fulfillment of the Requirements
For the Degree of Masters of Science, Geospatial Science in Geography and Geology

May 2018

Approved:

_____
Kevin Ray Evans, PhD

_____
Robert Pavlowsky, PhD

_____
Xin Miao, PhD

_____
Julie Masterson, PhD: Dean, Graduate College

ACKNOWLEDGEMENTS

I would first like to thank my thesis advisor Dr. Kevin Evans for introducing me to Jamaica and providing me the opportunity to work in such an amazing place. Dr. Evans consistently allowed this thesis to be my own work, but provided proper guidance as needed. Dr. Evans treated me as a professional throughout this project and for that I am forever grateful.

I would also like to thank my other committee members, Dr. Robert Pavlowsky and Dr. Xin Miao, for their invaluable time, expertise and knowledge during my graduate studies and completion of my thesis. Also, I would like to extend a thank you to Dr. Douglas Faulkner and Sarah LeTarte for showing genuine interest in my research area and assisting me in the data collection process.

I am deeply grateful to Mr. Wolde Kristos and RAJ Tours for hosting us in Jamaica as well as providing transportation and security on the island. Thank you to Decieta, Veda, and Merna in Bluefields and Suzett, Renée, and Denzil in Treasure Beach for providing hospitality and friendship during our stays. A special thanks is due to Captain Dennis for providing transportation to and from our study site in Treasure Beach.

This thesis was made possible through financial support from a thesis research grant and a Faculty Research Grant with Dr. Evans from the Missouri State University Graduate College, OEWRI, College of Natural & Applied Sciences, and the MSU Study Away program. Without this support, this project would not have been possible.

Finally, I would like to thank my parents, siblings, and friends for showing me unwavering support and encouragement throughout this process.

TABLE OF CONTENTS

LIST OF TABLES

LIST OF FIGURES

INTRODUCTION

Global climate oscillations between warm and cold periods have occurred naturally throughout geologic history due to various factors, such as biotic processes, orbital variations (eccentricity, rotational obliquity, and precession), solar-intensity variations, volcanic activity, and plate tectonics (Riebeek, 2010; Blois et al., 2013; Feng and Bailer-Jones, 2015; Goelzer et al., 2016). However, studies of the observed warming trend over the past century cannot be explained by natural causes alone, indicating the significance of human activities on the climate system (Riebeek, 2010). The Intergovernmental Panel on Climate Change (IPCC) has reported it is extremely likely that anthropogenic greenhouse gas emissions have been the dominant driving force of the past centennial warming trend being responsible for approximately 75 percent (with a 95 percent confidence) of global warming trends experienced since the middle twentieth century (IPCC, 2014). The onset of the current warming trend has resulted in observed changes that are unprecedented over decades to millennia (IPCC, 2014). These changes include global temperature rise, warming oceans, sea-level rise, ocean acidification, shrinking continental ice sheets, glacial retreat, decreased snow cover, and increased numbers of extreme storm events. Current predictive climate models suggest that these trends are likely to continue at the current alarming rate or possibly accelerate by the end of this century having continued profound effects on global climate, especially marine ecosystems and coastal communities (IPCC, 2014). As these trends develop further and the associated changes become more pronounced, the need for accurate predictive climate models becomes increasingly apparent.

Identifying the processes involved in past climate systems and understanding the operating mechanisms that allow for rapid shifts is fundamental to predicting future climate trends (Dutton et al., 2015; Hearty and Tormey, 2017). High-resolution studies of proxy indicators, such as ice cores, tree rings, corals, sediment cores, and speleothems, allow for the reconstruction of paleoclimatic conditions. Studies on deep-sea cores, specifically the carbon and oxygen isotope ratios of benthic foraminifera, provide a calibrated proxy record for the evolution of the ocean, atmosphere, and ultimately, past climates (Emiliani, 1955; Shackleton, 1987). Secular variations within these isotopic records are interpreted as representing temporal trends of glacial-interglacial oscillations during Quaternary time, with peaks indicating glacials and troughs indicating interglacials (Emiliani, 1955; Hays et al., 1976; Shackleton, 1987; Railsback et al., 2015). From these records, paleoclimatologists have been able to categorize these isotopic packages into marine isotope stages (MIS) (Emiliani, 1955). With over 100 stages being identified, the MIS timescale represents the standard to which Quaternary climate records are calibrated (Railsback et al., 2015). Although the MIS timescale is widely used across many disciplines of Quaternary climate studies, the interpretations are continuously being refined as additional data becomes accessible.

In addition to high-resolution studies of climate proxy record, direct, non-proxy geologic data provides information towards understanding the potential magnitude of future climate changes. While composite isotopic studies on deep-sea sediments provide a calibrated timescale of past climate conditions, direct, non-proxy geologic evidence can provide information toward understanding the potential magnitude of future climate changes (Hearty and Tormey, 2017). Coastal sequences of marine terraces formed during

sea-level highstands associated with interglacial stages are correlative to marine isotope stages and provide direct evidence of past elevated stadial positions (e.g., marine terraces and wave-cut notches). These features occur on both active and passive margins where tectonic uplift and subsidence are responsible for emerged or submerged sequences, respectively (Pedoja et al., 2011). Comprehensive studies have attempted to compile previous work on emergent sequences at a regional scale to correlate the described features and evaluate global sea-level change during the associated interglacial stages. A significant example of one of these well-documented and globally correlated emergent coastal sequences is known as the marine isotope stage 5e or the last interglacial maximum, which occurred approximately between 130-115 ka (Kukla et al., 2002; Shackleton et al., 2003; Hearty and Tormey, 2017).

Detailed stratigraphic and geomorphic studies have characterized the relative sea-level movements during the last interglacial maximum as several well-defined sea-level intervals with a maximum sea-level reaching heights of +6 to +9 m above modern sea-level (Hearty et al., 2007). The last interglacial maximum corresponds to the marine isotope stage 5e, a proxy record for low global ice cover and high sea-levels, and represents the last time global sea levels were at or near modern levels (Stirling et al., 1995; Kukla et al., 2002; Hearty et al., 2007; Hearty and Tormey, 2017). Although the onset, duration, and emergent coastal sequences of the last interglacial maximum corresponding MIS 5e are well documented on a global scale (e.g., Huon Peninsula in New Guinea, Barbados, Vanuatu archipelago, Italy, Australia, Japan), the influence of rapid sea-level rise and fall remains unclear at a regional scale, especially last interglacial maximum sites lacking in previous studies (Pedoja et al., 2011). By increasing the

available literature regarding the last interglacial maximum, the accuracy of predictive climate models at both global and regional scales would greatly increase, which would lead to improved risk assessment for future changes.

The purpose of this study is to analyze the depositional patterns and ages of fossil reef terraces in the Coastal Group in southern St. Elizabeth Parish, southwestern Jamaica. Within these parameters, it is hypothesized that deposition of the sequence of the Coastal Group coincided with the last interglacial maximum or MIS 5e. If the ages are confirmed to be MIS 5e, then it is expected that the exposures will exhibit similar stratigraphic, sedimentologic and geomorphic characteristics (e.g., wave-cut notches, unconformities) exhibited in other MIS 5e deposits. Paleoecological studies of coral reef community structure from previously published studies on modern Jamaican fringing reefs (e.g., Goreau, 1959; Liddell and Ohlhorst, 1987) were used to assess the relationships between community composition and reef environment.

Since the coral taxonomy of Pleistocene reefs are essentially identical to modern coral reefs, identification of key reef-building coral species and associated fauna is used to interpret the depositional environment as well as the orientation of the coral heads in outcrop exposure. For example, large, branching coral colonies of *Acropora palmata* are thought to be indicative of a reef crest zone (Goreau, 1959). However, species diversity and relative abundance of key coral species can increase uncertainty of environment interpretations. The caveat to paleoecological studies of coral reef communities is that there is an interdependence between environmental interpretation and ecological analysis, as many coral species are capable of living in more than one environment.

In this study, sequence stratigraphy, in combination with geochronology, geomorphologic features, coral paleoecology and gamma-ray profiles, were used for high-resolution correlations of Coastal Group outcrops with outcrops in other areas of Jamaica, and potentially other MIS 5e sites. An approximation of sea-level was taken to establish a datum for stratigraphic correlations because there is an approximately 30-40 cm maximal tidal range in the study area. Establishing sea-level as the datum also allowed for observations on the variability of each section's maximum thickness as well as correlating any significant indicators of past sea-level position. A disconformable, hardground surface at the base of the Coastal Group, characterized by encrusting corals and borings, was identified at several outcrops in the study area and is interpreted as sequence boundary. A shift from mixed siliciclastic and carbonate marine deposition to non-marine eolian sedimentation is interpreted as a sequence boundary at the top of the succession.

Utilizing lithostratigraphic relationships, strata stacking patterns, and depositional trends, all of the measured and described sections have been placed into a systems tract model. This allows for interpretations for base level change, reef environment conditions, and indirectly paleoclimate change. Once the regional depositional environments and sea-level trends are understood, geochronology of corals present in the succession was applied to better constrain the time of deposition. If the resulting age can confirm a depositional age during MIS 5e, then the past sea-level indicators present in the Coastal Group exposures of southwestern Jamaica could be compared to other sites in Jamaica, the Caribbean and around the world that have confirmed MIS 5e ages. After MIS 5e confirmation, the Coastal Group exposures of southwestern Jamaica can be added to the

comprehensive global framework of data available. By comparing significant features indicative of past sea-level position between the globally abundant MIS 5e sites, a more detailed understanding of the magnitude of global sea-level fluctuations during the last interglacial maximum may be gained.

This investigation of the Coastal Group includes description of a mixed siliciclastic-carbonate system that experienced dynamic sea-level fluctuations that were influenced by glacioeustatic changes, but also has been affected by neotectonism and influxes of siliciclastic components from terrestrial as well as marine sources. Outcrop studies have identified at least six different lithostratigraphic units within the identified mixed siliciclastic-carbonate system that characterizes most of the coastal exposures between Great Pedro Bay and Fort Charles Bay. Electron-Spin Resonance (ESR) spectroscopy techniques performed on three corals within the succession suggests that the elevated coral reef assemblage was deposited during the MIS 5e and should be added to the comprehensive global framework of data available from the last interglacial maximum.

BACKGROUND

Sequence Stratigraphy

Carbonate and siliciclastic systems have been studied through the application of sequence stratigraphic principles. Sequence stratigraphy focuses on changes in facies of rock strata and the identification of key surfaces to determine the chronological order of basin-filling and erosional events. A variety of different datasets is required to build a sequence-stratigraphic framework. Seismic data, well log data, core data and outcrop data can all be used for an integrated approach to create a reliable and complete sequence stratigraphic model. Packages of distinct rock sequences are divided into stratal stacking patterns in order to interpret the changes in rates of sedimentation and base level. These stacking patterns reflect the evolution of a depositional environment (Catuneanu et al., 2009).

Each stacking pattern defines different types of deposits based on the geometry and facies preservation style. A systems tract outlines the depositional setting and may contain several age-equivalent deposits with a variety of lithologies. Some generic types of deposits include normal regression, forced regression and transgression (Catuneanu et al., 2009). A normal transgression systems tract is where progradation is driven by sediment supply. Sedimentation rates outpace the rates of base level rise at the coastline. This causes the shoreline to migrate slowly seaward and is commonly observed in a deltaic system. A forced regression systems tract is driven by base level fall. Deposits along the coastline become exposed as the sea level drops. In this type of systems tract, the coastal deposits become subjected to higher rates of erosion, which commonly results

in an unconformity: a period of non-deposition. A regressive systems tract is the opposite of a normal transgression systems tract. The rates of base sea-level rise outpace the sedimentation rates at the coastline forcing the coastline to migrate landward (Catuneanu et al., 2009).

Depositional Controls of Mixed Carbonate-Siliciclastic Systems

Mixed carbonate-siliciclastic sedimentation systems are common to shelf and platform settings in low latitude, tropical environments (Dunbar and Dickens, 2003; D'agostini et al., 2015; Harper et al., 2015). Major mixed systems are found today in Austrailia, Papua New Guinea, Panama, and Belize (Francis et al., 2008; Harper et al., 2015). These systems are characterized as displaying high variability of lateral and vertical facies relationships as well as lithological variability. These stratigraphic variations are created by complex interactions between allochtonous and autochtonous sedimentation processes and complicate the application of sequence stratigraphic interpretations (Zeller et al., 2015).

The reciprocal sedimentation model, based on classic sequence stratigraphic models, has been applied to interpret observed sedimentation processes of mixed carbonate-siliciclastic systems among the shelf, slope and basin in tropical environments (D'agostini et al., 2015). These systems exhibit alternating sedimentation patterns between siliciclastic-dominated and carbonate-dominated sediment influx, where the main control on the sediment source is dependent on the relative sea level position (Zeller et al., 2015). During periods of relatively low sea levels (lowstand systems tract, LST), siliciclastic sediments are carried into the basin after intense erosion on the exposed

continent resulting in a progradational stacking pattern. During periods of relatively high sea levels (highstand systems tract, HST), the siliciclastic input is essentially cut-off due to less intense erosion on the continent allowing for carbonate production to ensue on the flooded shelf, creating a carbonate dominated facies (D'agostini et al., 2015; Zeller et al., 2015). While this relatively simple concept provides a reasonable explanation for the control on mixed carbonate-siliciclastic systems, studies of modern and ancient mixed sedimentation systems suggest a much more dynamic environment consisting of multiple controls rather than just one (Dorsey and Kidwell, 1999; Dunbar and Dickens, 2003; Francis et al., 2008; Harper et al., 2015; Zeller et al., 2015).

Marine Isotope Stages

The study of oxygen isotope ratios in foraminifera found in deep sea cores has revealed a cyclical pattern representing climate change over long periods of time. Cesare Emiliani was the first to publish a report on the variance of oxygen isotope ratios in foraminifera found in deep sea cores in support of the Milankovitch theory (Emiliani, 1955; Ravelo and Hillaire-Marcel, 2007). In general, the Milankovitch theory describes the overall effect of changes in the Earth's astronomical movements, such as eccentricity, axial tilt, and precession, on climate. Major shifts in the isotopic ratios representing climate change and designated stage numbers for each peak and trough are referred to as Marine isotope stages (Emiliani, 1955). Shackleton (1967) subdivided marine isotope stage 5 from Emiliani (1955) into lettered substages. These studies created marine isotope stage and substage division of the Quaternary period. These marine isotope stages begin

in the Holocene and date back in time as MIS 1, MIS 2, MIS 3, and so on, where MIS refers to various marine isotope stage (Railsback et al., 2015).

Other researchers assigned different peaks and troughs in oxygen isotopic record as marine isotope substages. However, the research following Shackleton's report lacked consistency and had different researchers assigning different nomenclature to any one interval (Shackleton, 1969). Railsback et al. (2015) recognized the conflicting nomenclature for the different substages and generated a more consistent scheme. Their scheme, which is used herein, provides a continuous record of marine benthic oxygen isotopic records representative of changes in ice volume that can be useful for global correlation (Figure 1). This record serves as the basis for global correlation of Pleistocene marine successions (Railsback et al., 2015).

Marine Isotope Substage 5e

MIS 5e is the warmest of the MIS 5 substages and representative of the Eemian period, the last interglacial period in northwestern Europe, which occurred between 130±2 and 119±2 ka (Hearty et al., 2007). During the MIS 5e, global mean surface temperatures were roughly 1 - 2ºC warmer and sea level reached heights of several meters higher than today (Irvali et al., 2012; Hansen et al., 2015; Hearty and Tormey, 2017). This interval is characterized by rapid, multi-meter shifts in sea level as the major ice sheets were reduced (e.g., Greenland ice sheet) (Figure 2; Hearty et al., 2007; Rohling et al., 2007; Hearty and Tormey, 2017). Because of global sea levels being higher than today, fossil coral reef complexes that developed during the peak of the MIS 5e are abundant and widespread on many stable and uplifted coastlines of the world (Hearty et

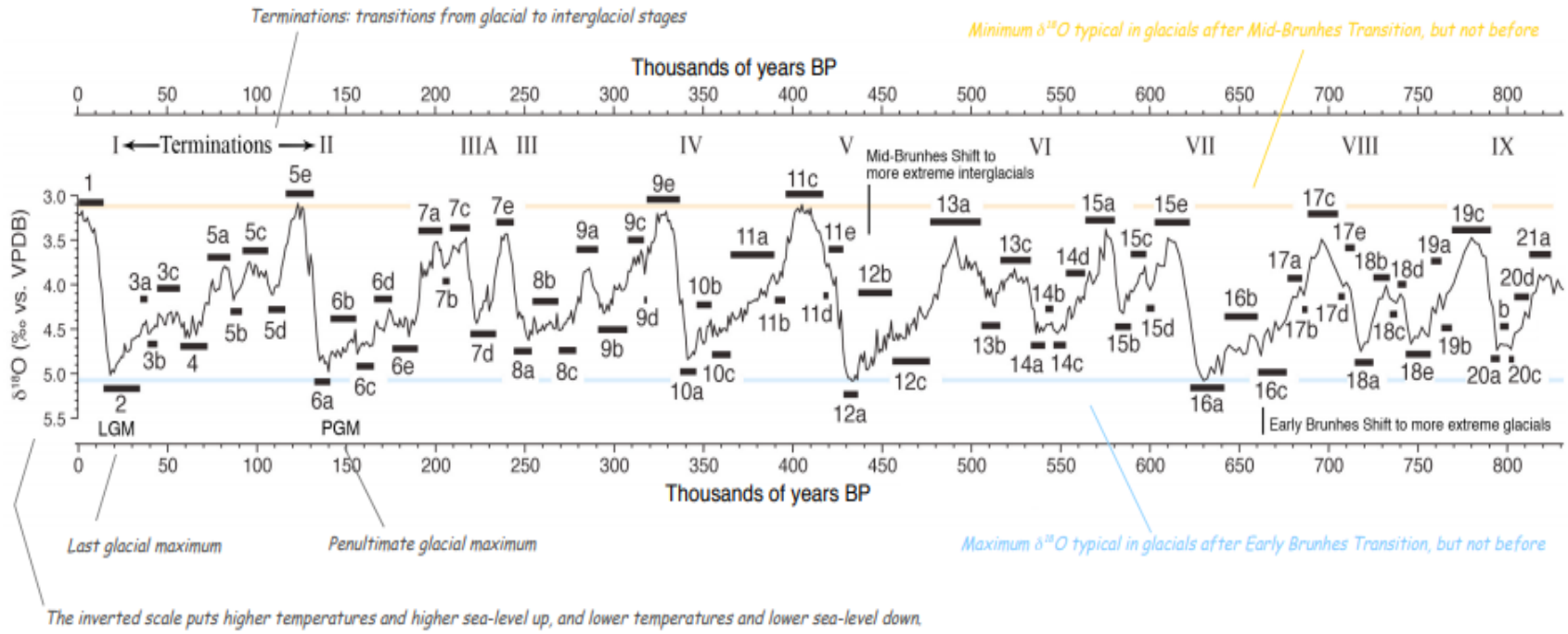

Figure 1. Marine oxygen isotope nomenclature scheme extending back to Marine Isotope Stage 28c at 1.0 mya (Railsback et al., 2015).

al., 2007). These exposures represent the most accessible and widespread evidence for climate changes during the MIS 5e.

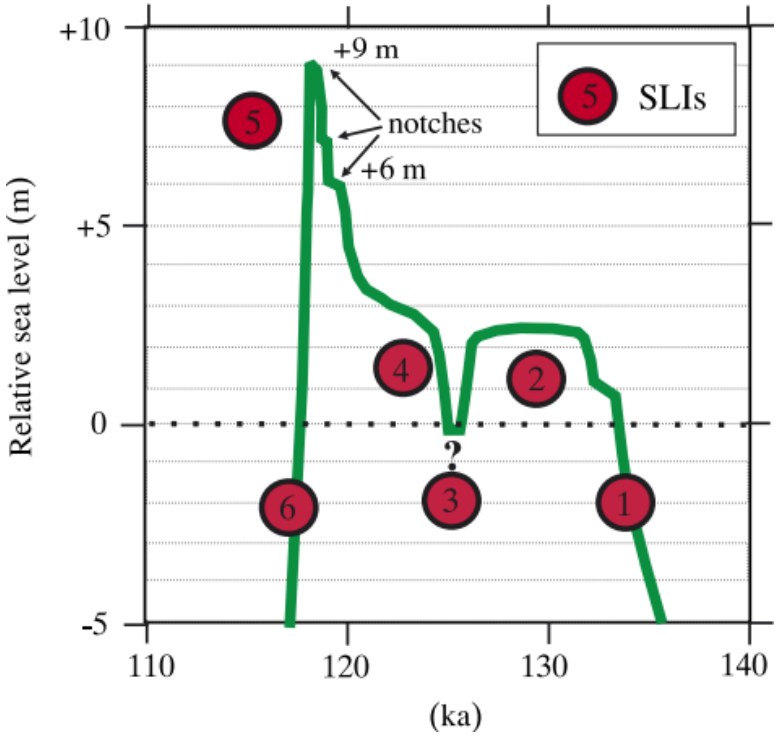

Figure 2. Composite reconstruction of MIS 5e sea-level fluctuations from 15 MIS 5e sites (Hearty et al., 2007).

Fossil Coral Reefs During the Last Interglacial Maximum

Extensive studies on the development of fossil coral reefs during the last interglacial maximum are widespread and reflect past eustatic sea-level fluctuations on both tectonically stable and active regions. Previous work on fossil coral reefs during the last interglacial have documented the ages of corals present in the succession as well as any potential indicators for past sea-level positions.

In tectonically stable regions, past sea level change cannot be explained by uplift or down faulting. Therefore, fossil coral reefs directly reflect eustatic sea-level

fluctuations during the last interglacial maximum (Dutton and Lambeck, 2012). Some examples of fossil reef occurrences from tectonically stable areas include Bermuda, Bahamas, Florida Keys, Hawaii, Seychelles, and Australia (Sherman et al., 1993; Fruijtier et al., 2000; Hearty and Neumann, 2001; Hearty, 2002; Zazo et al., 2010; Pan et al., 2018).

In tectonically active regions, the history of past sea level fluctuations during the last interglacial maximum are recorded in uplifted reef terraces. Positive vertical components of tectonic movement places terraces and older reef successions at high levels along the coast, which conveniently increases their accessibility. However, interpreting the magnitude of past sea-level changes is difficult because of unknown rates of uplift and, in some cases, a lack of coral fauna for accurate radiometric dating (Dutton and Lambeck, 2012). Some examples of fossil reef occurrences from tectonically unstable areas include Indonesia, New Guinea, and Barbados (Hantoro et al., 1994).

Florida Keys. The Florida Keys island chain provide an ideal location for past sea-level reconstruction studies during the Quaternary because of the tectonic stability of the region, abundant records of past sea-level positions, and available materials (i.e. corals) for geochronological analysis (Muhs et al., 2003). Extensive stratigraphic studies in the northeastern Florida Keys on the Key Largo Formation have identified at least five distinct parasequences separated by disconformable surfaces (Muhs et al., 2003; Precht and Miller, 2007). These parasequences consist of coral dominated limestone facies with the disconformable surfaces recognized by hardgrounds, root structures, solution surfaces, and overlying soils (Multer et al., 2002; Muhs et al., 2003).

Amino acid racemization combined with numerical methods such as U-series or ^{14}C dating have constrained the uppermost (youngest) unit of the Key Largo Formation, referred to in places as the Key Largo Limestone, to the peak of the last interglacial (Multer et al., 2002; Muhs et al., 2003). Fossil coral samples from several onshore locations of Key Largo Limestone exposures confirmed ages that range from approximately 130,000 to 121,000 years (Fruijtier et al., 2000). A southeast trending slope of the Key Largo Limestone was identified through extensive core studies that can be traced laterally offshore (Multer et al., 2002). TIMS U-series dating techniques performed on fossil corals from water depths of about 16 to 22 m yielded ages of approximately 127 ka – 124 ka (Multer et al., 2002).

In addition to stratigraphic and geochronologic data collection, elevation measurements were gathered from onshore exposures of the uppermost unit of the Key Largo Limestone to determine amount of sea-level fluctuations and their respective magnitudes during the last interglacial. A few locations where measurements were taken are at Windley Key, Grassy Key, and Key Largo. The youngest unit of the Key Largo Limestone is about 3-5 m above present sea-level at Windley Key, 1-2 m above present sea-level at Grassy Key, and 3-4 m above present sea-level at Key Largo (Muhs et al., 2003). These elevation measurements and optimal growth depths of present corals suggest that sea-level during the last interglacial period rose to at least 5-8 m above present sea-level (Multer et al., 2002; Muhs et al., 2003).

Bermuda. The Quaternary stratigraphy of Bermuda is regarded as one of the world's most complete sedimentary records of interglacial highstands (Hearty, 2002). The Rocky Bay Formation was deposited during the MIS 5e interglaciation. The ages of

the Rocky Bay Formation were constrained through thermal ionization mass spectrometry (TIMS) U-series dating techniques and were then correlated back to the oxygen isotope curve of ODP core 677 from Shackleton et al. (1990). The Belmont member of the Rocky Bay Formation recorded a highstand, which peaked at about + 2.5m. This highstand elevation agrees with what was recognized as the highstand elevation in the Bahamas (Hearty and Kaufmann, 2000; Hearty and Neumann, 2001; Hearty, 2002). The Devonshire member of the Rocky Bay Formation records a similar sea level change observed in the Bahamas where there is a lowstand separating the lower highstand from a second highstand (Hearty and Neumann, 2001). Additionally, there is evidence of notches and rubble benches due to erosion with terrestrial deposits and plant remains that have back filled the breaks in slope (Hearty, 2002).

Bahamas. MIS 5e outcrops found in the Bahamas record climatic events during and at the close of this critical interval (Hearty and Neumann, 2001). Long-term changes are recorded by radiometrically dated fossil reefs and speleothems that provide climatic data from stable isotope ratios (Hearty and Neumann, 2001). In addition to stable isotope ratios, geochronology was performed through TIMS U-series dating to provide better constraints on the timing and magnitude of sea level changes during the MIS 5e (Hearty and Neumann, 2001). Within the Geologic outcrops, Hearty and Neumann (2001) identified six different depositional stages throughout the MIS 5e. Outcrops included chevron ridges, run-up deposits, giant boulders, and massive oolitic and eolian dunes. These different lithologies display a visible change in sea level over the geologic timescale. There was an initial sea level rise that was capped at an approximate height +2.5 meters from ~132-122 ka (Hearty and Neumann, 2001). A second sea-level

highstand that peaked briefly at levels of +6 and possibly +8 meters (Hearty and Neumann, 2001). These highstands were separated by a single lowstand which resulted in the incision of channels in the carbonate platform (Hearty & Neumann, 2001). As the MIS 5e ended, sea level rapidly fell with the onset of MIS 5d.

Hawaii. Sherman et al. (1993) described the Barbers Point section on Oahu, Hawaii, which provides an exposure of the Waimanalo Formation. The Waimanalo Formation, composed of a coral-algal boundstone, is the basal layer of the section and is truncated by an unconformable surface and overlain by grainstone and rudstone of the Leahi Formation. (Sherman et al., 1993). The Waimanalo Formation's age has been constrained to MIS 5e through TIMS U-series dating (Sherman et al., 1993; Hearty et al., 2000). The TIMS analysis yielded ages ranging from 160 ± 15 ka to 115 ± 10 ka (Sherman et al., 1993).

Sediments found at Oahu correlate well in regards to the timing, magnitude, and sea level changes originally suggested by Aharon et al. (1980) from sediments found near New Guinea, which also span the MIS 5e. These sediments display definitive evidence for two different highstands separated by a single lowstand. Two wave cut notches in lithified dune successions indicate two highstands at 6.7 and 8.2 meters in height (Sherman et al., 1993). Indicators of separation between these different highstands can be found within an unconformable surface between the Waimanalo and Leahi Formations, which represents a lowstand (Sherman et al., 1993).

Seychelles. In the Seychelles, patches of limestones containing small coralline algae-vermetid remnants are found as encrustations and cavity fillings between granitic boulders (Israelson and Wohlfarth, 1999). Israelson and Wohlfarth (1999) selected fossil

corals from elevated reefs elsewhere in the Seychelles to perform U-Th radiometric dating. These yielded age dates ranging between 131-122 ka. The elevation of the corals in the sucession and the respective U-Th age dates, combined with fabric analyses in previous studies allowed for a detailed outline of the past sea-level history, which suggests that a gradual sea level rise until 131 ka, followed by a sea-level fall between 131-122 ka (Israelson and Wohlfarth, 1999).

Dutton et al. (2015) surveyed similar fossil reefs on the Seychelles Islands and obtained age dates from corals as well in order to establish peak sea level for the region. The results from the U-Th dating techniques yielded similar results to those from Israelson and Wohlfarth (1999). Dutton et al. (2015) observed a pattern of gradual sea level rise between approximately 129-125 ka with peak sea level being reached at ~128 ka at a position of +5.9 m above current sea level.

Australia. Western and southern Australia represent some of the world's most distant and remote locations from the centers of the major ice sheets during the Pleistocene (Stirling et al., 1998; Murray-Wallace, 2002; Hearty, 2003; Murray-Wallace et al., 2016; Pan et al., 2018). Coastlines in Western Australia are characterized by successions of reef platforms and calcarenites containing in situ corals. Through U-series dating, the ages of the fossil corals have been determined within 131 to 116 ka (Stirling et al., 1998; Camoin and Webster, 2015; Murray-Wallace et al., 2016; Pan et al., 2018). In general, coastal successions in Australia corresponding to the last interglacial or MIS 5e suggest that the magnitude of base-level change range between +2 and +6 m (Murray-Wallace, 2002; Pan et al., 2018).

Indonesia. Coral reef terraces found in the Indonesia region are commonly surveyed and correlated to track Quaternary deformation. Hantoro et al., (1994) identified a series of six major coral reef terraces reaching elevations of about 700 m. Three different radiometric dating techniques were used (^{14}C, $^{230}Th/^{234}U$, ESR) on coral samples found in growth position (Hantoro et al., 1994). Collected coral samples were analyzed to determine the abundance of calcite and samples with a minimal composition of calcite were chosen for radiometric dating.

In addition to radiometric samples, topographic transects were measured across the series of terraces to account for the regional tectonic uplift. Radiometric analyses on three corals yielded apparent ages of the peak of the last interglacial, but it was noted that these ages are to be interpreted with caution due to the samples being affected by recrystallization and dissolution (Hantoro et al., 1994). Similar Pleistocene reef terrace studies in Indonesia have concluded similar results with similar levels of uncertainty regarding radiometric ages (Bard et al., 1996; Voris, 2000; Imran et al., 2016).

Tectonic Evolution of the Caribbean

The Caribbean Plate is located in a very active tectonic region amidst the Cocos, Panama, North Andes, and South American and North American plates (Figure 3). Continental fragments making up the Caribbean plate include the majority of north Central America, the Greater Antilles, and the Lesser Antilles. To the west, the Caribbean plate is bounded by the Middle American subduction zone and in the east by the Lesser Antilles subduction zone (Bachmann, 2001). The northern and southern boundaries are more complex and not as well defined. Strike-slip motions along major fault systems,

such as the Motagua-Polochic fault zone and the Oriente fault, dominate the northern Caribbean plate boundary. This boundary extends from Central Guatemala through Jamaica, Hispaniola, and Puerto Rico to the northern Lesser Antilles (Bachmann, 2001). Important structures included in this boundary is the Cayman Trough, a complex transform fault zone pull-apart basin, the Gonâve microplate, which includes a spreading center west of Jamaica and the south of Cayman Islands. The southern Caribbean plate boundary has been characterized as a very complex zone of thrusting, transcurrent motion and rifting (Bachmann, 2001; Pindell and Barrett, 1990). Plate tectonic models have been created based on the relative motion of the involved plates. While these studies have been successful in delineating the evolution of the Caribbean plate, the genesis of the plate remains inconclusive (Bachmann, 2001).

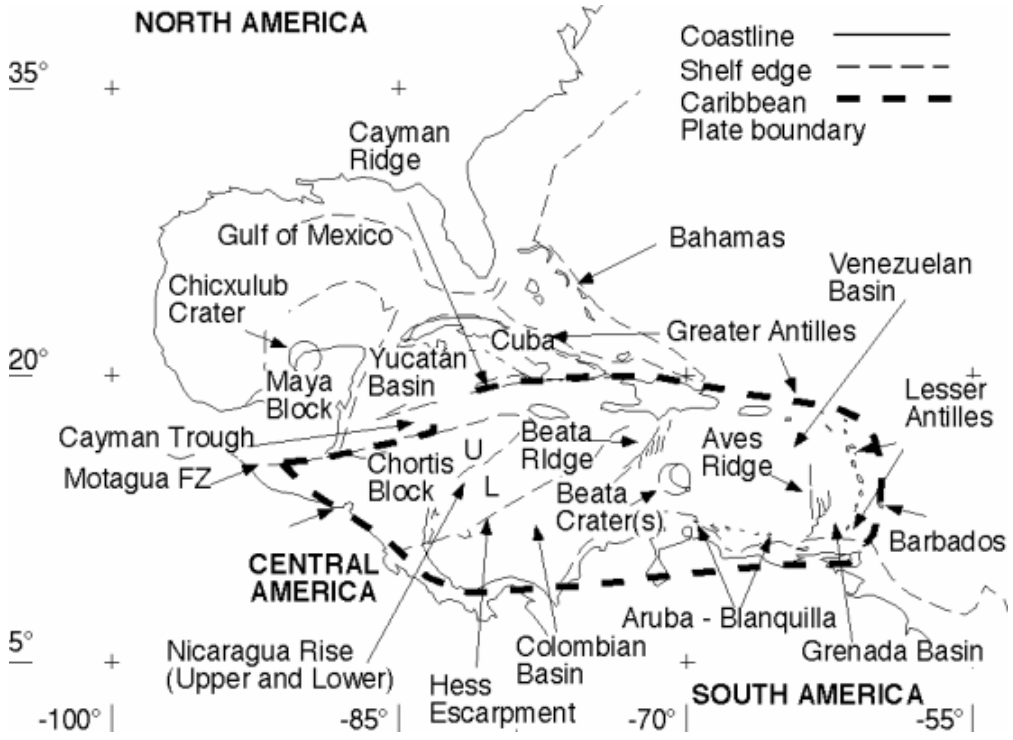

Figure 3. Map displaying major geographic and tectonic provinces of the Caribbean region (James, 2005).

Tectonic Models

There are numerous models attempting to explain the origin of the Caribbean plate. The tectonic environment in pre-Jurassic times remains in dispute with disagreements occurring in using references in reconstruction such as, 1000 m isobaths, paleomagnetic poles, or realignment of marginal offsets (Bachmann, 2001). Currently, at least two models suggest an origin beginning in Jurassic times, the Pacific Model and the Alternative Model (Pindell and Barrett, 1990; Meschede and Frisch, 1998; Bachmann, 2001).

The Pacific Model (Figure 4), preferred by Pindell and Barrett (1990), suggests a late Mesozoic origin of the Caribbean plate within the Pacific Ocean. The evolution of the Caribbean plate with a Pacific provenance can be summarized by five phases: 1) middle to late Jurassic rifting between North America, the Bahamas, the Yucatán block, and northern South America, 2) late Jurassic through late Cretaceous/early Tertiary passive margins and the widening of the proto-Caribbean Basin, 3) Late Cretaceous to recent orogenic event between the eastward migrating Caribbean plate and the stable passive margins, 4) Eocene to recent development of complex strike-slip boundary zones along the northern and southern Caribbean plate margins, 5) Miocene to recent period of widespread deformation across the entire Caribbean (Pindell and Barrett, 1990). The fifth phase for evolution of the Caribbean plate is a result of interactions between the Caribbean, North American, and South American plates. These interactions include compression from the convergence of North and South America, northwestward migration of the Andean Terranes of southwest South America, and the convergence of

the Hispaniolan Restraining Bend along the Orient-Puerto Rico Trench transform fault (Pindell and Barrett, 1990).

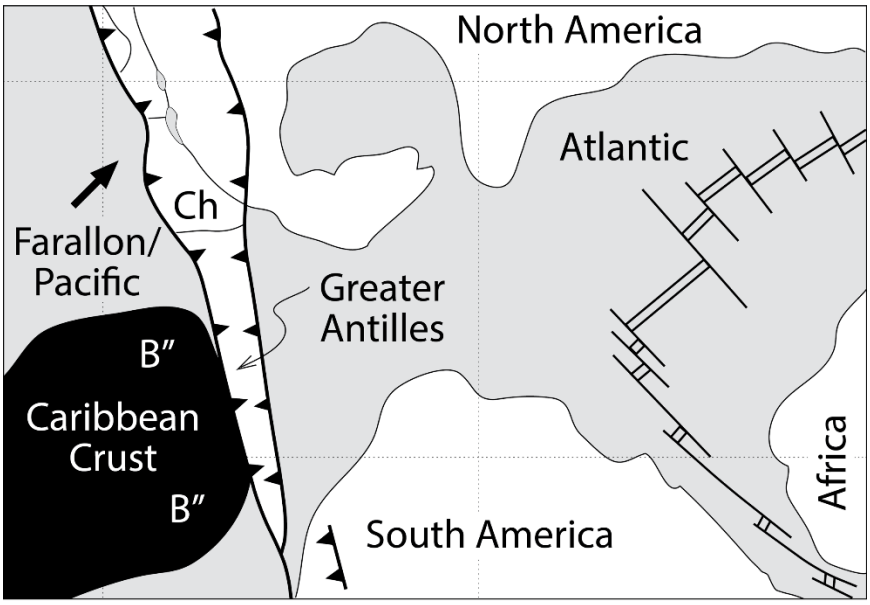

Figure 4. The Pacific model for the origin of the Caribbean Plate. B'' corresponds to the uppermost level of the plateau basalt. CH stands for the Chortis Block (modified from Meschede and Frisch, 1998; Bachmann, 2001).

The Alternate Model (Figure 5), suggested by Meschede and Frisch (1998), proposes that the Caribbean plate formed to the west of its current position, but still between North and South America (Meschede and Frisch, 1998). This model recognizes the following seven evolutionary phases for the Caribbean plate: 1) middle Jurassic rifting between North and South America, 2) late Jurassic through middle Cretaceous widening of the proto-Caribbean Sea, 3) middle to late Cretaceous thickening of the oceanic crust by the formation of a basalt plateau in the Caribbean area, 4) middle to late Cretaceous subduction in the Cuban-Aves Ridge arc and the collision of southern Cuba with the North American plate, 5) middle to late Cretaceous opening of the South

Atlantic Ocean and the Caribbean plate becoming an independent plate, 6) late Cretaceous to recent eastward movement of the Caribbean plate relative to the North and South American plates causing subduction in the Lesser Antilles Arc and the development of complex strike-slip boundary zones, 7) Miocene to recent widespread deformation across the entire Caribbean region (Meschede and Frisch, 1998).

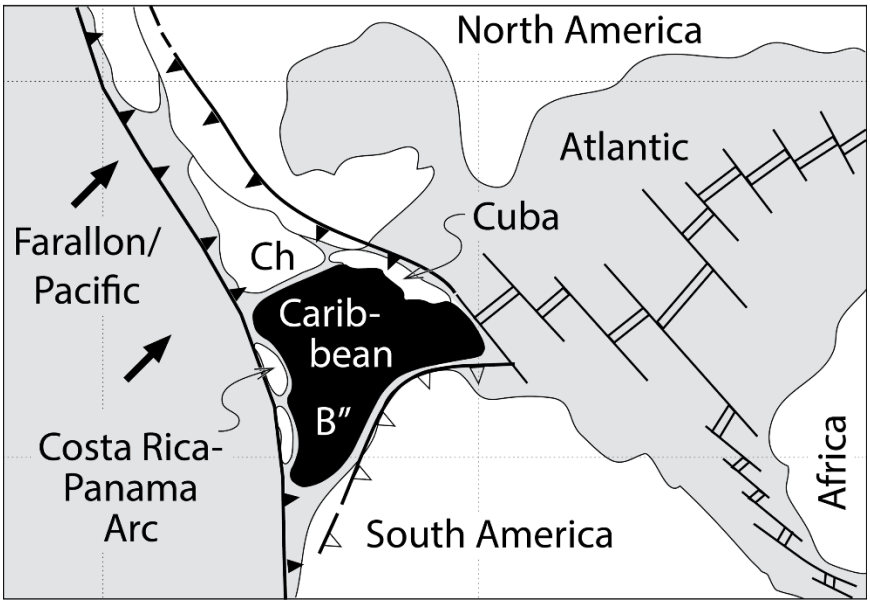

Figure 5. The Alternate model for the origin of the Caribbean Plate. B'' corresponds to the uppermost level of the plateau basalt. CH stands for the Chortis Block (modified from Meschede and Frisch, 1998; Bachmann, 2001).

During the 1990's, the Pacific Model served as the standard model for explaining the genesis of the Caribbean plate and its associated tectonic features. However, some inconsistencies remained regarding the full explanation of how the Caribbean plate formed. Some of the major inconsistencies include the distribution of land and sea during the Jurassic, the amount of space present between North and South America at the beginning or during the Mesozoic, the lack of isotopic indicators for the Galapagos

hotspot, and the existence of the Costa Rica-Panama arc during the early Cretaceous (Albian age) (Bachmann, 2001). While the alternative model attempts to explain the major inconsistencies for the evolution of the Caribbean within the Pacific Model, it does not explain the existence of a thickened oceanic crust whereas the Pacific model does. If the provenance for the Caribbean plate is located near the Galapagos hotspot, then further research is needed to explain the disagreements between the two proposed models.

Geologic Setting of Jamaica

Jamaica is located at the easternmost extent of the Nicaragua rise in what has been described as a 200-kilometer-wide seismically active zone between the North American plate and Gonâve microplate to the north and Caribbean plate to the south (Figure 6) (James-Williamson et al., 2014). The Nicaragua Rise is a Cretaceous submarine volcanic plateau overlain by 5-7 kilometers of Neogene carbonates and is bounded by the Cayman Trough and Colombian Basin to the north and south, respectively (James-Williamson et al., 2014; Benford et al., 2014).

The geologic evolution of Jamaica can be divided into four separate phases: a Cretaceous to early Eocene island arc; Paleocene to Eocene extensional rifting; a middle Eocene to middle Miocene period of quiescence allowing for development of a large carbonate bank; and a middle Miocene to recent left-lateral transpression which led to the prominent uplift of Jamaica (James-Williamson et al., 2014; Benford et al., 2014; Robinson and Mitchell, 1999). The period of tectonic and volcanic inactivity in the second phase of the geologic evolution of Jamaica provided enough stability for large-scale carbonate deposition, which covers about two-thirds of the island (Donovan, 2003).

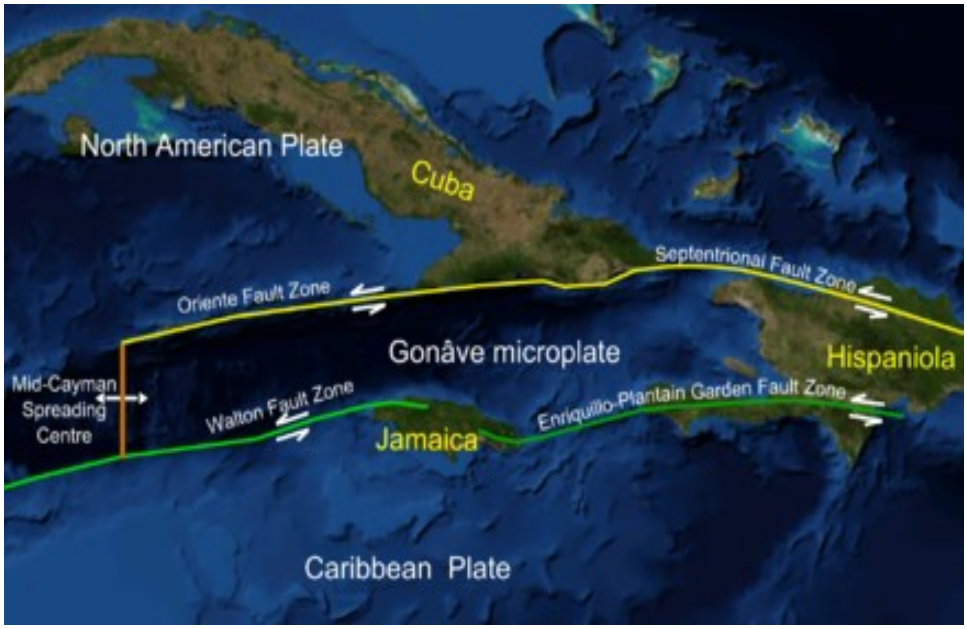

Figure 6. Map displaying the geographic and tectonic setting of Jamaica and the surrounding Caribbean region (Norton, 2006).

The western portion of the island is dominated by post-Eocene carbonates (White Limestone Group) overlying the Cretaceous basement rock and older carbonate sediments of the Yellow Limestone Group. A series of structural elements, including folds and faults, have deformed the pre-Pleistocene strata, and exposures of the carbonates are extensively karstified.

Regional Stratigraphy of Jamaica

Due to the complex tectonic and geologic history, the lateral stratigraphic relationships between geologic units display high levels of variance across the entire island. Detailed geologic mapping at various scales has been executed to establish correlative stratigraphic relationships. In general, Jamaican stratigraphy consists of five units: the basal volcanic rocks, the Yellow Limestone Group, the White Limestone

Group, the Coastal Group, and the recent alluvium deposits (Figure 7). For this study, locations of the recent alluvium deposits are noted (Figure 7), but are not discussed in detail.

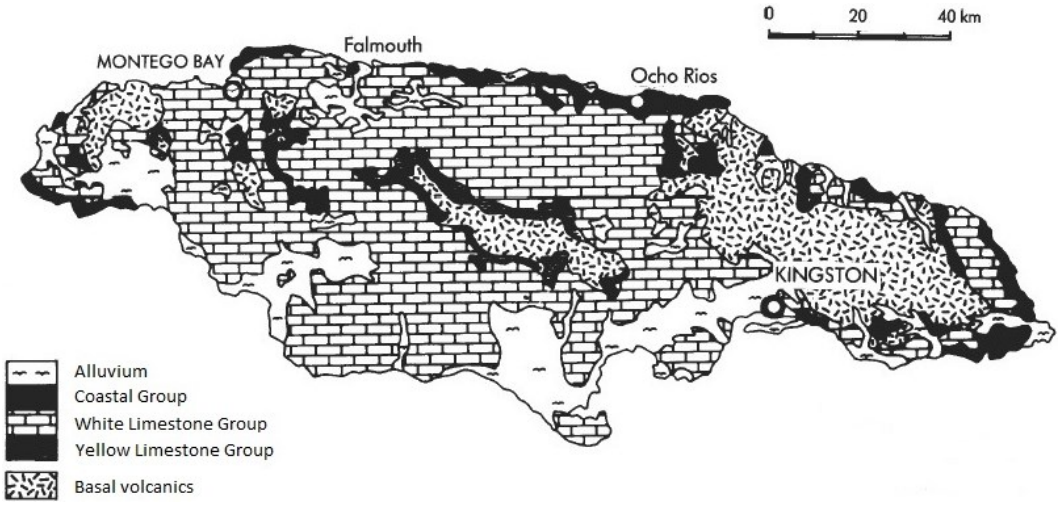

Figure 7. Simplified geologic map of Jamaica showing the major geologic (modified from Donovan, 2003).

Basal volcanic rocks. The basement rocks of Jamaica are exposed at the surface in a series of about 27 inliers that are bounded by faults and surrounded by younger rocks (Robinson, 1994). The series of inliers can be divided into the following groups: Blue Mountains Inlier, Sunning Hill Inlier, Benbow Inlier, Above Rocks Inlier, Lazaretto Inlier, Central Inlier, St Ann's Great River Inlier, the St. James Inliers, and the Hanover Block Inliers (Mitchell, 2001; Mitchell, 2006; Mitchell, 2013; Mitchell, 2016).

These exposures are distributed across Jamaica containing successions of lava flows, intrusives, volcaniclastics, carbonates, and some metamorphic suites (Robinson, 1994; Mitchell, 2003). In general, the inliers are reported as Cretaceous in age (Mitchell, 2006). Recent studies have documented the successions within the different inliers

through geologic mapping at a 1:12,500 scale to revise the regional lithostratigraphy and reconstruct the geologic evolution of Jamaica (e.g., Gunter and Mitchell, 2005; Brown and Mitchell, 2010; Mitchell et al., 2011; Fisher and Mitchell, 2012; Mitchell, 2013; Mitchell and Edwards, 2016; Mitchell, 2016).

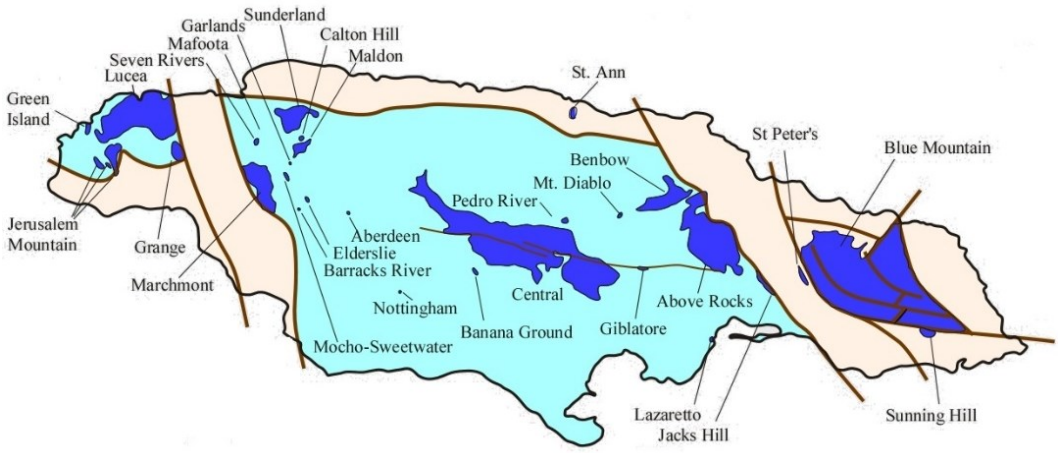

Figure 8. Simplified geologic map of Jamaica showing the distribution of the 27 different Cretaceous Inliers represented in dark (modified from Mitchell, 2016).

Yellow Limestone Group. The Yellow Limestone Group unconformably overlies the Cretaceous basement complex consisting of a succession of impure limestones and clastics, which include claystones, siltstones, shales, and sandstones (Mitchell, 2013; Mitchell, 2016). The geology of the Yellow Limestone Group is best understood from exposures around the margins of the Central Inlier, where it is represented by the Guys Hill, Freemans Hall, Stettin, and Chapleton Formations (Robinson and Mitchell, 1999; Mitchell, 2013; Mitchell, 2016).

The Stettin Formation consists of a sequence of fine-grained, fossiliferous, wackestones, packstones, and grainstones containing algae, foraminifera, echinoids,

molluscs, and a minor abundance of corals (Robinson and Mitchell, 1999). The Guys Hill Formation consists of a succession of quartz-rich sandstones and conglomerates that is capped by an irregularly bedded limestone containing a rich molluscan fauna and large foraminifera. In the lower portion of this irregular limestone unit, fragments of crocodile, turtle, and sea cow remains have been found (Robinson and Mitchell, 1999). The Chapleton Formation creates the upper part of the Yellow Limestone Group and consists of medium to thick bedded wackestones and packstones with interbedded sandstones, mudstones, and marls (Robinson and Mitchell, 1999).

White Limestone Group. The White Limestone Group covers about two-thirds of Jamaica (Figure 9) consisting of shallow-water and deep-water carbonates that were deposited from the middle Eocene to the early or middle Miocene, ranging from approximately 45 million years to 12 million years ago (Robinson and Mitchell, 1999; Mitchell, 2013).

Extensive research on the stratigraphy of the White Limestone Group by previous investigators has identified that rocks belonging to the group were deposited when Jamaica was composed of a series of shallow carbonate platforms separated by deep-water marine troughs, which have been subsequently uplifted (Robinson and Mitchell, 1999; Mitchell, 2003; Mitchell, 2013).

On the Clarendon Block, the White Limestone Group consists of massively bedded limestones with a fossil assemblage containing corals, algae, molluscs, echinoids, and benthic foraminifera (Robinson and Mitchell, 1999). Macrofossils characteristic of the sublittoral zone may be locally abundant, however, they are commonly poorly preserved and difficult to extract (Robinson and Mitchell, 1999).

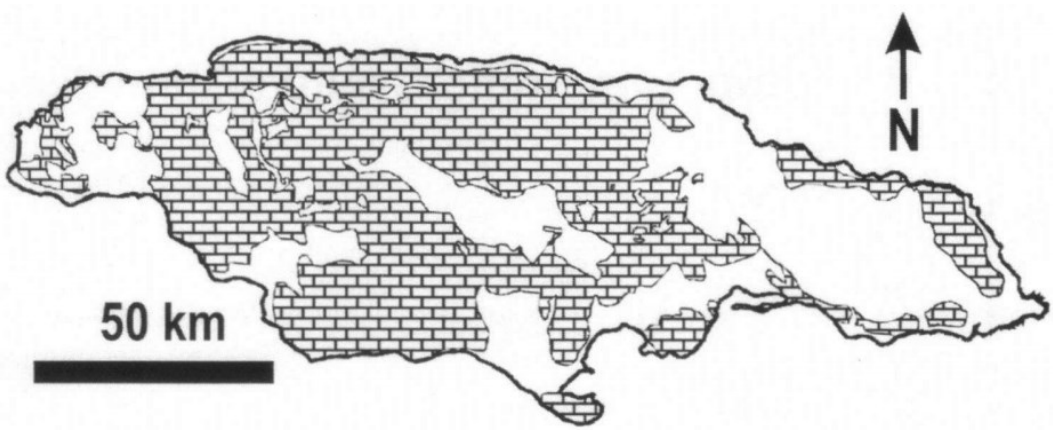

Figure 9. Simplified geologic map of Jamaica showing the distribution of the White Limestone Group, which is marked by the block pattern (modified from Robinson, 1994; from Stemann, 2004).

Within the Wagwater, North Coast, and Montpelier-Newmarket belts, the White Limestone Group consists of successions of bedded chalks containing layers of chert. The fossil assemblages in these localities contain planktonic foraminifera indicating a deeper marine environment (Robinson and Mitchell, 1999). The White Limestone Group has been extensively eroded to form the tower and cone karst formations characteristic of the famed Cockpit Country of St. James, Trelawney, Manchester, and St. Elizabeth parishes.

Since being originally introduced as a formation in 1825, the White Limestone Group has undergone many revisions to the regional lithostratigraphy being applied (Robinson and Mitchell, 1999; Mitchell, 2003; Mitchell, 2013). Mitchell (2013) provided a provisional lithostratigraphic scheme where previous formation names were abandoned and new names were defined at lithological boundaries based on changes in texture and/or color. While further revisions are under review, the current lithostratigraphic nomenclature of the White Limestone Group consists of eight different geologic formations (Table 1; Mitchell 2013). From oldest to youngest, the units include: Healthy

Hill Formation, Troy Formation, Swanswick Formation, Claremont Formation, Somerset Formation, Walderston Formation, Browns Town Formation, and Newport Formation (Mitchell, 2013).

Table 1. Generalized lithostratigraphy of the White Limestone (Mitchell, 2013).

Formation	Period	Lithology
Newport Formation	Late Oligocene – Early Miocene	Thick bedded white wackestones and carbonate mudstones
Browns Town Formation	Late Oligocene – Early Miocene	White packstones, wackestones, and carbonate mudstones containing abundant large foraminifers and corals
Walderston formation	Early Oligocene	Medium to thick bedded grainstones and packstones
Somerset Formation	Late Eocene	Foraminiferal grainstones and packstones containing abundant molluscs and corals
Claremont Formation	Late Eocene	Medium to thick bedded carbonate mudstones and wackestones
Swanswick Formation	Middle Eocene	Thin to thick bedded white grainstones
Troy Formation	Middle Eocene	Massive to medium bedded limestones and dolostones
Healthy Hill Formation	Early Middle Eocene	White grainstones, packstones, and wackestones containing abundant foraminifera

Coastal Group. Sedimentary successions of the Coastal Group were deposited along the flanks of Jamaica during its tectonic uplift over the last 12-14 million years (James-Williamson et al., 2013). In general, the Coastal Group's depositional history can be divided into two phases: an older part consisting of mid/late Miocene to early

Pleistocene age units and a younger part consisting of late Pleistocene age units (Mitchell, 2016). In eastern Jamaica, the older part consists of five identified formations including the August Town Formation, Low Layton Formation, Layton Formation, Manchioneal Formation, and Old Pera Formation (James-Williamson et al., 2013).

The August Town Formation (mid-Miocene – Pliocene) consists of a mixed clastic-carbonate succession that unconformably overlies the White Limestone Group (James-Williamson et al., 2013). The Low Layton Formation (upper Miocene) is a succession of pillow basalts from a submarine fissure eruption, which occurred near Black Hill in Portland Parish (Wadge, 1982). The Layton Formation (late Miocene – Pliocene) consists of a series of marlstones and can be divided into three members: the Buff Bay member, the San San Member, and the Bowden Member (James-Williamson et al., 2013). The Bowden Member has been upgraded to formation status at its type section, which consists of the upper Pliocene Bowden Shell Beds, a highly fossiliferous conglomerate to coarse-grained sandstone containing over 800 identified taxa (Donovan et al., 2014). The Manchioneal Formation and Old Pera Formation (early Pleistocene) contain abundant transported reef-building corals and consist of impure limestones and sandstones, respectively (Mitchell et al., 2000).

In northwestern Jamaica, the older part of the Coastal Group consists of the Hopegate Formation, a Pliocene coral reef terrace found along the coast and is often dolomitized (Land, 1991; Donovan et al., 2004; Skrivanek et al., 2017). The upper part of the Coastal Group is represented by the Falmouth Formation, an uplifted coral reef complex and associated lagoonal deposits, and the Port Morant Formation, a mixed carbonate-siliciclastic succession interpreted as a dissected fan-delta (Mitchell et al.,

2000; Skrivanek et al., 2017). These formations are considered to be penecontemporaneous (e.g., Collins et al., 2009) representing deposits from the MIS 5e, the last interglacial episode (Mitchell et al., 2000).

Study Area

Jamaica, the third largest island of the Greater Antilles in the Caribbean Sea, located at approximately 18º North latitude and 77º West longitude. The island has an area of 10,939.7 square kilometers and is 236 kilometers long by 35-82 kilometers wide (Richards, 2008). Jamaica's topography consists of high interior mountain ranges reaching 2,256 m high in the eastern Blue Mountains, surrounded by flat, narrow coastal plains. The coastline, approximately 895 km long, has been described as irregular varying between sandy beaches, estuaries, mangrove swamps, cays, coral reefs, and seep rocky shores. White sand beaches and a plunging sea floor allowing for extensive fringing reef development dominate the northern coastline. On the other hand, long, steep cliffs (e.g., Lover's Leap), mangrove swamps, and black sand beaches characterize the south coast of the island. There is little reef development on the south coast due to a shallow shelf environment of less than 36 m in depth. The shallow shelf extends 8-32 km offshore where barrier reefs and small islands or cays are found (Richards, 2008).

The parish of St. Elizabeth is located in southwest Jamaica (Figure 10). It is one of Jamaica's oldest and largest parishes (Jamaica Information Service, 2017). Originally, the parish covered a greater portion of southwestern Jamaica. However, the area underwent subdivisions in 1703 and 1814 into the parishes of Westmoreland and Manchester, respectively (National Library of Jamaica, 2018). The resulting area was

named St. Elizabeth after Lady Elizabeth Modyford, the wife of the first Governor of Jamaica (National Library of Jamaica, 2018). Today, St. James and Trelawny border St. Elizabeth on the north, the Caribbean Sea on the south, Westmoreland on the east and Manchester on the west (Jamaica Information Service, 2017).

Figure 10. Geographic map displaying the boundaries of Jamaican parishes. The study area is in St. Elizabeth parish, outlined in white, located in southwestern Jamaica (Google Earth, https://earth.google.com/web/).

The area of interest for this study includes roughly 10 kilometers of the coastal region of St. Elizabeth parish. The area begins roughly 5 km east of Parrottee Point in Fort Charles Bay and ends 1.5 km northwest of Great Pedro Bluff in Pedro Bay (Figure 11-A). This section of coastline in St. Elizabeth is composed of sandy beaches and rocky shorelines.

The principal exposures in this study appear in several of the major bays, which includes Fort Charles Bay, Billy Bay, Frenchmans Bay, Calabash Bay, and Pedro Bay (Figure 11-A). Fort Charles Bay and Billy Bay exhibit vertical rocky exposures separated by sandy beaches. Some of these sandy beaches (e.g., Billy Bay) are protected and serve

as sea turtle sanctuaries. In Fort Charles Bay, these vertical exposures terminate along a modern dune field. Frenchmans Bay, Calabash Bay, and Pedro Bay are dominated by sandy beaches, sporadic vertical rock exposures, and wave-cut platforms. The entire coastline has fringing wave-cut platforms extending about 40 m offshore with some being emergent in areas along with the vertical exposures. These emergent sequences have likely been uplifted as a result of neotectonic activity in the area. Based on the geologic map (Figure 11-B), the White Limestone Group covers the majority of the region and has been mapped as the Newport Formation (Late Oligocene – Early Miocene). The Coastal Group, mapped as the Falmouth Formation, is represented along the coastline between Calabash Bay and Fort Charles Bay with a small amount fringing Great Pedro Bluff and Boatmans Bay (Figure 11-B). In some areas, exposures of these units have been covered by eolian sand (Quaternary) and recent alluvium deposits (Figure 11-B).

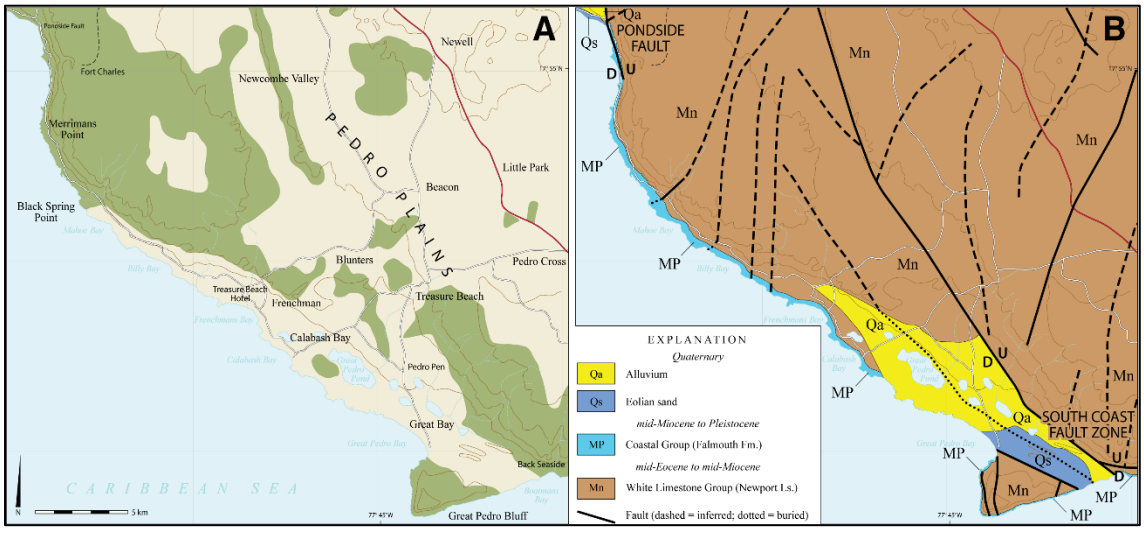

Figure 11. Geographic and geologic maps of the study area. A) Map of geographic locations within the study area of St. Elizabeth Parish. B) Geologic map of southwestern St. Elizabeth Parish (Modified from Benford et al., 2012).

Additionally, there are two main fault systems within the study area, the Pondside Fault to the northwest at Fort Charles Bay and the South Coast Fault Zone to the southeast near Great Pedro Bluff as well as several minor inferred faults intersecting the coastline. These have been documented as being recently active and have likely displaced the geologic units (Evans et al., 2018).

METHODS

Geologic Field Mapping

Detailed, geologic field mapping was conducted to define the local distribution of outcrops belonging to the Coastal Group along the coast of southwestern St. Elizabeth Parish. Exposures were documented using standard geologic field survey techniques to establish age relationships in the strata present, with additional data collected from photographs, Geographic Positioning System (GPS) and aerial drone imagery.

While traversing the coast, Coastal Group exposures were documented through a total of 1,837 photographs taken using an Olympus Tough TG-4 waterproof camera. This camera contains a GPS device and allowed a geographic map to be created showing the location of each photograph taken (Figure 12). The photographs provide a digital catalog of observed features along the coast as well as locations for each observed feature (Appendix A).

In addition to standard field survey techniques, aerial drone imagery of the study area was collected to better outline the regional distribution of Coastal Group exposures. Orange markers were placed in areas with unobstructed aerial views to provide ground control points and allow each individual photo to be properly georeferenced. The imagery was collected on January 9, 2018 using a DJI Phantom 4 Professional Unmanned Aerial vehicle (i.e. a drone; Figure 13) equipped with a 12.4-megapixel camera covering an area of approximately 3.51 km^2. The flight pattern used to collect the orthogonal imagery was approximately a grid centered along the coast and criss-crossed with some randomly oriented overflights with the drone at approximately 100 +/- 50 m altitude.

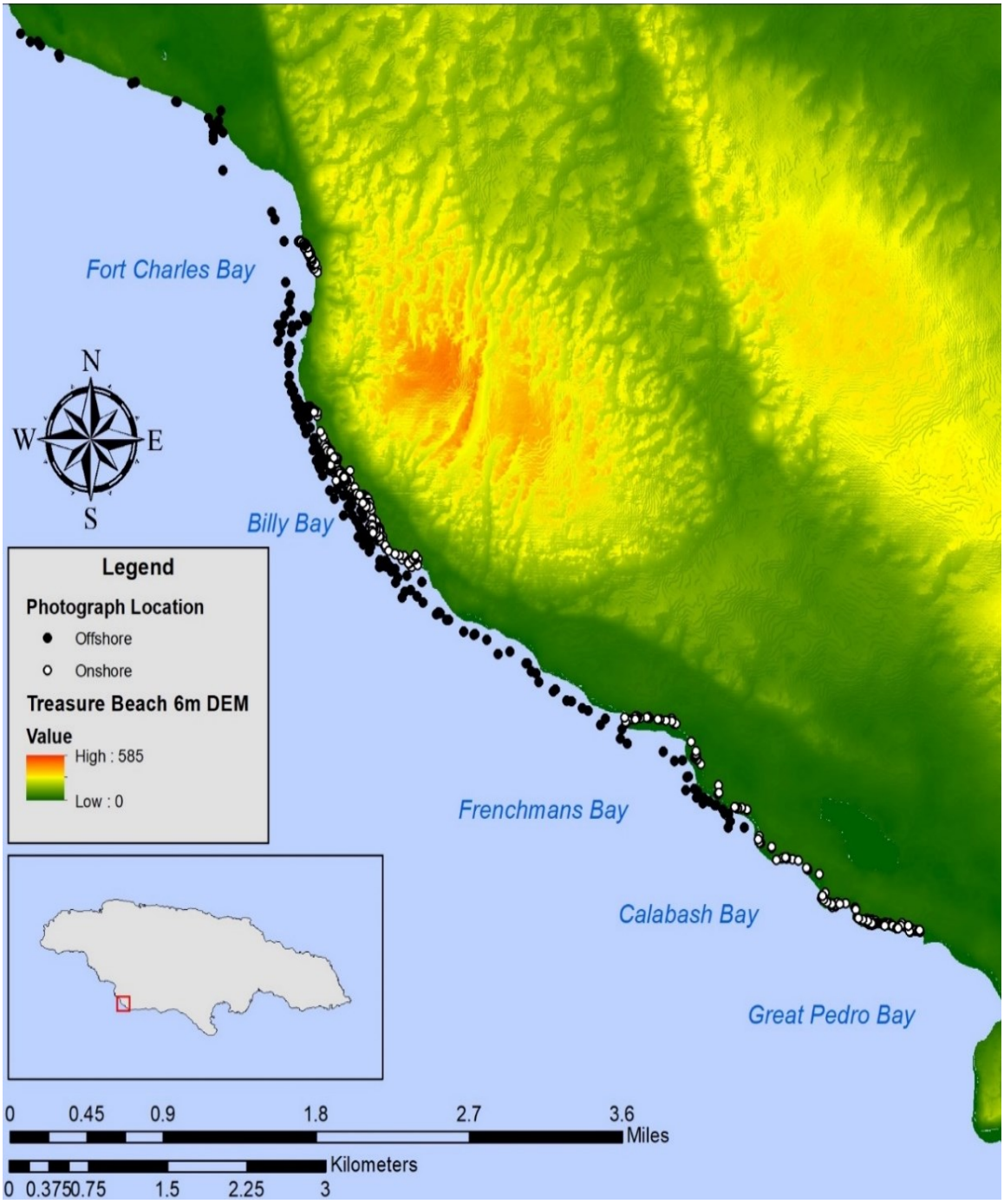

Figure 12. Location and distribution of photographs taken in the field. Black dots indicate photos taken offshore. White dots indicate photos that were taken onshore. DEM was provided by Mona Geoinformatics at the University of West Indies, Mona.

Figure 13. Image of the drone, a DJI Phantom 4 Professional Unmanned Aerial Vehicle, and the orange marker used to establish ground control points.

The imagery was processed using AGI Photoscan software with markers and ultrahighest quality. In total, 235 photographs were aligned to generate 858,949 tie points. An ultra-high quality dense cloud was generated into a three-dimensional model. The resulting orthomosaic image and digital elevation models (DEM) have resolutions of 7.83 cm per pixel. After generating the orthomosaic image and DEMs, they were brought into ArcGIS and overlain on top of a different DEM provided by Mona Geoinformatics at the University of West Indies, Mona.

Stratigraphic Sections

Detailed descriptions of each section can be found in the results section. Descriptions of carbonate rock textures are based on the classification scheme of Dunham (1962) (Figure 14). Reefal limestone fabrics were characterized using Embry and Klovan

(1972), an adaptation to the Dunham (1962) classification system (Figure 14). Accompanying drafted stratigraphic columns and corresponding GPS coordinates are in Appendix B.

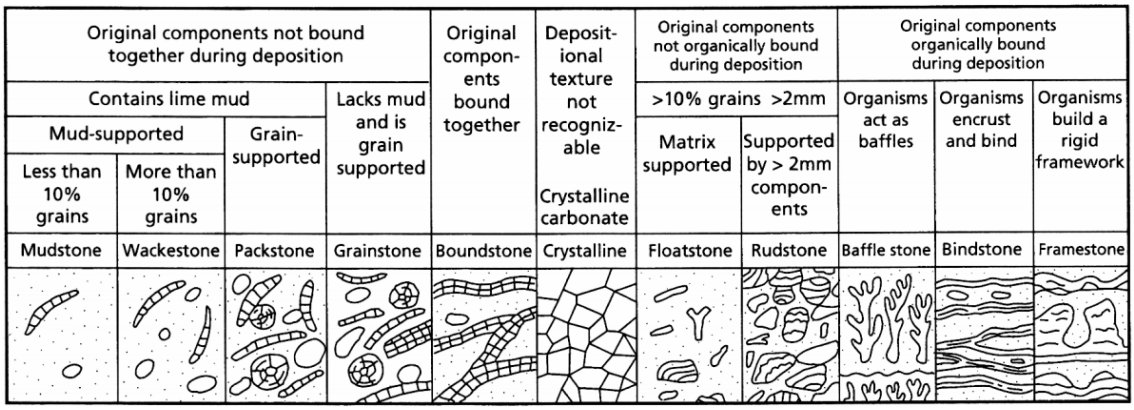

Figure 14. Classification of limestones based on depositional (Embry and Klovan, 1972; after Dunham, 1962).

Stratigraphic sections were measured and described on a sub-meter scale at eleven different locations along the coast of southwestern St. Elizabeth Parish, southwestern Jamaica (Figure 15). Each section, selected based on the quality of exposure of the coral cobble-boulder rudstone unit, was measured and discreetly marked using a Jacob's staff. Detailed descriptions of lithofacies, sedimentary structures, and contacts were made along with accompanying digital photographs. A focus was placed on surfaces of significance, such as unconformities and lithologic transitions, as these contacts determine the placement of systems tracts and allow for interpretations about relative sea-level and paleo-depositional environment evolution. Additionally, identified coral heads were photographed and cataloged to document biological changes and understand the development of the coral reef community through time (Appendix C).

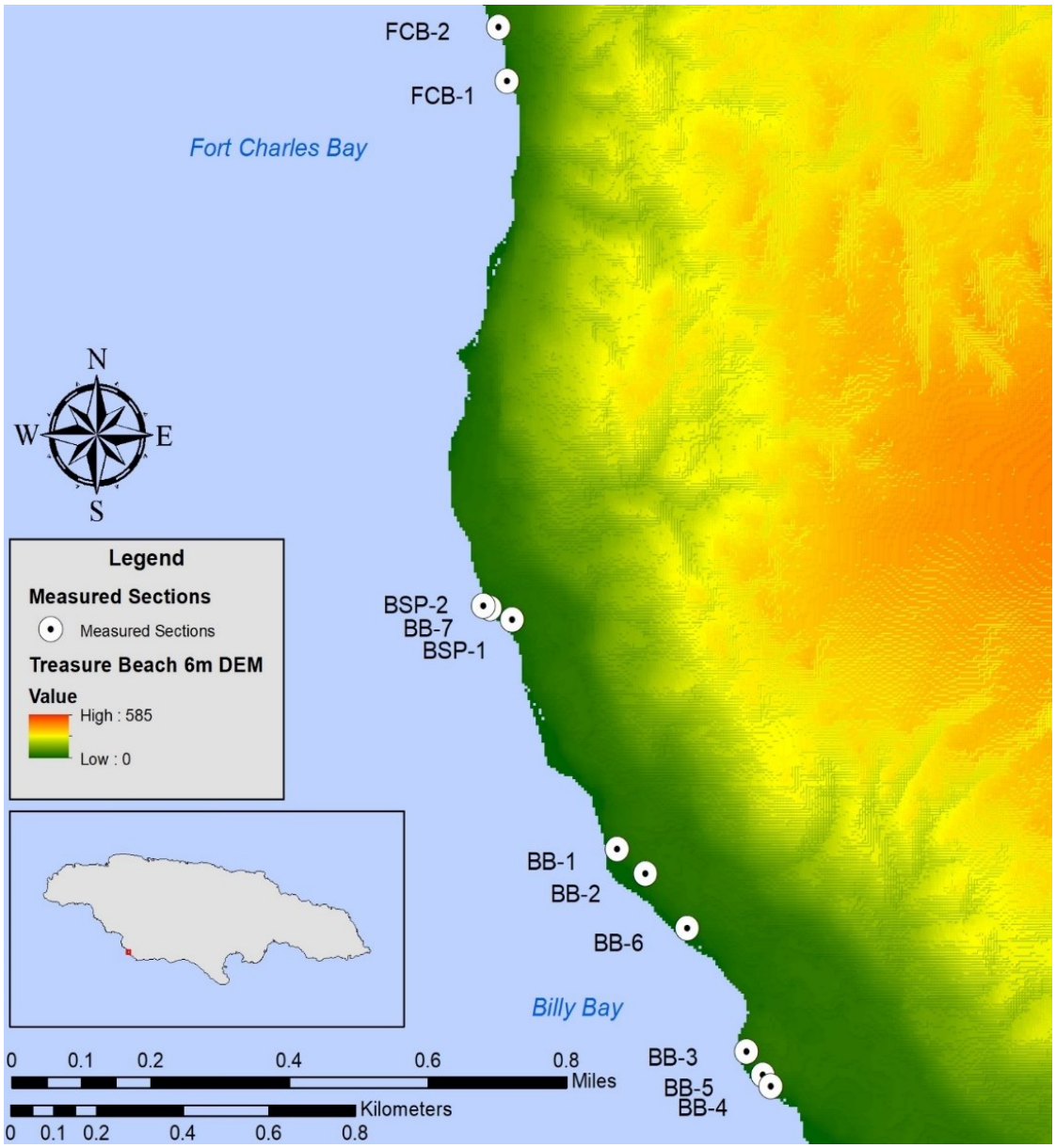

Figure 15. Location of the eleven measured stratigraphic sections. Each section is marked by a white circle with a black dot in the center. 6m DEM was provided by Mona Geoinformatics at the University of West Indies, Mona.

Gamma-Ray Profiles

While gamma-ray logs commonly are used in the oil and gas industry, they support precise correlations over large distances between near shore and offshore facies. Various rock types emit different amounts and different spectra of gamma radiation

through the natural decay of radiogenic nuclides, such as uranium, thorium, and potassium. Typically, these elements are found in higher concentrations in clay-rich rocks, such as shales and siltstones. Fine-grained mudrocks often contain potassium as part of their clay content and clays are susceptible to absorbing uranium and thorium. Therefore, fine-grained mudstones with high clay content will yield higher values, while rocks with low clay content, such as mature quartz sandstone and limestone, will yield lower values. When a gamma-ray interacts with a NaI crystal within scintillometer, there is a chance the gamma ray will be captured. Upon capture, photons will be emitted and brought into a photonmultiplier mounted on the side of the crystal, which will convert the emitted photons into an electronic pulse. This pulse is counted and displayed as a numerical value in Counts Per Second (CPS). This is a relative value, rather than absolute, and are not directly comparable between different sections. However, identified trends or shifts in the gamma-ray log can be used to correlate significant geologic attributes over significant distances and differentiate between regionally controlled strata from local depositional effects.

For this study, gamma-ray profiles were measured using an Urtec Miniscint UG130 solid-state crystal spectral scintillometer. Values were recorded as a ten second average in CPS. The raw gamma-ray data in CPS can be found in Appendix D, along with the stratigraphic position of each measurement. Appendix E contains the gamma-ray profiles from five of the eleven measured and described stratigraphic sections.

Electron-Spin Resonance (ESR) Spectroscopy

Corals are abundant and relatively diverse in the coastal outcrops of southwestern St. Elizabeth parish. Common identified corals include: *Acropora palmata*, *Acropora cervicornis*, *Diploria strigosa*, *Diploria labrinthiformis*, *Montastrea cavernosa*, *Montastrea annularis*, *Porites* spp., and *Siderastrea* spp (Appendix C). Fossil coral samples that seemed well preserved within the exposures were collected from a coral cobble-boulder rudstone facies to obtain a suggestive age of the succession (Table 2). The coral samples were sent to Dr. Anne Skinner at Williams College to conduct Electron-Spin Resonance Spectroscopy. This method was previously performed by Mitchell et al. (2000) on the Port Morant Formation in southeastern Jamaica and yielded an age of approximately 125 ka, Additional dating methods have been implemented in other parts of Jamaica on the Falmouth Formation with similar results (Skrivanek et al., 2017). These dating methods have provided reliable ages that confirmed an age coinciding with marine isotope stage 5e and agree with the ages of the ESR analysis results of Mitchell et al. (2000).

Table 2. Collected coral samples for Electron-Spin Resonance (ESR) Spectroscopy.

Sample	Lab ID	Site	Position	Comments
CD-1	CL1	BB-2	1.6 m above base	Field sketch says 1.7 m
CD-2	CL2	BB-3	6.2 m above base	At contact with skeletal grainstone unit
CD-3	CL3	Float	Float	Potential alteration

Three coral samples, CD-1, CD-2, and CD-3, were collected from a coral cobble-boulder rudstone facies at various locations and elevations (Table 2). Each sample was carefully examined to be as unweathered as possible to ensure maximum preservation of an aragonitic composition. Sample CD-1 was collected at section BB-2 (17.902222 N, -77.794998 W) from a *Montastrea spp.* coral head, which was encrusting the unconformable hardground layer at the base of the coral cobble-boulder rudstone facies at an approximate height of 1.6 meters. Sample CD-2 was collected at section BB-3 (17.898724 N, -77.792885 W) from a *Diploria labrinthiformis* coral head at an approximate height of 6.2 meters, which marks a contact between the coral cobble-boulder rudstone facies and a skeletal grainstone facies. Sample CD-3 was collected from a disarticulated branch of *Acropora palmata*, which came from a toppled block composed of the coral cobble-boulder rudstone facies. Although this sample is considered float, petrologic analysis suggests it came from the same unit as the previous samples and the internal structures of the coral had been preserved; hence, ESR analysis can be applied to this sample to obtain a suggestive age. In addition to the coral samples, the surrounding fine-grained skeletal grainstone matrix of the coral cobble-boulder rudstone facies was collected.

After collection, samples were sent to McMaster University in Hamilton, Ontario, Canada for neutron activation analysis (NAA) to determine the radioisotope concentrations of uranium, thorium, and potassium. NAA is a highly sensitive and non-destructive method for determining minor amounts of various elements in a sample (Figure 16). The analysis hinges on the fact that stable, naturally occurring are capable of absorbing neutrons into their atomic nuceli (McMaster, 2015). The sample is exposed to

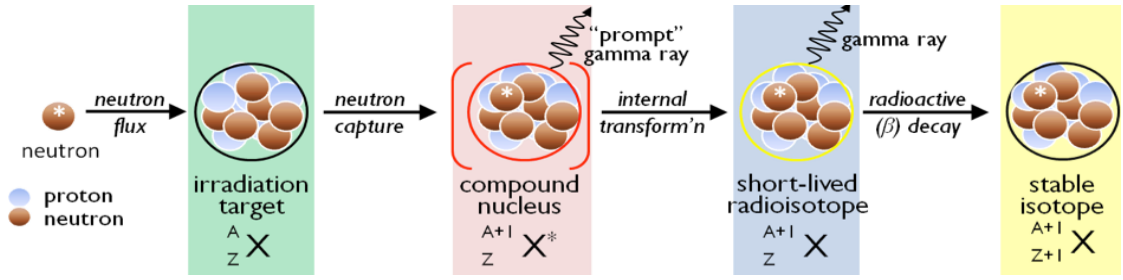

Figure 16. Neutron Activation Analysis (NAA) process (McMaster, 2015).

neutrons in a nuclear reactor causing some of the atoms to undergo neutron capture producing a high-energy compound nuclei that converts into radioactive isotopes of the original element(s) (McMaster, 2015). As these radioactive isotopes decay, the sample is placed on a high purity germanium detector that records the emission of gamma rays (McMaster, 2015). Different radioactive isotopes emit gamma rays at specific energies and intensities allowing for radioisotopes and their parent isotope to be identified.

Following NAA, the coral samples were sent to the ESR-age-dating laboratory of Dr. Anne Skinner at Williams College in Williamstown, Massachusetts. Samples were cut from the cobble-sized corals and surface material (lichens, etc.) was removed. Then, the cut samples were reduced to a powder. The resulting powder was divided into aliquots of approximately 80 mg for each sample. These powders were transferred to the New York State Public Health lab in Albany, New York where irradiations were performed yielding 12-16 samples with doses ranging from 0 to 1000 Gy.

ESR dating, also known as Electron Paramagnetic Resonance (EPR), is a trapped charge dating method that allows precipitated minerals, such as tooth enamel, volcanic minerals, speleothems, mollusc shells, and corals, to be dated (Grün, 1997; Rink, 1997). Recently, attempts have been made to apply ESR dating techniques to assess the resetting

of ESR signals during fault movement to establish the timing of neotectonic processes (Grün, 1997). Natural radioactivity in the environment from uranium, thorium, potassium, and other cosmogenic sources provide enough energy to unpaired electrons causing them to migrate from the valence band to a higher energy level (Grün, 1997). After a short amount of time, these electrons will recombine with the positively charged holes left behind in the valence band. However, some electrons become trapped in between energy levels or impurities within the sample. The amount of trapped electrons corresponds to the magnitude of the ESR signal, which is directly proportional to the number of trapped electrons in the mineral, the applied dosage of radioactive substances, and the age (Grün, 1997; Rink, 1997).

For corals, an ESR signal is produced when unpaired electrons become trapped within impurities of coralline aragonite (Mitchell et al., 2000). The magnitude of the resulting ESR signal directly depends on the total radiation experienced by the coral sample during its geologic history. Therefore, the sample can be dated as long as the dose rate generated from the coral itself and its environment can be measured accurately (Mitchell et al., 2000). ESR dates of corals can be calculated using the equation below (Figure 17).

For this equation to be applied, the total environmental radiation dose rate, $\boldsymbol{D_{\Sigma}(t)}$, must have remained constant throughout the sample's geologic history. Typically, corals do not incorporate thorium or potassium into their chemical structure, and rarely lose radon (Radtke et al., 1988; Skinner, 1988; Mitchell et al., 2000). Additionally, coralline aragonite uptake minor amounts of uranium relatively quickly in terms of geologic time allowing for the presence of an early uranium uptake model to be assumed (Radtke, et al.,

1988; Skinner, 1988; Mitchell et al., 2000). This method has been proven to produce reliable dates from coral samples up to 500 ka (Skinner, 1988; Mitchell et al., 2000) and, in some cases, as old as 800 ka (Radtke et al., 1988).

$$t = \frac{A_\Sigma}{D\Sigma(t)} = \frac{A_\Sigma}{D_{int}(t) + D_{ext}(t)}$$

Figure 17. Equation for calculating ESR dates of corals; t = the age of the sample; A_Σ = the total accumulated dose in the sample; $D_\Sigma(t)$ = the total environmental radiation dose rate; $D_{int}(t)$ = the internal radiation dose rate arising from the coral itself; $D_{ext}(t)$ = the external radiation dose rate (e.g., cosmic radiation) derived from the coral reef matrix (Mitchell et al., 2000).

Sequence Stratigraphy

Prior to any paleoclimatological interpretations being made, the sedimentation patterns and depositional environments must be understood. For this study, a sequence stratigraphic framework model was developed to better understand variables controlling sedimentation, such as sediment influx variations, base-level changes, subsidence rates, and accommodation (Catuneanu, 2006). Physical features of the exposures at various scales were taken into consideration to generate the stratigraphic model. In general, these physical features are surfaces of sedimentary significance, such as unconformities and flooding surfaces, which provide the basis for interpretations regarding changes in relative or eustatic base level and depositional environments (Christie-Blick and Driscoll, 1995).

The accuracy of sequence stratigraphic models relies on the amount and quality of the available data for any given study area (Catuneanu, 2006). All of the available data is integrated in generating a sequence stratigraphic model. The types of data used include studies of outcrops, cores, well logs, and seismic data. Data is more abundant in well-studied sedimentary basins and less abundant in understudied sedimentary basins (Catuneanu, 2006). Sequence stratigraphic principles generate model-based predictions that enable for the most viable and admissible interpretations to be made regarding the evolution of the associated depositional environments within the study area. A typical workflow of sequence stratigraphic analysis for any given area utilizes a systematic approach, which has been outlined by Catuneanu (2006).

First, the understanding of the tectonic setting hosting the sedimentary succession is fundamental in the early stages of sequence stratigraphic analysis (Catuneanu, 2006). Various tectonic controls and structural mechanisms directly affect stratigraphic architecture, subsidence patterns, and trends in the active depositional environments. Reconstruction of the tectonic setting requires a compilation of all available regional data, including seismic data, well-log cross-sections, large-scale outcrop relationships, and paleoecology (Catuneanu, 2006). For this study, a general understanding of the tectonic interactions responsible for the formation of the Caribbean region, and subsequently, Jamaica was gathered from all available data.

Following the reconstruction of the tectonic setting, the interpretation of depositional environments is the next step in the workflow. Vertical and lateral stratigraphic relationships between are examined to understand the spatial and temporal changes between each unit. These spatial and temporal changes in are critical to the

interpretation of sequence stratigraphic surfaces and systems tracts (Catuneanu, 2006). Outcrop analysis allows for direct assessment of the geology and the associated sequence stratigraphic boundaries. For this study, outcrop analysis was performed along the southwestern coast of St. Elizabeth parish to document the geometric relations between strata and the nature of their bounding stratigraphic surfaces.

Once the regional tectonic regime is understood and depositional environment interpretations are made, a sequence stratigraphic framework can be prepared. This framework places the significant stratigraphic surfaces and the strata they separate into a model that displays all the spatial and temporal relationships of the facies that fill the sedimentary basin (Catuneanu, 2006). The model takes into account the nature of the stratal terminations (e.g., onlap, downlap, offlap, etc.) to provide information towards the trend and type of syndepositional shoreline shift (Christie-Blick and Driscoll, 1995; Catuneanu, 2006). Sequence stratigraphic surfaces contribute to the chronostratigraphic framework of a sedimentary succession. These surfaces are based on several properties, including the nature of the contact, the nature of depositional systems, types of associated stratal terminations, and depositional trends observed above or below the surface (Catuneanu, 2006). Typically, these significant surfaces can be traced laterally. However, additional data (e.g., biostratigraphy, magnetostratigraphy, isotope geochemistry, or lithological marker beds) in structurally complex regions may be needed to constrain stratigraphic correlations (Catuneanu, 2006). At this point, all available data is incorporated to provide a viable and admissible sequence stratigraphic model.

After the available data is fully integrated, the final step for creating a sequence stratigraphic model is the identification of systems tracts. Each systems tract is

characterized by specific stratal stacking patterns or depositional trends that are bounded by significant stratigraphic surfaces. The identification of these depositional trends allows for interpretations to be made regarding base-level fluctuations as depositional environments respond in a predictive manner to such changes (Catuneanu, 2006). The predictability of these responses allows for observed lateral facies changes to be related to various stages in the evolution of a sedimentary basin (Catuneanu, 2006).

RESULTS

Regional Distribution

The coastline examined in this study is characterized by laterally discontinuous low cliff exposures, separated by modern beach deposits and tectonically raised shore platforms composed of the White Limestone Group and sedimentary units belonging to the Coastal Group. Appendix A contains representative photographs of the different bays within the study area, selected to illustrate the regional variability of exposures seen along the coastline.

Aerial drone imagery captured the entire coastline within the study area and provided a view of the more inland area that was not visited during field research excursions (Figure 18). The total amount of area covered is approximately 3.51 km^2. The resulting image (Figure 18) and generated DEM (Figure 19) were effective at showing the lateral distribution of the tectonically raised, emergent and submergent, shore platforms. Location of vertical exposures can be inferred based on the locations of rocky shorelines and sandy beaches. Typically, vertical exposures are found along the rocky shorelines that are separated by the sandy beaches. However, the drone imagery is not effective at displaying the lateral distribution of the sedimentary units in the Coastal Group.

Stratigraphic Sections

Identification of stratigraphic trends are fundamental to the interpretation of geologic successions. Following lithologic descriptions, drafted stratigraphic columns

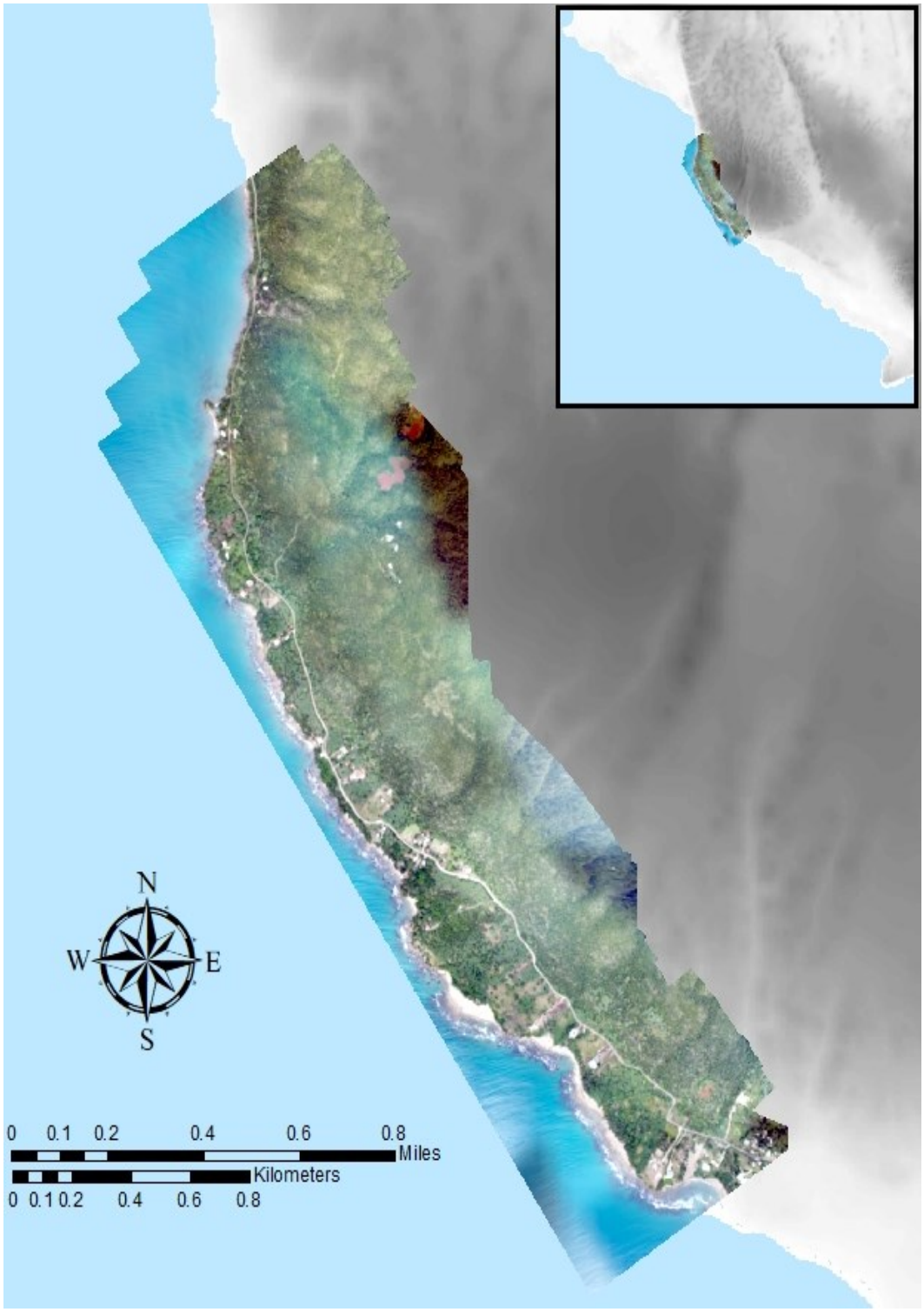

Figure 18. Orthomosaic image of the study area. Underlying 6 m DEM was provided by Mona Geoinformatics at the University of West Indies, Mona.

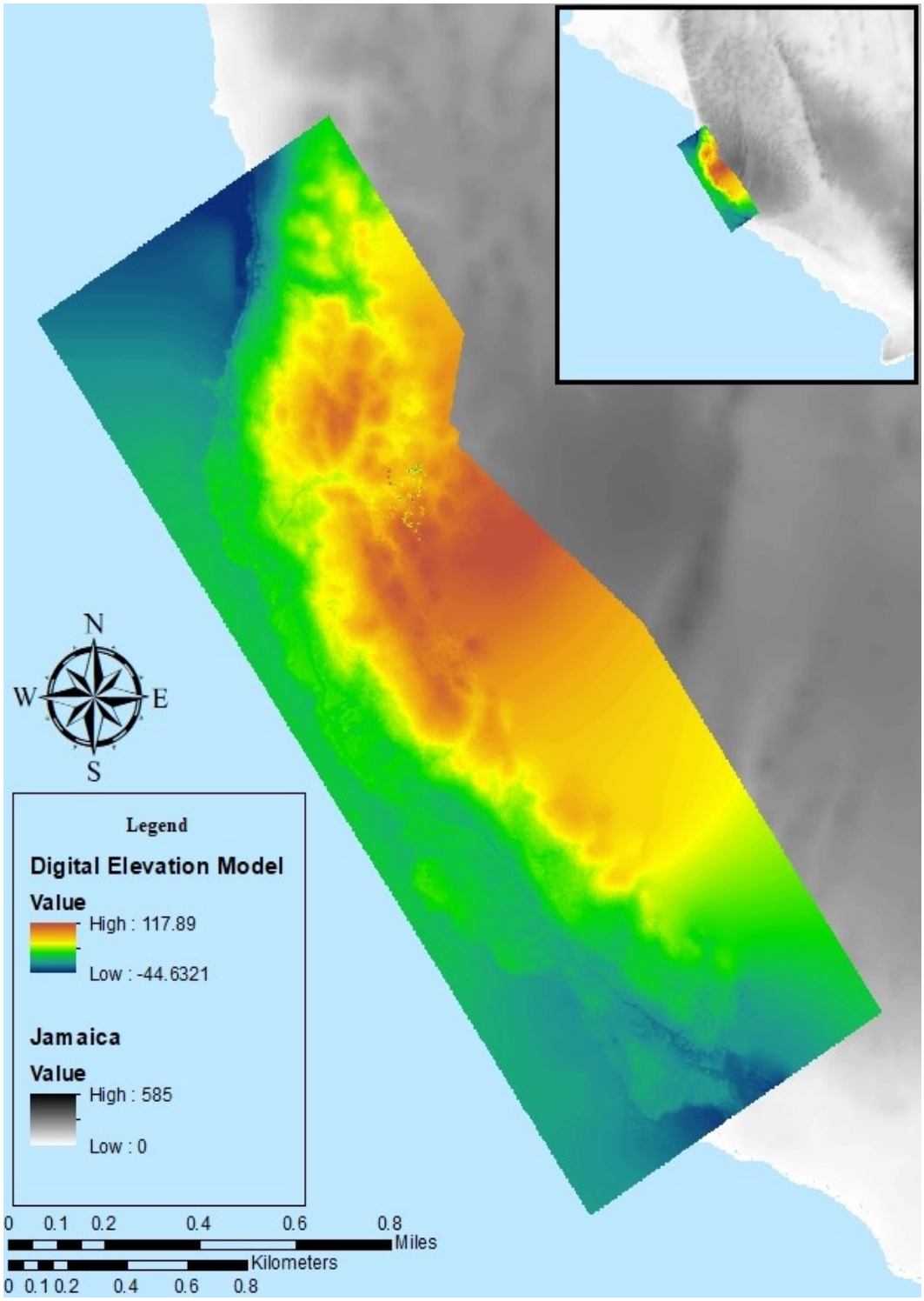

Figure 19. Generated digital elevation model of the study area. Red indicates the high elevations and blue indicates the low elevations. Values represent elevation in feet. Underlying 6 m DEM was provided by Mona Geoinformatics at University of West Indies, Mona.

provide an illustrative model to better understand potential variables controlling sedimentation as well as permit the construction of regional correlations and interpretation of ancient depositional environments. Potential controlling variables of sedimentation include sediment influx, subsidence, and accommodation.

This section provides detailed descriptions of lithologies and stacking patterns present at each of the eleven measured sections. These descriptions are intended to complement the drafted stratigraphic sections that can be found in Appendix B. Drafted stratigraphic sections are interpretive illustrations that represent the lithologies and fauna present in each unit. While these illustrations deliver the general geology present at each location, the specifics and details of each section may not be apparent. All stratigraphic sections were drafted using Inkscape, a vector graphics editor.

Overall, there were a total of six different facies described at the eleven measured sections. These include: encrusting coral bindstone, coral rudstone to framestone, very fine-grained calcareous quartz lithic arenite with seaward dipping bedding planes, burrowed coarse-grained calcareous lithic quartz arenite, a cross-bedded lithic sandstone with skeletal fragments, and overlying paleosol. In the vertical exposures, these sedimentary units have a general trend where units begin to pinch out to the southeast. The variation of measured thicknesses for the units can likely attributed to this observed trend as well as neotectonic activity.

Section BB-1. This succession is located in Billy Bay (17.902706 N, -77.795586 W) with an established datum of +1.2 meters above base level and a total measured height of 8.5 meters (Figure 20). The base of this section begins in the White Limestone Group, where it is a white to light-gray to yellow-gray skeletal wackestone.

Figure 20. Photograph of section BB-1. The unconformity between the White Limestone Group and Coastal Group is indicated. Author is pictured.

The measured thickness of the White Limestone Group at this section is 1.5 meters. The top of the White Limestone Group is marked by an unconformable hardground surface, where abundant borings in the upper surface of the White Limestone Group and encrusting corals belonging to the overlying unit (Figure 21).

Figure 21. Borings and encrusting coral observed at Section BB-1.

In addition, systematic fracture and joint sets within the White Limestone Group terminate along the unconformable hardground surface. These fractures commonly have been filled by fine-grained skeletal material containing fragments of corals, gastropods, bivalves, and other indistinguishable skeletal fragments.

Overlying the White Limestone Group, is a 7.0 meter thick coral cobble-boulder rudstone unit belonging to the Coastal Group. At the base of this unit, there are *in situ* corals found encrusting the unconformable hardground layer. Other than the encrusting corals, corals within this unit are interpreted to be out of place. Although disaggregation of the corals increases towards the top of the unit, the coral fauna present and their average size appear to remain consistent. At this section, identified corals include *Acropora cervicornis* and *Diploria* spp.

Section BB-2. This succession is located in Billy Bay (17.902222 N, -77.794998 W) with an established datum of +1.0 meters above base level and a total measured height of 7.9 meters (Figure 22). The base of this section begins in the White Limestone Group, where it is white to light-gray skeletal wackestone. At this section, the measured thickness of the White Limestone Group is 1.6 meters and is capped by the unconformable hardground surface.

Figure 22. Photograph of section BB-2 with a large boulder of the coral rudstone unit. Author is pictured.

Overlying the White Limestone Group, the coral cobble-boulder rudstone unit is observed with a measured thickness of 6.3 meters. At the base of the section, the corals are cobble-sized surrounded by a skeletal grainstone matrix. A progressive increase in coral diameter and decrease in skeletal grainstone matrix abundance occurs towards the top of the unit. In addition to an increase in size, the coral fauna transitions to being dominated by large, branching corals. A large *in situ* branch of *Acropora palmata* was identified at an approximate height of 5.0 meters (Figure 23). Along the flanks of the section, there are large boulders of float composed of the coral cobble-boulder rudstone unit that have fallen from the vertical exposure.

Figure 23. Photograph of large in situ branching coral *Acropora palmata*. Pocket knife for scale (13 cm long).

Section BB-3. This succession is located in Billy Bay (17.898724 N, -77.794998 W) with an established datum of +0.6 meters above base level and a total measured height of 7.3 meters (Figure 24). The White Limestone Group could not be identified at the base of the section due to sand cover. The base of this section begins in a coral cobble floatsone-framestone unit with a measured thickness of 2.4 meters.

Figure 24. Photograph of section BB-3. Author is pictured.

This unit includes a high abundance of corals surrounded by a minor abundance of a fine-grained skeletal grainstone matrix. Identified corals within this unit include *Diploria* spp. and possible branches of *Acropora cervicornis* that have been weathered away. This unit transitions into a 3.8 meter thick coral cobble-boulder rudstone unit surrounded by an abundant fine-grained skeletal grainstone matrix. Identified corals within this unit include *Acropora cervicornis*, *Acropora palmata*, *Diploria* spp., and *Montastrea* spp. Within this coral cobble-boulder rudstone unit, there are several lenses with an approximate thickness of 0.4 meters that are dominated by disarticulated branches of *Acropora cervicornis* (Figure 25). A coral sample (*Diploria* spp.) was taken from the top of this unit at a height of 6.2 meters for ESR analysis.

Figure 25. Photograph of *Acropora cervicornis* lens at four meters from the base of the section. Pocket knife for scale (13 cm long).

Near the top of the section there is a significant lithological transition between the coral cobble-boulder rudstone, a 0.5 meter thick skeletal grainstone, and a significantly less resistant unit without any corals. This 0.6 meter thick less resistant unit caps the vertical exposure and is composed of a calcareous quartz-rich sandstone containing cross-beds that terminate along the skeletal grainstone unit beneath (Figure 26). There are skeletal grains present within the sandstone unit. However, they are extremely small and scarce throughout.

Figure 26. Cross-bedded calcareous quartz-rich sandstone. Cross-beds dip toward the offshore direction.

Section BB-4. This succession is located in Billy Bay (17.898262 N, -77.792542 W) with an established datum of +1.5 meters above base level and a total measured height of 5.3 meters (Figure 27). The base of the section is covered by large amounts of

sand and coral debris. The units within this section display a gentle dip towards the southeast before terminating along the base of the exposure. However, these units do not provide reliable surfaces for recording strike and dip measurements.

Figure 27. Photograph of section BB-4. The top surface of a calcareous marine sandstone facies at the base of the photo dips to the right (southeast). Author is pictured.

Measuring began in a 3.4 meters thick coral cobble-boulder rudstone unit. The base and top of the unit consists of a coral cobble-boulder facies containing large, disarticulated branches of *Acropora palmata* and other assorted coral fauna, while the middle portion of the unit is an *Acropora cervicornis* rudstone (Figure 28). The *Acropora cervicornis* rudstone is more resistant than the bounding units of the coral cobble-boulder rudstone containing a much more mixed coral fauna assemblage. Both of these facies have a fine-grained skeletal grainstone matrix. A 1.5 meters thick fine-grained skeletal grainstone overlies the coral rudstone unit and a 0.4 meters thick calcareous sandstone

caps the section. There are no visible cross-beds observed in the sandstone unit at this section.

Figure 28. Photograph of coral rudstone at BB-4 with abundant *Acropora cervicornis* being weathered out. Non-resistant calcareous sandstone with coral fragments present in the middle part of the photo.

Section BB-5. This succession is located in Billy Bay (17.898040 N, -77.792542 W) with an established datum of +0.9 meters above base level and a total measured height of 9.5 m (Figure 29). The base of this section consists of a 2.0 meter thick calcareous sandstone unit containing large conch shells, cobble-sized solitary corals, and bivalve fragments. In some areas near the measured section, coral abundance gradually

increases towards the top of the unit, where it develops into a coral cobble-boulder rudstone facies.

Figure 29. Photograph of section BB-5. Note calcareous sandstone facies at base and small channel in middle left photo overlain by allochthonous coral rubble beds that slope to the right (southeast).

At the 2.0 meter mark of the section, this sandstone unit abruptly transitions into a 0.5 meters thick, thinly-bedded skeletal grainstone and a 5.0 meter thick coral cobble-boulder rudstone. However, while laterally tracing the contacts, the thinly-bedded

skeletal grainstone becomes obscured where the sandstone unit transitions into a coral cobble-boulder rudstone facies. The overlying coral cobble-boulder rudstone unit consists of a coral assemblage containing abundant, disarticulated *Acropora palmata*. At the top of the section, another 0.5 meters thick, thinly-bedded skeletal grainstone occurs and is overlain by a 1.5 meters thick, calcareous sandstone with cross-beds.

Section BB-6. This succession is located in Billy Bay (17.901154 N, -77.794121 W) with an established datum of +1.0 meters above base level and a total measured height of 6.4 meters (Figure 30).

Figure 30. Photograph of section BB-6. Note that the base of the section has been reinforced by concrete and the wooden fence at the top of the section. Author is pictured.

The White Limestone Group appears again at the base of this section as the previously described skeletal wackestone unit. However, the base of the section was strengthened with a layer of concrete to increase stability for a house that had been built on top of the vertical exposure (Figure 30). The estimated thickness of the White Limestone Group at this section is 1.0 meter. The unconformable hardground layer that is typically found at the top of the White Limestone Group was not observed, but there are systematic fractures and joint sets similar to other sections where it was found.

The overlying coral cobble-boulder rudstone unit has a thickness of 5.4 meters with abundant branches of *Acropora palmata*. This is the only section where the top of the section could not be described due to steepness as well as location adjacent to private property. It is important to note that units overlying the coral cobble-boulder rudstone could have potentially been removed during construction of the house at the top of the section.

Section BB-7. This succession is located in Billy Bay (17.907223 N, -77.797775 W) with an established datum of +1.3 meters above base level and a total measured height of 7.7 meters (Figure 31). The base of the section is within the White Limestone Group where it has a thickness of 1.8 meters and is capped by the unconformable hardground layer. At this section, the unconformable layer could be traced laterally with a 15º slope seaward before being covered by sand and water. A 5.3 meters thick coral cobble-boulder rudstone unit overlies the White Limestone Group. A coral sample, *Diploria* spp., was collected from the base of this unit for ESR analysis. Overlying the coral cobble-boulder rudstone unit is a 0.6 meters thick skeletal grainstone unit. On top of the section is an abandoned homestead, which potentially resulted in the removal of the

uppermost units. A red, fine-grained siltstone – sandstone soil horizon is found surrounding the area where the homestead was built, this is not included in the stratigraphic section.

Figure 31. Photograph of the base of section BB-7.

Section BSP-1. This succession is located at Black Spring Point (17.907447 N, -77.798240 W) with an established datum of +1.0 meters above base level and a total measured height of 7.5 meters (Figure 32). This section, as well as section BSP-2, were

measured with a stadia rod, rather than a Jacob's staff, due to the vertical nature of the exposure at Black Spring Point and the inability to climb to the top. The White Limestone Group forms the base of the measured section and has been characterized as a skeletal wackestone with a thickness of 1.5 meters. The entire unit has been heavily fractured with these fractures terminating along an unconformable surface at the top of the unit.

Figure 32. Photograph of section BSP-1.

In some areas, these fractures have been backfilled by the overlying unit consisting of coral debris (Figure 33-A). Near the base of some of these backfilled fractures, rounded limestone pebbles are found (Figure 33-B). These pebbles were only

found and described at the Black Spring Point sections and are not widely distributed at this location. This surface, similar description to other sections, is characterized by an abrupt change in lithologies, borings found on the surface, and corals from the above unit found encrusting the surface.

Overlying the White limestone Group is the coral cobble-boulder rudstone unit with a thickness of approximately 6.5 meters. This thickness was estimated using a stadia rod. The coral faunal assemblage remains consistent with descriptions at other measured sections and additional outcrop observations. At the top of the section, there appears to be a possible thinly-bedded unit. However, this unit was unable to be examined up close. Therefore, this was generalized and grouped with the coral cobble-boulder rudstone unit.

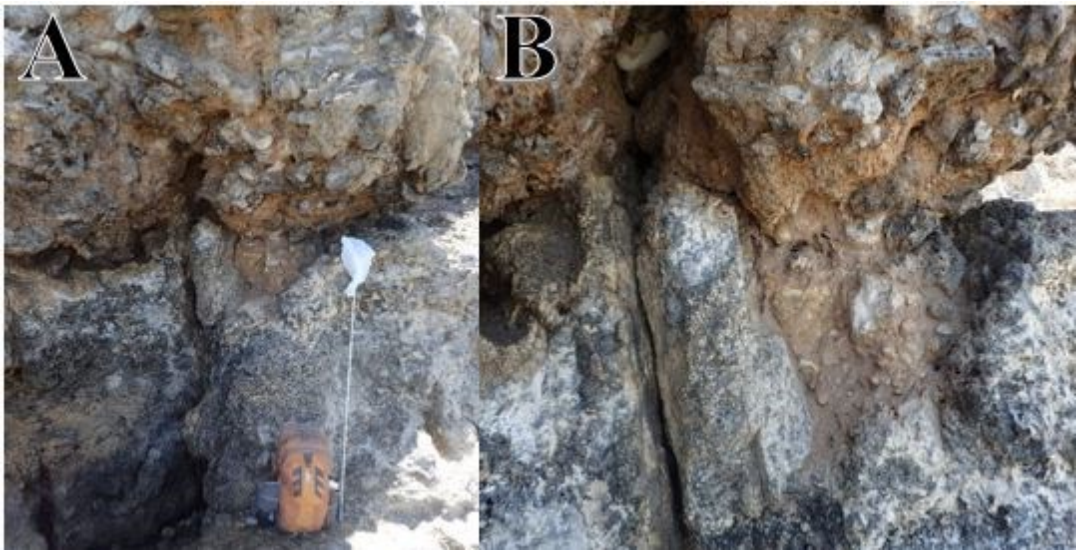

Figure 33. Photograph of fracture in White Limestone Group. A) Photograph of White Limestone Group with overlying coral cobble-boulder rudstone unit backfilling a fracture. B) Closer view at the backfilled fracture in A.

Section BSP-2. This succession is located at Black Spring Point (17.907497 N, -77.798378 W) with an established datum of +1.3 meters above base level and a total

measured height of 7.6 meters (Figure 34). This section was measured with a stadia rod instead of a Jacob's staff. A unique aspect to this section is that it was measured at the mouth of a large sea cave opening.

Figure 34. Photograph of section BSP-2.

Our guide, Captain Dennis, informed us that Black Spring Point has a freshwater spring in a sea cave near the base of the section on the north side of Black Spring Point. The spring rises from a fracture in the White Limestone Group. A small cylindrical sinkhole approximately 5.0 meters across is present approximately 10.0 meters into the cave. A second cave passage is found about 3.0 meters south of the entrance to the north cave. It has a shorter passage that terminates in the small sinkhole.

The described units present at this section resemble those at section BSP-1 closely. Although there are a few minor differences. The skeletal wackestone unit assigned to the White Limestone Group is 2.0 meters thick and exhibits similar characteristics to the other described locations. It is capped by the unconformable layer, which is very distinct here, and overlain by the coral cobble-boulder framestone to rudstone containing the typical coral faunal assemblage. Since the section was at a sea cave opening, a somewhat three-dimensional aspect could be gained. This was more apparent for the coral cobble-boulder framestone to rudstone unit. Upon walking into the sea cave, massive branching corals (possible *Acropora palmata*) appear to be in growth position. However, the coral was too high in the section and the lighting was too poor to provide an accurate identification.

Section FCB-1. This succession is located in Fort Charles Bay (17.917833 N, -77.797882 W) with an established datum +0.0 meters above base level and a total measured height of 4.1 meters (Figure 35). Measurements were taken at sea level starting from the modern beach sand. Outcrops of the White Limestone Group were not found at this location, as they were at the measured sections at Black spring point and Billy Bay. The basal unit of this section is a 3.5 meter thick cobble coral-boulder rudstone with a

skeletal grainstone matrix. The coral faunal assemblage is mixed at this location containing similar corals described at other measured sections. At the base of the unit, the corals and surrounding matrix appear to be more cemented than its equivalence at the top of the unit. In addition to decrease in diagenetic cementation, the color of the out shifts from a light gray at the base to orange-reddish brown color at the top. To the left of the measured section, there is a fractured block of float that has been extensively oxidized within the fractured areas. A red claystone unit containing minor silt and sand particles overlies the entire section and outcrop forming the soil the small grasses and plants grow within.

Figure 35. Photograph of section FCB-1.

Section FCB-2. This succession is located in Fort Charles Bay (17.918888 N, -77.798058 W) with an established datum of +0.0 meters above base level and a total measured height of 4.3 meters (Figure 36). This section is unique and consists of lithologies that have not been observed or described in any of the other measured sections. The base of the section is a 1.7 meter thick, massively bedded, fine-grained quartz lithic arenite that has been extensively burrowed.

Figure 36. Photograph of section FCB-2 with minor offset observed along a fault at the base of the Jacob's staff.

The second unit in the section consists of two different facies. The lower facies is a heavily weathered, thinly bedded (1.0 – 3.0 cm thick), quartz lithic arenite containing small skeletal fragments. This facies has extensive horizontal and vertical burrow networks that sometimes cross-cut the bedding planes. The upper facies is similar to the facies below. However, there is a lack of skeletal grain fragments and no obvious bedding planes. At this point in the section, the section needed to be offset to include the upper portion. The uppermost unit of the measured section is a 1.2 meter thick, thinly bedded (0.1 – 0.2 meter thick), friable, reddish-brown silty-sandy claystone. There a few fractures and some mineralized veins were described in hand-sample.

Gamma-Ray Profiles

Five of the measured stratigraphic sections were selected for gamma-ray profiles. Three sections are located in Billy Bay, BB-1, BB-2, and BB-3, and two are located in Fort Charles Bay, FCB-1 and FCB-2. The names of the gamma-ray profiles correspond to the associated measured stratigraphic columns. The raw gamma-ray data in CPS, along with the stratigraphic position can be found in Appendix E. The gamma-ray profiles can be found in Appendix D.

These sections display high levels of variability for exposed units, their associated thicknesses and the elevations of the top of the logged sections. These are likely a result of neotectonic area causing units to become exposed and units to become removed. Profiles were plotted in Microsoft Excel, allowing for potential trends in the gamma-ray data to be identified.

Once the gamma-ray profiles were generated, each profile was carefully examined for any potential trends within the data between each section. Each unit produced very similar ranges of data. Therefore, the gamma-ray data could not indicate the presence of a change in lithology and, consequently, no trends within the data could be reliably interpreted.

Since there were no visually identifiable and reliable trends within the profiles, the raw gamma-ray data (Appendix E) was imported into IBM SPSS statistics software to perform a discriminant function analysis. In general, discriminant analysis is a function for classifying a set of mutually exclusive categories based on numerical values. This method has been utilized as a supplementary analysis for the mud-logging industry to improve the identification of lithologies in complex and heterogeneous basins (Busch et al., 1987). Typically, discriminant analysis for lithology identification is performed in core studies, but a similar analysis can be performed on an outcrop study. For this study, each described lithology was assigned a number (1 – 8). These values were compared to the gamma-ray data. The numbers representing the described lithologies was the independent value and the gamma-ray values served as the dependent value.

The results showed that are no statistically significant trends present within the gamma-ray data, which backs up the inability to visually identify any significant trends within the gamma-ray profiles. The gamma-ray values have a low level of variance and are too close together to serve any statistical significance. Each gamma-ray value from various lithologies falling within the range of values for a rudstone would be classified as such. In an attempt to better understand the data and correct for this classification error, gamma-ray values of the rudstone were removed and the analysis was run again. While

readings were not classified as a rudstone, the statistical software classified the majority of readings as wackestone contradicting the field classifications.

Electron-Spin Resonance (ESR) Spectroscopy

Prior to ESR analysis, neutron activation analysis (NAA) was required to account for the total amount of external radiation received during exposure to cosmogonic rays (Table 3). Cosmic radiation varies with factors such as the amount of cover and the presence of water. These factors should be less significant for sample CD-1 than sample CD-2 as a result of where they were sampled from; Sample CD-1 was collected lower in the exposure than sample CD-2.

Table 3. NAA results.

Sample		[U] ppm	[Th] ppm	[K] ppm
CD1		4.89		
	±			
CD1sed		3.83	0.39	352
	±	0.02	0.03	25
CD2		2.19		
	±	0.02		
CD2sed		0.85	0.36	762
	±	0.02	0.02	30
CD3		1.73		
	±	0.02		
CD3sed		1.15	0.31	712
	±	0.02	0.02	37
CD3sed2		1.80	0.18	212
	±	0.02	0.01	16

However, the rate of cover accumulation and the depth of immersion have varied. Therefore, three different scenarios for cosmic radiation exposure were taken into account. These scenarios include: minimal to no protection from cosmic radiation, time-averaged dose between the time the sample was exposed and the time the sample was covered, which is half the total dose, and full protection from cover for almost the entire period of formation (Table 3). In past studies, calculations based on sea level and sedimentation rates tend to support the half-dose model (Deely et al., 2011).

Each of three coral samples were assumed to be aragonitic. X-ray diffraction of the coral samples were consistent with this assumption. However, the spectra were dominated by non-carbonate signals, predominantly manganese and, in some cases, iron, which suggests that the aragonite may have been diagenetically altered to carbonate. If there is any kind of secondary mineralization, then any ESR date for the sample can only be a minimum age at best. Although there are indicators for secondary mineralization, the growth curves were adequate, if not statistically excellent. In addition to the coral samples, the skeletal grainstone matrix was analyzed to serve as the sediment cover and source of an external radiation dose. The analysis of the matrix surrounding the corals is the largest source of uncertainty as the contribution of the fine grains within the skeletal grainstone to the external radiation dose cannot be calculated. However, the coral cobble-boulder rudstone unit from which the corals were collected from are clearly dominated by individual corals. Therefore, the dose rate calculated from the corals should result in a reasonable age as a first approximation.

Each of three coral samples collected for ESR analysis yielded varying age ranges (Table 4). Sample CD-1 produced ages of 70.9 ± 4.0 kyr in a setting with minimal cosmic

radiation protection, 60.5 ±3.5 kyr in a setting receiving half the total cosmic radiation dose, and 65.3 ±3.6 for a setting with complete protection from cosmic radiation. Sample CD-2 produced ages of 137.9 ± 8.9 kyr, 120.1 ± 7.9 kyr, and 106.1 ± 7.1 kyr. Sample CD-3 was collected from an out of place block and produced the youngest range of ages, 47.3 ± 3.5 kyr, 38.3 ± 2.9 kyr, and 32.0 ± 2.4 kyr. While the ages produced by sample CD-2 fell within the expected range, a range of dates from a single sample in hypothesized settings can be considered completely accurate and reliable by itself.

Table 4. ESR dating results for corals from the Coastal Group, southwestern Jamaica.

Sample	Accumulated dose, A_Σ (Grays)	Internal dose rate, $D_{int}(t)$ (mGrays/y)	External dose rate, $D_{ext}(t)$ (mGrays/y)	Age t (kyr)
CD-1	101.0 ± 3.9	511 ± 30	0	70.9 ± 4.0
	101.0 ± 3.9	511 ± 30	150 ± 25	60.5 ±3.5
	101.0 ± 3.9	511 ± 30	300 ± 50	65.3 ±3.6
CD-2	113.3 ± 5.7	285 ± 17	0	137.9 ± 8.9
	113.3 ± 5.7	285 ± 17	150 ± 25	120.1 ± 7.9
	113.3 ± 5.7	285 ± 17	300 ± 50	106.1 ± 7.1
CD-3	26.2 ± 1.6	276 ± 17	0	47.3 ± 3.5
	26.2 ± 1.6	276 ± 17	150 ± 25	38.3 ± 2.9
	26.2 ± 1.6	276 ± 17	300 ± 50	32.0 ± 2.4

DISCUSSION

Record of Sea-Level Change

Overall, the sedimentary units described in this study provide an extensive record of sea-level fluctuations in southwestern Jamaica. Coastal Group outcrops in southwestern St. Elizabeth Parish exhibit a dynamic mixed siliciclastic – carbonate depositional system that shifts to a non-marine eolian-based depositional environment (Figure 37) and consists of two distinctive sequence boundaries.

The depositional environments and sequence boundaries, in order of interpreted occurrence, include: transitional phase between deep-water to shallow-water marine environment, the first sequence boundary represented by a disconformable hardground surface, a coral reef depositional environment and associated lagoonal environment, a progradational lagoonal environment deposited on top of the coral reef, a fossil beach environment, the second sequence boundary marked by a significant increase in siliciclastic input and abrupt decrease in coral fauna abundance, an expansive coastal dune field, and a recent paleosol. The significant influx of siliciclastic material covering the stranded coral reef suggests a rapid marine regression for this region.

The skeletal wackestone facies, assigned to the White Limestone Group, forms the base of several of the eleven described sections and the majority of the coastline in the study area. This facies was likely deposited during a transitional period of deposition from a deep marine to shallow marine environment. A disconformable hardground surface marks the contact between the White Limestone Group and the overlying coral rudstone facies, which has been assigned to the Coastal Group. This hardground surface

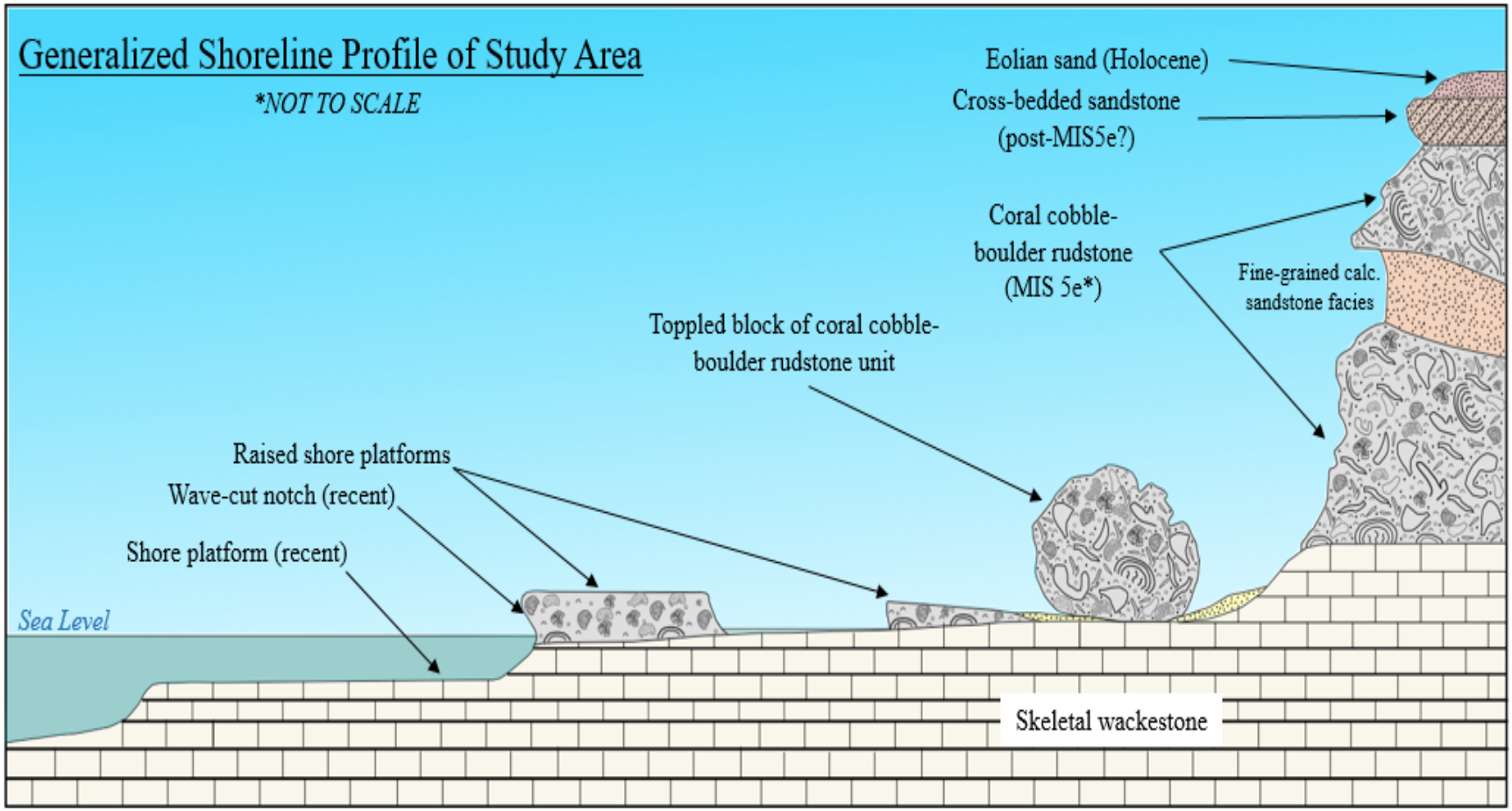

Figure 37. Generalized shoreline profile showing described sedimentary units and various features.

is indicated by borings and encrusting organisms (e.g., corals). Joint sets are found truncated at this surface and filled with overlying sediment indicating erosion and subsequent burial. In some areas (e.g., Black Spring Point), these fractures are filled with rounded pebbles of the White Limestone Group suggesting some level of transport prior to deposition. These joints commonly show indications of iron oxidation with changes in color of the weathered surface as a result of subaerial exposure. Lateral identification of this surface and associated indicators provides further evidence suggesting a regional sea-level fall.

At most locations along the coast, a coral rudstone facies, which has been assigned to the Coastal Group, overlies the White Limestone Group. This unit indicates a regional rise in sea-level that allowed for extensive coral reefs to become established. In addition to abundant coral fauna, there is a minor siliclastic component at the base and middle sections of this unit that was likely introduced through predominantly eolian sedimentation. At section BB-5, the White Limestone Group was overlain by a fine-grained, calcareous sandstone unit containing abundant conch shells and solitary corals. In some areas, this facies slowly transitioned into the coral rudstone facies that is typically overlying the White Limestone Group. The appearance of this sandstone facies is likely a lagoonal facies located near or at the base of the reef slope and could have a similar depositional age as the coral rudstone facies.

Corals present in this fossil reef assemblage include *Acropora* spp., *Diploria* spp., *Montastraea* spp., and other minor coral species. The dominant coral genera present in the assemblage are *Acropora*, which include the species *A. palmata* and *A. cervicornis*, and *Diploria*, which include the species *Diploria strigosa* and *Diploria labrinthiformis*.

These genera are the typical reef-building corals and provide indicators for sea-level based on their distribution modern marine environments. *Acropora* spp., some of the major reef corals, are most common in shallow reef environments ranging from 1.0 to 5.0 meters deep with an abundance of light and water circulation (Goreau, 1959). *A. palmata* is typically found at water depths up to 10 meters in the reef crest to seaward slope regions of the coral reef, whereas *A. cervicornis* is typically found on the seaward slope in water depths up to 15 meters (Goreau, 1959). *Diploria* spp., also known as brain corals, occurs in reef environments as well as muddy seafloors where many other coral species cannot survive. These muddy seafloor environments can exist in both the back reef and fore reef regions of the coral reef ranging up to a depth of 30 meters (Goreau, 1959). Fossil remains of *Diploria strigosa* have been found together with massive, boulder corals, such as *Siderastrea siderea* and *Solenastrea bouroni*, in Coastal Group units (Goreau, 1959; Mitchell et al., 2000).

While the distribution of genera and species serve as useful indicators for past sea-levels, they can only provide an approximation as each coral species can survive within a range of water depths. Corals within the Coastal Group units in southwestern Jamaica have largely been reworked resulting in the redistribution of corals with minimal amounts corals interpreted to be in growth position. Coral debris of the described coral rudstone facies can possibly be attributed to waves during storm events that redistributed the coral assemblage closer to the shore. The coral reef likely became unconsolidated as a result of the environment transitioning to less favorable conditions where corals were not able to produce skeletons at a fast enough rate to withstand erosional forces. Possible

factors affecting reef development may include changes in temperature, light availability, nutrient availability, sediment influx, water depth, and lack of water circulation.

The upper portion of the exposures exhibits a shift from a mixed siliciclastic-carbonate marine depositional environment to a non-marine eolian depositional environment. An increase in siliciclastic input is seen near the top of the coral rudstone facies. This coincides with an abrupt reduction in coral abundance. In Fort Charles Bay, a burrowed carbonate sand facies was seen overlying the coral rudstone facies. Based on the proximity to the coral rudstone facies and basinward dipping stratal geometry, this facies can be assigned to a fore-reef depositional setting.

Found overlying the coral rudstone unit in other exposures, a yellow to light brown to red colored, thinly-bedded lithic quartz arenite with patchy coral growth is likely the result of shallow marine environment and little to no water circulation. This unit has been interpreted as a shallow back-reef lagoonal facies. This unit is closely related to the overlying cross-bedded sandstone facies. These two units are similar in their color and composition, red oxidation and high quartz content. However, the cross-bedded sandstone facies contains a significant amount of skeletal carbonate fragments. This facies has a strong resemblance to the previously described “old eolianite” unit by Hendry and Head (1985) and likely formed during a period of sea-level fall.

In northwestern Great Pedro Bay, a light brown to brown, fine-grained lithic quartz arenite with a gentle seaward slope overlies the coral rudstone facies and underlies the cross-bedded sandstone facies with no signs of iron oxidation. This unit has been interpreted as a beach and is likely part of the same or similar regressive sequence as the lagoonal facies.

The overlying cross-bedded sandstone facies likely represents a coastal dune field deposited during a significant regional sea-level fall. The general trend of the cross-beds suggests that the winds likely came the southeast, the direction of Great Pedro Bluff, and were sourced by the underlying beach facies. Similar trends of the cross-beds are seen at various areas of the exposures between Great Pedro Bay and Fort Charles Bay suggests that there was significant dune migration. Proxy data for large-scale dune migration are established modern dune fields near the modern shoreline at eastern side of Great Pedro Bluff, Great Pedro Bay, Frenchman's Bay, and the northwestern region of Fort Charles Bay. Additionally, there are cross-cutting joints that are truncated on the base of the cross-beds and have been filled in by the "old eolianite" facies. This suggests that area experienced tectonic activity prior to the lithification of the eolian dune facies.

A thinly bedded, friable, reddish-brown, silty-sandy claystone caps the entire succession and can be considered a relatively modern deposit. Similar deposits can be seen near buildings, roads, drainage ditches, etc. This unit likely extends further inland from the top of the coastal cliff exposures to the hills made up of the White Limestone Group. This has been interpreted as a recent paleosol deposit.

Stratigraphic Trends of Gamma-Ray Values

Significant stratigraphic trends in the gamma-ray data were unable to be identified through visual correlation attempts as well as statistical analysis. While the described units show great changes in lithology, the gamma-ray values did not display enough variance to be considered statistically significant. Although trend identification of the

gamma-ray profiles was a failed attempt for this study, the results are interesting and could be improved through more data collection.

Ages from ESR Analysis

Samples CD-1 and CD-2, the two samples collected from *in situ* position within the vertical exposures, were not collected from the same measured stratigraphic section. Although the applied radiation doses to each sample are similar, both the internal and external dose rates are significantly different. These differences likely resulted in the diverse range of ages between the two samples. In order to refine this, additional samples of the matrix surrounding the corals would need to be collected and analyzed.

Based on the spectral analysis, the coral samples likely underwent diagenetic alteration to some degree. Consequently, any age obtained using a compositionally mixed sample can only provide a minimum age at best for each of the various settings relative to the degree of exposure to cosmic radiation. Therefore, CD-1 must be greater than 70.9 ± 4.0 kyr for no cover, greater than 60.5 ± 3.5 kyr for half cover, and greater than 65.3 ± 3.6 kyr for full cover. Sample CD-2 must be greater than 137.9 ± 8.9 kyr for no cover, greater than 120.1 ± 7.9 kyr for half cover, and greater than 106.1 ± 7.1 kyr. Sample CD-3 produced a much younger age range than the other two samples. This supports the suggestion that the aragonite has been diagenetically altered to carbonate minerals.

Based on previous studies (Table 5), the estimated age range for these corals was between 120 and 140 ka. The Falmouth Formation and Port Morant Formation are have been described as being penecontemporaneous with the Marine Isotope Stage 5e, the last interglacial period (Mitchell et al., 2000). The range of dates obtained from sample CD-2

fall within the hypothesized range. This range is in agreement with the range of ages documented in previous studies on corals from similar stratigraphic successions in Jamaica suggesting that the succession in southwestern Jamaica was deposited during MIS 5e. However, more dates are required to confirm this result.

Table 5. Published dates for Falmouth and Port Morant Formations reef material (from Skrivanek et al., 2017).

Sample Description	Age (ka)	Method	Source
EAST RIO BUENO Falmouth Formation corals (*Acropora*, *Orbicella sp.*, *Siderastrea*, *Colpophyllia*: one sample collected at +1 m (125 ka), one from a cave 300 m inland at +5m	140 – 117	Alpa-counting U-series techniques	Moore and Somayajulu, 1974 Also, Moore, 1969 (personal communication, *in* Land and Epstein, 1970)
Falmouth Formation corals from an upper and a lower unit, separated by a zone of heavy algal encrustation	Lower unit: 134 – 127 Upper unit: 124 - 199	U-series dating of pristine coral	Precht, 1993
NORTH COAST Shelly material and coral from lowest terrace between Discovery Bay and East Rio Bueno	ca. 120	Radiometric dating	R.V. Cant (personal communication *in* Horsfield, 1972)
ORACABESSA Aragonitic corals of the lowest terrace, occurring as high as 17 m (Horsfield, 1975)	ca. 120	U-Th dating (unspecified)	Cant, 1972
PORT MORANT Port Morant Formation corals (*Solenatrea bournoi and Solenastrea radians*) from the upper part of the unit	132 - 125	ESR dating techniques	Mitchell et al., 2000

Implications for Future Climate Change

Widespread variability, both locally and longshore, is expressed within the sedimentary units within the Coastal Group in southwest Jamaica, leading to complications in correlation between the eleven stratigraphic sections. Complications arise due to the representation of sedimentary units within each section as well as variations in unit thicknesses. These exposures have been subjected to extensive weathering that may have resulted in the removal of units within the succession. At some of the measured sections, the uppermost units may have been disturbed or completely removed during the building phases of some of the resorts and other structures along the coastline (e.g., section BB-7, section BB-6).

Additionally, the southwestern coast of Jamaica has been disturbed by neotectonic forces. Evidence for neotectonic movement has been documented in a series of raised shore platforms northwest of Billy's Bay that are approximately 0.5 – 1.2 meters above sea level indicating uplift along the Pond Side Fault (Evans et al., 2018). The upper surfaces of these raised platforms are encrusted with serpulid worms, which were sampled and yielded a ^{14}C age date of 1184-948 cal BP (95.4% CI) suggesting recent tectonic movement along the southwestern coast of Jamaica. Therefore, these vertical exposures cannot be used as a standard for determining relative mean sea level (RMSL).

The disconformity between the White Limestone Group and Coastal Group represents a period of subaerial exposure and provides a correlative surface for interpreting regional sea-level fluctuations. The measured sections where this disconformity is observed include section BB-1, section BB-2, section BB-6, section BSP-1, and section BSP-2. At section BB-1, the White Limestone Group is observed at

the base of the section and is capped by a disconformity at approximately +2.7 meters asl, which is overlain by a 7.0 meters thick coral rudstone unit. At section BB-2, the White Limestone Group is observed at the base of the section, capped by a disconformity at approximately +2.6 meters asl, and is overlain by a 6.3 meters thick coral rudstone unit. At section BB-6, the White Limestone Group is observed at the base, capped by a disconformity at approximately +2.0 meters asl, and is overlain by a 5.4 meters thick coral rudstone unit. At sections BSP-1 and BSP-2, the White Limestone creates the base of the sections and is capped by a disconformity at approximately +3.5 – 3.8 meters asl, and is overlain by a 7.0 meters thick coral rudstone unit. The thickness of the coral rudstone units at sections BB-6, BSP-1, and BSP-2 are may not reflect the total thickness as measurements were unable to be taken from the tops of these sections. Overall, these five sections suggest a period of sea-level stability, followed by a minor sea-level fall, then a rapid sea-level rise. The disconformity representing a minor sea-level fall does display a topographic relief, which may factor in to why it is not represented at each measured section. In other sections along southern coast of St. Elizabeth Parish, these units are overlain by beach and eolian deposits signifying an abrupt sea-level fall.

The southwest coast of Jamaica likely had sea-levels rise within the range of +2 – 4 meters above modern sea level and +6 – 9 meters above modern sea level during deposition of coral rudstone unit belonging to the Coastal Group. The extent of sea-level fall separating these two separate highstands is unknown. These estimated regional sea-level fluctuations for these highstands are in agreement with the composite sea-level models for the MIS 5e (Hearty et al., 2007).

CONCLUSIONS

This study presents the first detailed measured and described stratigraphic sections for Coastal Group exposures in southwestern Jamaica. By documenting the Coastal Group outcrops in southwestern Jamaica, we are able to record and preserve the spatial distribution as well as the variability of thickness, geometry and depositional facies for the sedimentary units before they are no longer available as they are rapidly weathering away.

The vertical exposures in southern St. Elizabeth Parish indicate changes in sedimentation patterns that reflect regional sea-level fluctuations and stratal geometries indicating the overall platform and coastal evolution during a period of rapid sea-level change. However, this region is tectonically active with highly variable sedimentation rates and cannot be used for a reliable model for these developments. Further work needs to be done to survey geographical landmarks relative to modern sea-level in order to potentially calculate for the regional uplift rate.

This study also reports approximate age dates from three fossil coral samples that allow us to tentatively assign the coral reef facies to the MIS 5e (~ 130±2 - 119±2 ka). Sample CD-1 yielded ages of 70.9 ± 4.0, 60.5 ±3.5, and 65.3 ±3.6. Sample CD-2 yielded ages of 137.9 ± 8.9, 120.1 ± 7.9, and 106.1 ± 7.1. Sample CD-2 yielded ages of 47.3 ± 3.5, 38.3 ± 2.9, and 32.0 ± 2.4. Although samples were carefully examined, the degree of diagenetic alteration and exposure to cosmic radiation remain unknown. Therefore, these ages are can only be considered as a minimum. Sample CD-2 is believed to have the least amount of diagenetic alteration and suggests an age of at least 100 ka. Assignment to the

MIS 5e is in agreement with age dates from similar sedimentary units (e.g., Falmouth Formation and Port Morant Formation) from previous studies in other areas of Jamaica. However, more age dates are required to confirm this.

While these exposures cannot serve as a proxy for correlation of MIS 5e strata due tectonism, potential exhumation of sedimentary units and siliciclastic influxes, they provide an example of the potential magnitude for accelerated sea-level rise with current trends in climate change. The MIS 5e interval experienced rapid sea-level fluctuations that peaked at about +6 - +9 meters above modern sea level. Based on measurements from the vertical exposures in this study, the southwestern coast of Jamaica likely experienced similar magnitudes of sea-level change to previously documented sea-level fluctuations at MIS 5e sites.

REFERENCES CITED

Aharon, P., Chappell, J., Compston, W., 1980. Stable isotope and sea level data from New Guinea supports Antarctic ice-surge theory of ice ages: Nature, v. 283, p. 649–651.

Bachmann, R., 2001, The Caribbean Plate and the question of its formation: http://citeseerx.ist.psu.edu/viewdoc/download?doi=10.1.1.693.9074&rep=rep1&type=pdf (accessed November 2017).

Bard, E., Jouannic, C., Hamelin, B., Pirazzoli, P., Arnold, M., Faure, G., Sumosusastro, P., and Syaefudin, 1996, Pleistocene sea levels and tectonic uplift based on dating of corals from Sumba Island, Indonesia: Geophysical Research Letters, v. 23, no. 12, p. 1473-1376.

Benford, B., Tikoff, B., and DeMets, C., 2014, Interaction of reactivated faults within a restraining bend: Neotectonic deformation of southwest Jamaica: Lithosphere, v. 7(1), p. 21-39.

Benford, B., DeMets, C., Tikoff, B., Williams, P., Brown, L., and Wiggins-Grandison, M., 2012, Seismic hazard along the southern boundary of the Gônave microplate: block modeling of GPS velocities from Jamaica and nearby islands, northern Caribbean: Geophysical Journal International, v. 190, no. 1, p. 59-74, doi: 10.1111/j.1365-246X.2012.05493.x.

Blois, J.L., Zarnetske, P.L., Fitzpatrick, M.C., and Finnegan, S., 2013, Climate change and the past, present and future of biotic interactions: Science, v. 341, p. 499-504.

Brown, I. and Mitchell, S.F., 2010, Lithostratigraphy of the Cretaceous sucession in the Benbow Inlier, Jamaica: Caribbean Journal of Earth Science, v. 41, p. 25-37.

Busch, J.M., Fortney, W.G., and Berry, L.N., 1987, Determination of lithology from well logs by statistical analysis: Society of Petroleum Engineers, vol. 2, no. 4, p. 412-418, doi: 10.2118/14301-PA.

Camoin, G.F., and Webster, J.M., 2015, Coral reef response to Quaternary sea-level and environmental changes: State of the science: Sedimentology, v. 62, p. 401-428, doi: 10.1111/sed.12184.

Cant, R.V., 1972, Jamaica's Pleistocene reef terraces: Journal of the Geological Society of Jamaica, v. 12, p. 13–17.

Catuneanu, O., 2006, Principles of Sequence Stratigraphy: Elsevier, p. 279-291.

Catuneanu, O. Abreu, V., Bhattacharya, J.P., Blum, M.D., Dalrymple, R.W., Eriksson, P.G., Fielding, C.R., Fisher, W.L., Galloway, W.E., Gibling, M.R., Giles, K.A., Holbrook, J.M., Jordan, R., St.C. Kendall, C.G., Macurda, B., Martinsen, O.J., Miall, A.D., Neal, J.E., Nummedal, D., Pomar, L., Posamentier, H.W., Pratt, B.R., Sarg, J.F., Shanley, K.W.m Steel, R.J., Strasser, A., Tucker, M.E., and Winker,

C., 2009, Towards the standardization of Sequence Stratigraphy: Earth-Science Reviews, v. 92, no. 1-2, p. 1-33, doi: 10.1016/j.earscirev.2008.10.003.

Christie-Blick, N., and Driscoll, N.W., 1995, Sequence Stratigraphy: Annual Reviews Earth Planet Science, v. 23, p. 451-478.

Collins, J.S.H., Donovan, S.K., and Stemann, T.A., 2009, Fossil crustacea of the late Pleistocene Port Morant Formation, west Port Morant Harbour, southeastern Jamaica: Scripta Geologica, v. 138, no. 7, p. 23-53.

D'Agostini, D.P., Bastos, A.C., and Dos Reis, A.T., 2015, The modern mixed carbonate-siliciclastic Abrolhos Shelf: Implications for a mixed depositional model: Journal of Sedimentary Research, v. 85, p. 124-139, doi: http://dx.doi.org/10.2110/jsr.2015.08.

Deely, A.E., Blackwell, B.A.B., Mylroie, J.E., Carew, J.L., Blickstein, J.I.B., and Skinner, A.R., 2011, Testing cosmic dose rate model for ESR: Dating corals and molluscs on San Salvador, Bahamas: Radiation Measurements, v. 46, no. 9, p. 853-859, doi: 10.1016/j.radmeas.2011.02.008.

Donovan, S.K., 2003, A karst of thousands: Jamaica's limestone scenery: Geology Today, v. 18, no. 4, p. 143-151, doi: 10.1046/j.0266-6979.2003.00356.x.

Donovan, S.K., Pickerill, R.K., and Keighley, D.G., 2014, The upper Pliocene Bowden shell beds, southeast Jamaica: Geology Today, v. 30, no. 6, p. 232-238, doi: 10.1111/gto.12079.

Donovan, S.K., Portell, R.W., and Stemann, T.A., 2004, Macropaleontology of the Hopegate Formation, Jamaica, An Upper Pliocene raised reef: Geological Society of America *Abstracts with Programs*, v. 36, no. 2, p. 110.

Dorsey, R.J. and Kidwell, S.M., 1999, Mixed carbonate-siliciclastic sedimentation on a tectonically active margin: Example from the Pliocene of Baja California Sur, Mexico: Geology, v. 27, no. 10, p. 935-938.

Dunbar, G.B. and Dickens, G.R., 2003, Late Quaternary shedding of shallow-marine carbonate along a tropical mixed siliciclastic-carbonate shelf: Great Barrier Reef, Australia: Sedimentology, v. 50, p. 1061-1077, doi: 10.1046/j.1365-3091.2003.00593.x.

Dunham, R.J., 1962, Classification of carbonate rocks according to depositional texture: American Association of Petroleum Geologists Memoirs, v. 1, p. 108-121.

Dutton, A. and Lambeck, K., 2012, Ice volume and sea level during the last interglacial: Science, v. 337, p. 216-219, doi: 10.1126/science.1205749.

Dutton, A., Carlson, A.E., Long, A.J., Milne, G.A., Clark, P.U., CeConto, R., Horton, B.P., Rahmstory, S., and Raymo, M.E., 2015, Sea-level rise due to polar ice-sheet mass loss during past warm periods: Science, vol. 349, 11 p., doi: 10.1126/science.aaa4019.

Dutton, A., Webster, J.M., Zwartz, D., Lambeck, K., and Wohlfarth, B., 2015, Tropical tales of polar ice: evidence of last interglacial polar ice sheet retreat recorded by fossil reefs of the granitic Seychelles islands: Quaternary Science Reviews, v. 107, p. 182-196, doi: https://doi.org/10.1016/j.quascierev.2014.10.025.

Embry, A.F., and Klovan, J.E., 1972, A late Devonian reef tract on northeastern Banks Island, N.W.T.: Bulletin of Canadian Petroleum Geology, v. 19, no. 4, p. 730-781.

Emiliani, C., 1955, Pleistocene temperatures: The Journal of Geology, v. 63, no. 6, p. 538-576.

Evans, K.R., Dogwiler, T., Faulkner, D.J., Jacobs, P.M., Kenning, B., Lecce, S.A., and Pavlowsky, R.T., 2018, Late Holocene raised shore platforms in southwestern Jamaica: Geological Society of America Abstracts with Programs, v. 50, no. 4, doi: 10.1130/abs/2018NC-312468.

Feng, F. and Bailer-Jones, C. A. L., 2015, Obliquity and precession as pacemakers of Pleistocene deglaciations: Quaternary Science Reviews, 19 p.

Fisher, J.D. and Mitchell, S.F., 2012, Lithostratigraphy of the Grange Inlier, Westmoreland, Jamaica: Caribbean Journal of Earth Science, v. 44, p. 19-24.

Francis, J.M., Daniell, J.J., Droxler, A.W., Dickens, G.R., Bentley, S.J., Peterson, L.C., Opdyke, B.N., and Beaufort, L., 2008, Deep water geomorphology of the mixed siliciclastic-carbonate system, Gulf of Papua: Journal of Geophysical research, v. 113, F01S16, 22 p., doi: 10.1029/2007JF000851.

Fruijtier, C., Elliott, T., and Schlager, W., 2000, Mass-spectrometric ^{234}U-^{230Th} ages from the Key Largo Formation, Florida Keys, United States: Constraints on diagenetic age disturbance: GSA Bulletin, v. 112, no. 2, p. 267-277.

Goelzer, H., Huybrechts, P., Loutre, M.F., and fichefetm T., 2016, Last interglacial climate and sea-level evolution from a coupled ice sheet-climate model: Climate of the past, v. 12, p. 2195-2213, doi: 10.5194/cp-12-2195-2016.

Goreau, T.F., 1959, The ecology of Jamaican coral reefs 1. Species composition and zonation: Ecology, v. 40, no. 1, p. 67-90, doi: 10.2307/1929924.

Grün, R., 1997, Electron Spin Resonance Dating, *in* Taylor, R.E., Aitken, M.J., eds, Chronometric Dating in Archaeology: Advances in Archaeological and Museum Science, Volume 2: Boston, MA, Springer, p. 217-260.

Gunter, G.C. and Mitchell, S.F., 2005, The lithostratigraphy of the Maldon Inlier, parish of St. James, northwestern Jamaica: Caribbean Journal of Earth Science: v. 38, p. 1-10.

Hantoro, W.S., Pirazzoli, P.A., Jouannic, C., Faure, H., Hoang, C.T., Radtke, U., cause, C., Best, M.B., Lafont, R., Bieda, S., and Lambeck, K., 1994, Quaternary uplifted coral reef terraces on Alor Island, East Indonesia, Coral Reefs, v. 13, p. 213-215.

Hansen, J., Sato, M., Hearty, P., Ruedy, R., Kelley, M., Masson-Delmotte, V., Russell, G., Tseloudis, G., Cao, J., Rignot, E., Velicogna, I., Kandiano, E., von

Schuckmann, K., Kharecha, P., Legrande, A.N., Bauer, M., and Lo, K.W., 2015, Ice melt, sea level rise and superstorms: evidence from paleoclimate data, climate modeling, and modern observations that 2ºC global warming is highly dangerous: Atomospheric Chemistry and Physics Discussions, v. 15, p. 20059-20179, doi: 10.5194/acpd-15-20059-2015.

Harper, B.B., Puga-Bernabéu, A., droxler, A.W., Webster, J.M., Gischler, E., Tiwari, M., Lado-Insua, T., Thomas, A.L., Morgan, S., Jovane, L., and Rõhl, U., 2015, Mixed carbonate-siliciclastic sedimentation along the Great Barrier Reef upper slope: A Challenge to the reciprocal sedimentation model, Journal of Sedimentary research, v. 85, p. 1019-1036, doi: http://dx.doi.org/10.2110/jsr.2015.58.1.

Hays, J.D., Imbrie, J., and Shackleton, N.J., 1976, Variations in the Earth's orbit: Pacemaker of the Ice Ages: Science, v. 194, no. 4270, p. 1121-1132

Hearty, P.J., 2002, Revision of the late Pleistocene stratigraphy of Bermuda: Sedimentary Geology, v. 153, p. 1-21.

Hearty, P.J., 2003, Stratigraphy and timing of eolianite deposition on Rottnest Island, Western Austrailia: Quaternary research, v. 60, p. 211-222, doi: 10.1016/S0033-5894(03)00063-2.

Hearty, P.J. and Kaufmann, D.S., 2000, Whole-rock aminostratigraphy and Quaternary sea-level history of the Bahamas: Quaternary Research, v. 54, p. 163-173, doi:10.1006/qres.2000.2164

Hearty, P.J., and Neumann, A.C., 2001, Rapid sea level and climate change at the close of the last interglaciation (MIS 5e): evidence from the Bahama Islands: Quaternary Science Reviews, v. 20, p. 1881-1895.

Hearty, P.J. and Tormey, B.R., 2017, Sea-level change and superstorms; geologic evidence from the last interglacial (MIS 5e) in the Bahamas and Bermuda offers ominous prospects for a warming Earth, v. 390, p. 347-365, doi: 10.1016/j.margeo.2017.05.009.

Hearty, P.J., Kaufman, D.S., Olson, S.L., and James, H.F., 2000, Stratigraphy and whole-rock amino acid geochronology of key Holocene and last interglacial carbonate deposits in the Hawaiian Islands: Pacific Science, v. 54, no. 4, p. 423-442.

Hearty, P.J., Hollin, J.T., Neumann, A.C., O'Leary, T.J., and McCulloch, M., 2007, Global sea-level fluctuations during the last interglaciation (MIS 5e): Quaternary Science Reviews, v. 26, p. 2090-2112. doi:10.1016/j.quascirev.2007.06.019

Hendry, M.D., and Head, S.M., 1985, Late Quaternary sea-level changes and the development of the raised/dune sequence at Great Pedro Bluff, south-west Jamaica, Proceedings of The Fifth International Coral Reef Congress: Tahiti, v. 6, p. 119-124.

Horsfield, W.T., 1972, A late Pleistocene sea level notch, and its relation to block faulting on the north coast of Jamaica: Journal of the Geological Society of Jamaica, v. 12, no. 6, p. 18–22, doi: 0.1080/00049188308702841.

Imran, A.M., Farida, M., Arifin, M.F., Husain, R., and Hafidz, A., 2016, Reef development as an indicatior of sea level fluctuation: A preliminary study on Pleistocene reef in Bulukumba, South Sulawesi: Indonesian Journal on Geosciences, v. 3, no. 1, p. 53-66, doi: 10.17014/ijog.3.1.53-66.

Intergovernmental Panel on Climate Change, 2013, Climate Change 2013: The physical science basis: Contribution of working Group I to the Fifth Assessment Report of the Intergovernmental Panel on Climate Change: Cambridge University Press, Cambridge, United Kingdom and New York, USA, 1535 p.

Irvali, N., Ninnemann, U.S., Galaasen, E.V., Rosenthal, Y., Kroon, D., Oppo, D.W., Kleiven, H.F., Darling, K.F., and Kissel, C., 2012, Rapid switches in subpolar North Atlantic hydrography and climate during the last interglacial (MIS 5e): Paleoceanography and Paleoclimatology, v. 27, 16 pp., doi: 10.1029/2011PA002244.

Israelson, C. and Wohlfarth, B., 1999, Timing of the last-interglacial high sea level on the Seychelles Islands, Indian Ocean: Quaternary Research, v. 51, p. 306-316.

Jamaica Information Service, 2017, St. Elizabeth heritage sites: http://jis.gov.jm/information/jamaica-heritage-sites/st-elizabeth-heritage-sites/ (Accessed March 2017).

James, K.H., 2005, A simple synthesis of Caribbean geology: Caribbean Journal of Earth Science, v. 39, p. 69-82.

James-Williamson, S.A., Mitchell, S.F., and Ramsook, R., 2014, Tectono-stratigraphic development of the Coastal Group of south-eastern Jamaica: Journal of South American Earth Sciences, v. 50, p. 40-47.

Kukla, G.J., Bender, M.L., de Beaulieu, J.L., Bond, G., Broecker, W.S., Clveringa, P., Gavin, J.E., Herbert, T.D., Imbrie, J., Jouzel, J., Keigwin, L.D., Knudsen, K.L., McManus, J.F., Merkt, J., Muhs, D.R., Müller, H., Poore, R.Z., Porter, S.C., Seret, G., Shackleton, N.J., Turner, C., Tzedakis, P.C.amd Winograd, I.J., 2002, Last interglacial climates: v. 58, p. 2-13, doi: 10.1006/qres.2001.2316.

Land, L.S., 1991, Dolomitization of the Hope Gate Formation (north Jamaica) by seawater: Reassessment of mixing-zone dolomite: Stable Isotope Geochemistry, Special Publication no. 3, p. 121-133.

Land, L.S., and Epstein, S., 1970, Late Pleistocene diagenesis and dolomitization, north Jamaica: Sedimentology, v. 14, no. 3-4, p. 187–200, doi: 10.1111/j.1365-3091.1970.tb00192.x.

Liddell, W.D., and Ohlhorst, S.L., 1987, Patterns of reef community structure, North Jamaica: Bulletin of Marine Science, v. 40, no. 2, p. 311-329.

Meschede, M., and Frisch, W., 1998, A plate tectonic model for the Mesozoic and early Cenozoic history of the Caribbean plate: Tectonophysics, v. 296, no. 3-4, p. 269-291, doi: 10.1016/S0040-1951(98)00157-7.

Mitchell, S.F., 2001, Lithostratigraphy of the late Cretaceous to Paleocene succession in the western part of the Central Inlier of Jamaica: Caribbean Journal of Earth Science, v. 35, p. 19-31.

Mitchell, S.F., 2003, Sedimentology and tectonic evolution of the Cretaceous rocks of central Jamaica: relationships to the plate tectonic evolution of the Caribbean: AAPG Memoir, v. 79, p. 605-623.

Mitchell, S.F., 2006, Timing and implications of late Cretaceous tectonic and sedimentary events in Jamaica: Geologica Acta, v. 4, no. 1-2., p. 171-178.

Mitchell, S.F., 2013, Lithostratigraphy of the Central Inlier, Jamaica: Caribbean Journal of Earth Science, v. 46, p. 31-42.

Mitchell, S.F., 2016, Geology of the western margin of the Benbow Inlier – implications for the relationship between the Yellow Limestone and White Limestone Groups (with the description of the Litchfield Formation, new name): Caribbean Journal of Earth Science, v. 48, p. 19-25.

McMaster University Nuclear Reactor, 2015, Neutron activation analysis: https://mnr.mcmaster.ca/index.php/products-and-services/neutron-activation-analysis (accessed December 2017).

Mitchell, S.F., 2016, SFM Geology: The Cretaceous Inliers of Jamaica: http://www.sfmgeology.com/Inliers.html (Accessed February 2018).

Mitchell, S.F. and Edwards, T.C.P., 2016, Geology of the Maastrichtian (Upper Cretaceous) succession of the Jerusalem Inlier in western Jamaica: Caribbean Journal of Earth Science, v. 48, p. 29-36.

Mitchell, S.F., Pickerill, R.K., Blackwell, B.A.B., and Skinner, A.R., 2000, The age of the Port Morant Formation, south-eastern Jamaica: Caribbean Journal of Earth Science, v. 34, p. 1-4.

Mitchell, S.F., Pickerill, R.K., Stemann, T.A., 2001, The Port Morant formation (Upper Pleistocene, Jamaica): High resolution sedimentology and paleoenvironmental analysis of a mixed-carbonate-clastic lagoonal succession: Sedimentary Geology, 16 p.

Mitchell, S.F., Ramsook, R., Coutou, R., and Fisher, J., 2011, Lithostratigraphy and age of the St. Ann's Great River Inlier, northern Jamaica: Caribbean Journal of Earth Science, v. 42, p. 1-16.

Moore, W.S., and Somayajulu, B.L.K., 1974, Age determinations of fossil corals using $^{230}Th/^{234}Th$ and $^{230}Th/^{227}Th$: Journal of Geophysical Research, v. 79, no. 33, p. 5065–5068, doi: 10.1029/ JC079i033p05065.

Muhs, D.R., Whmiller, J.F., Simmons, K.R., and York, L.L., 2003, Quaternary sea-level history of the United States: Developments in Quaternary Science, v. 1, p. 147-183, doi: 10.1016/S1571-0866(03)01008-X.

Multer, H.G., Gischler, E., Lundberg, J., Simmons, K.R., and Shinn, E.A., 2002, Key Largo Limestone revisited: Pleistocene self-edge facies, Florida Keys, USA: Facies, v. 46, no. 1, p. 229-271, doi: 10.1007/BF02668083.

Murray-Wallace, C.V., 2002, Pleistocene coastal stratigraphy, sea-level, highstands and neotectonism of the southern Australian passive continental margin – a review: Journal of Quaternary Science, v. 17, no. 5-6, p. 469-489, doi: 10.1002/jqs.717.

Murray-Wallace, C.V., Belperio, A.P., Dosseto, A., Nicholas, W.A., Mitchell, C., Bourman, R.P., Eggins, S.M., and Grün, R., 2016, Last interglacial (MIS 5e) sea-level determined from a tectonically stable, far-field location, Eyre Peninsula, southern Austrailia: Australian Journal of Earth Sciences, v. 63, no. 5, p. 611-630

National Library of Jamaica, 2018, The history of St. Elizabeth: http://www.nlj.gov.jm/history-notes/History%20of%20St.%20Elizabeth.pdf (accessed March 2018).

Pan, T.Y., Murray-Wallace, C.V., Dosseto, A., and Bourman, R.P., 2018, The last interglacial (MIS 5e) sea level highstand from a tectonically stable far-field setting, Yorke Penninsula, southern Austrailia: Marine Geology, v. 398, p. 126-136, doi: 10.1016/j.margeo.2018.01.012.

Pedoja, K., Husson, L., Regard, V., Cobbold, P. R., Ostanciaux, E., Johnson, M. E., Kershaw, S., Saillard, M., Martinod, J., Furgerot, L., Weill, P., and Delcaillau, B., 2011, Relative sea-level fall since the last interglacial stage: Are coasts uplifting worldwide?: Earth-Science Reviews, v. 108, p. 1-15, doi: 10.1016/j.earscirev.2011.05.002.

Pindell, J.L., and Barrett, S.F., 1990, Geological evolution of the Caribbean region: A plate-tectonic perspective, *in* Dengo, G., and Case, J.E., eds, The Caribbean region: Boulder, Colorado, Geological Society of America, The Geology of North America, v. H, p. 405-432.

Precht, W.F., 1993, Stratigraphic evidence from reef studies for a double-high sea stand during the Last Interglacial maximum: American Association of Petroleum Geologists Bulletin, v. 77, p. 1473, doi: 10.1306/ BDFF7890-1718-11D7-8645000102C1865D.

Precht, W.F., and Miller, S.L., 2007, Ecological Shifts along the Florida reef tract: The Past is a Key to the Future: Geological Approaches to Coral Reef Ecology, ch. 9, p. 237-312.

Radtke, U., Grün, R., and Schwarcz, H.P., 1988, Electron spin resonance dating of the Pleistocene coral reef tracts of Barbados: Quaternary Research, v. 29, no. 3, p. 197-215, doi: 10.1016/0033-5894(88)90030-0.

Railsback, B.L., Gibbard, P.L., Head, M.J., Voarintsoa, N.R.G., and Toucanne, S., 2015, An optimized scheme of lettered marine isotope substages for the last million years, and the climatostratigraphic nature of isotope stages and substages: Quaternary Science Reviews, v. 111, p. 94-106.

Ravelo, A.C., and Hillaire-Marcel, C., 2007, The use of oxygen and carbon isotopes of foraminifera in paleoceanography, *in* Hillaire-Marcel, C., and De Vernal, A., eds., Developments in Marine Geology: Proxies in Late Cenozoic Paleoceanography, v. 1, p. 735-764.

Richards, A., 2008, Development trends in Jamaica's coastal areas and the implications for climate change: Planning Institute of Jamaica: http://www.pioj.gov.jm/portals/0/sustainable_development/jamaica_climate_change_paper.pdf (accessed March 2017).

Riebeek, H., 2010, Global Warming, https://earthobservatory.nasa.gov/Features/GlobalWarming/page1.php, (accessed February 2018).

Rink, W.J., 1997, Electron spin resonance (ESR) dating and ESR applications in quaternary science and archaeometry: Radiation Measurements, v. 27, no. 5-6, p. 975-1025, doi: S1350-4487(97)00219-9.

Robinson, E., 1994, Caribbean geology: an introduction: *in* S.K. Donovan and T.A. Jackson, eds., University of the West Indies Publishers' Association, Kingston, Jamaica, p. 111-127.

Robinson, E, and Mitchell, S.F., 1999, Upper Cretaceous to Oligocene stratigraphy in Jamaica: *in* S.F. Mitchell ed., Contributions to Geology: University of the West Indies, Mona, no. 4, p. 1-47.

Rohling, E.J., Grant, K., Hemleben, C., Siddall, M., Hoogakker, B. A. A., Bolshaw, M., and Kucera, M., 2007, High rates of sea-level rise during the last interglacial period: Nature, v. 1, p. 38-42, doi: 10.1038/ngeo.2007.28.

Shackleton, N.J., 1967, Oxygen isotope analyses and Pleistocene temperatures re-assessed: Nature, v. 215, p. 15-17.

Shackleton, N.J., 1969, The last interglacial in the marine and terrestrial record: ser. B, v. 174, p. 135-154.

Shackleton, N.J., 1987, Oxygen isotopes, ice volume, and sea level: Quaternary Science Reviews, v. 6, p. 183-190.

Shackleton, N.J., Berger, A., and Peltier, W.R., 1990, An alternative astronomical calibration of the lower Pleistocene timescale based on ODP Site 677: Transactions of the Royal Society of Edinburgh: Earth Sciences, v. 81, p. 251-261.

Shackleton, N.J., Sánchez-Goñi, M.F., Pailler, D. and Lancelot, Y., 2003, Marine isotope substage 5e and the Eemian Interglacial: Global and Planetary Change, v. 36, p. 151-155, doi: 10.1016/S0921-8181(02)00181-9

Sherman, C.E., Glenn, C.R., Jones, A.T., Burnett, W.C., and Schwarcz, H.P., 1993, New evidence for two highstands of the sea during the last interglacial, oxygen isotope substage 5e: Geology, v. 21, p. 1079-1082. doi: 10.1130/0091-7613(1993)0212.3.CO;2.

Skinner, A.F., 1988, Dating of marine aragonite by electron spin resonance: Quaternary Science Reviews, v. 7, no. 3-4, p. 461-464, doi: 10.1016/0277-3791(88)90046-7.

Skrivanek, A., Dutton, A., Stemann, T., Vyverberg, K., and Mitrovica, J.X., 2017, Evidence of tectonism based on differential uplift of the Falmouth Formation of Jamaica: GSA Bulletin, 14. p, doi: 10.1130/B31796.1.

Stemann, T.A., 2004, Reef corals of the White Limestone Group, *in* Donovan, S.K., ed., The Mid-Cainozoic White Limestone Group of Jamaica: Cainozoic Research, v. 3, no. 1-2, p. 83-107.

Stirling, C.H., Esat, T.M., Lambeck, K., and McCulloch, M.T., 1998, Timing and duration of the Last Interglacial: evidence for a restricted interval of widespread coral reef growth: Earth and Planetary Science Letters, v. 160, p. 745-762.

Stirling, C.H., Esat, T.M., McCulloch, M.T., and Lambeck, K., 1995, High-precision U-series dating of corals from Western Austrailia and implications for the timing and duration of the Last Interglacial: v. 135, no. 1-4, p. 115-130, doi: 10.1016/0012-821X(95)00152-3.

Voris, H.K., 2000, Maps of Pleistocene sea levels in Southeast Asia: shorelines, river systems and time durations: Journal of Biogeography, v. 27, p. 1153-1167.

Wadge, G., 1982, A Miocene submarine volcano at Low Layton, Jamaica: Geological Magazine, v. 119, no. 2, p. 193-199, doi: 10.1017/S0016756800025875.

Zazo, C., Hoy, J.L., Hillaire-Marcel, C., Dabrio, C.J., González-Delgado, J.A., Cabero, A., and Bardají, T., 2010, Sea level changes during the last and present interglacials in Sal Island (Cape Verde archipelago): Global and Planetary Change, v. 72, p. 302-317.

Zeller, M., Verwer, K., Eberli, G.P., Massaferro, J.L., Schwarx, E., and Spalletti, L., 2015, Depositional controls on mixed carbonate-siliciclastic cycles and sequences on gently inclined shelf profiles, Sedimentology, v. 62, p. 2009-2037, doi: 10.1111/sed.12215.

APPENDICES

Appendix A. Regional Distribution

Appendix A-1. Photo of sea cliff (looking south) and toppled coral rudstone blocks at Fort Charles Bay. Merrimans Point is in the distance (17.917788 N, -77.797775 W).

Appendix A-2. Photo of sea cliff at Fort Charles Bay (looking north). Modern dune field at northwestern Fort Charles Bay in the distance (17.917809 N, -77.797775 W).

Appendix A-3. Photo (looking north) of burrowed lithic quartz arenite unit described at section FCB-2 at Fort Charles Bay (17.918962 N, -77.798286 W). Author is pictured.

Appendix A-4. Photo (looking south) of jointed and burrowed lithic quartz arenite unit at Fort Charles Bay (17.919212 N, -77.798363 W).

Appendix A-5. Photo of sea cliff (looking north) at Fort Charles Bay (17.919802 N, -77.799034 W).

Appendix A-6. Photo of modern dune field (looking south) at the northern portion of Fort Charles Bay (17.928644 N, -77.805901 W).

Appendix A-7. Photo of modern dune field (looking north) towards Parrotee Point at the northern portion of Fort Charles Bay (17.928333 N, -77.806389 W).

Appendix A-8. Photo of outcrop in the bay showing a wave-cut notch at fort Charles Bay (17.914143 N, -77.798401 W).

Appendix A-9. Photo (looking southeast) of modern beach and raised shore platforms at Billy Bay (17.896416 N, -77.788933 W).

Appendix A-10. Photo (looking southeast) of wave-cut platforms and coral rudstone boulders at Billy Bay (17.89855 N, -77.792999 W).

Appendix A-11. Photo (looking northwest) of raised shore platforms and vertical exposures separated by modern beach deposits at Billy Bay (17.902752 N, -77.795654 W).

Appendix A-12. Photo (looking southeast) of nearly continuous section of raised shore platforms at Billy Bay (17.902603 N, -77.795761 W).

Appendix A-13. Photo (looking northwest) of weathered raised shore platforms and coral rudstone boulders at Billy Bay. The top of section BB-3 is visible in the top right corner of the photo (17.898346 N, -77.792648 W).

Appendix A-14. Photo (looking northwest) of modern beach deposits separating vertical exposures with some raised shore platforms at Billy Bay. Section BB-6 can be seen in the distance (17.900278 N, -77.793053 W).

Appendix A-15. Photo (looking east) of coral rudstone boulders at Billy Bay (17.896101 N, -77.789017 W).

Appendix A-16. Photo (looking northwest) of vertical exposures, submerged raised shore platforms, and modern dune deposits at Frenchmans Bay (17.884781 N, -77.771332 W).

Appendix A-17. Photo (looking southeast) of coral rudstone to framestone facies with *in situ Acropora palmata* at Frenchmans Bay (17.884361 N, -77.77121 W).

Appendix A-18. Photo (looking northwest) of fine-grained calcareous sandstone facies with bedding planes gently sloping to the southeast at Frenchmans Bay (17.884882 N, -77.770332 W).

Appendix A-19. Photo (looking north) of lithified sandstone beneath stable modern dune deposits in a drainage passage at Frenchmans Bay (17.884718 N, -77.769318 W).

Appendix A-20. Photo (looking northwest) of vertical exposure of coral rudstone unit at Jake's hotel at Frenchmans Bay (17.879774 N, -77.763313 W).

Appendix A-21. Photo (looking southeast) of vertical exposures at Jake's Hotel at Frenchmans Bay (17.884781 N, -77.771332 W).

Appendix A-22. Photo (looking northwest) of a calcareous sandstone unit containing conch shells, patchy coral debris, and skeletal fragments found landward of coral rudstone facies at Calabash Bay. A wave-cut notch is also seen at + 2 meters asl (17.878189 N, -77.761925 W).

Appendix A-23. Photo (looking northwest) of calcareous sandstone unit with bedding planes gently sloping towards the sea at Calabash Bay (17.878113 N, -77.761681 W).

Appendix A-24. Photo (looking southeast) of thinly-bedded, fine-grained calcareous sandstone facies with bedding planes gently sloping to the south towards the sea at Pedro Bay. Great Pedro Bluff can be seen in the distance (17.870907 N, -77.753334 W).

Appendix A-25. Photo (looking southeast) of coral rudstone unit that has been heavily weathered by waves at Calabash Bay. The bottom portion of the exposure is submerged by modern sea level. Great Pedro Bluff can be seen in the distance (17.869884 N, -77.751205 W).

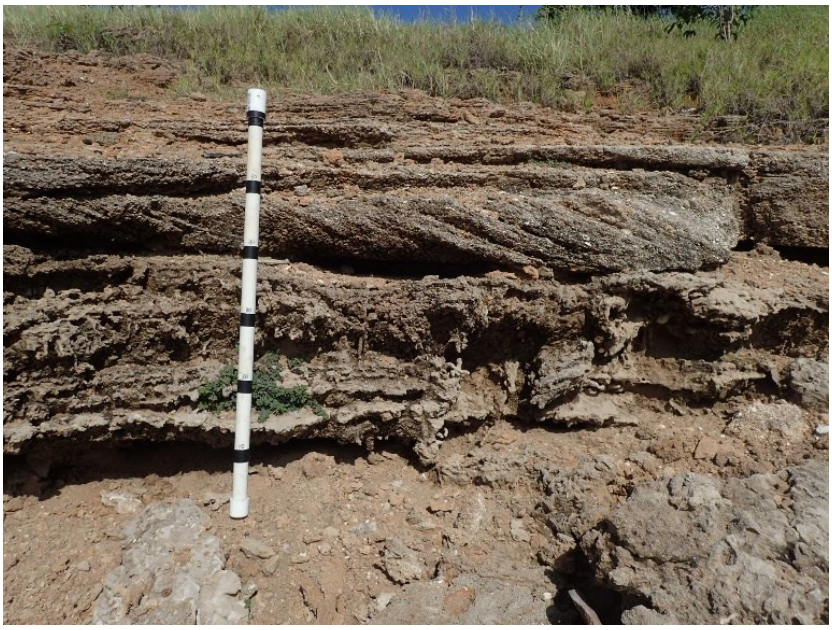

Appendix A-26. Photo (looking north) of lithic quartz arenite facies containing skeletal fragments at Pedro Bay. This unit is horizontally laminated at the base and top and cross-bedded in the middle. The cross-bedded sandstone facies contains abundant skeletal fragments (17.869106 N, -77.746323 W).

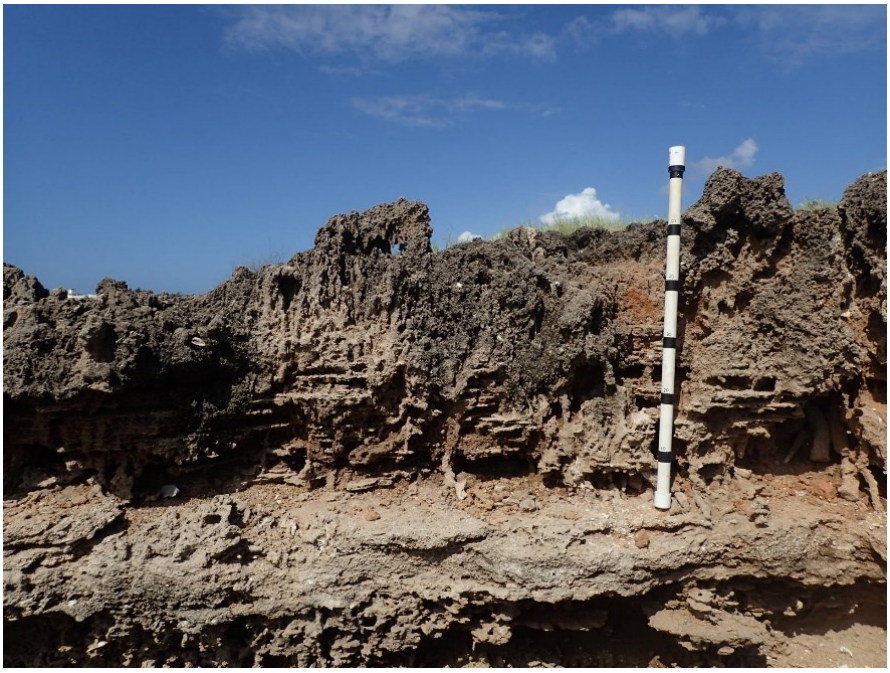

Appendix A-27. Photo (looking northwest) of possible lithified root casts (rhizocretions?) in a lithic quartz arenite facies at Pedro Bay (17.869143 N, -77.746498 W).

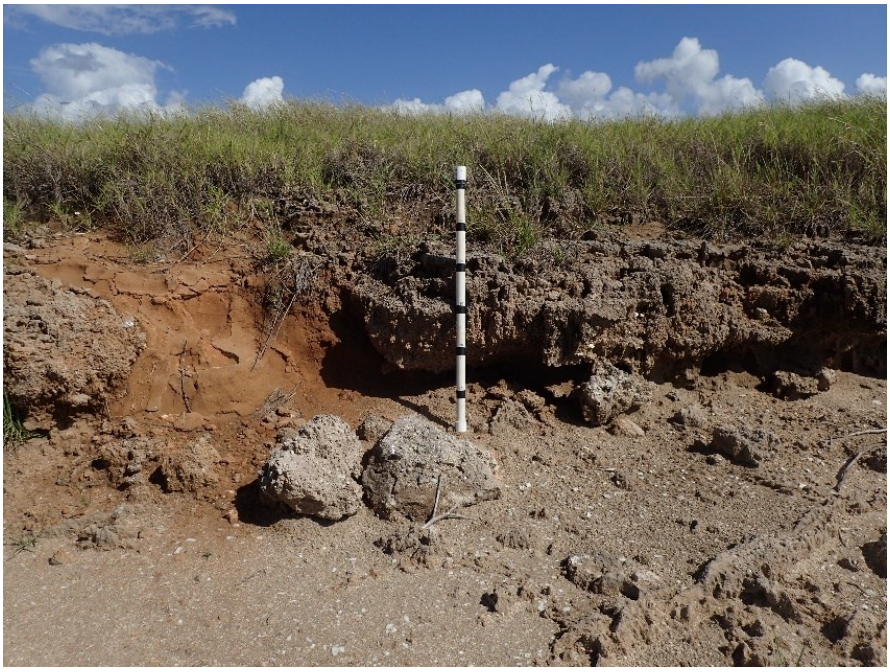

Appendix A-28. Photo (looking east) of horizontally laminated lithic quartz arenite with skeletal fragments overlain by a red silty – clay facies at Pedro Bay (17.869497 N, -77.748535 W).

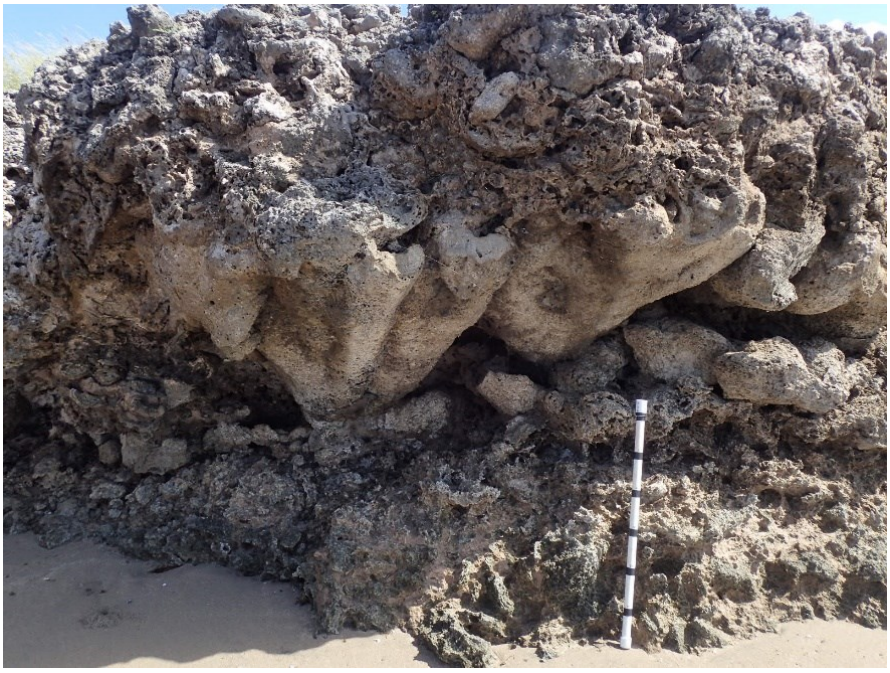

Appendix A-29. Photo (looking northeast) of a large *in situ Acropora palmata* at Pedro Bay (17.869341 N, -77.747116 W).

Appendix A-30. Photo (looking north) of well-cemented lithic quartz arenite with skeletal fragments interpreted to be filling in a joint at Pedro Bay. It has been surrounded by modern beach sand deposits. The originally jointed material may have been eroded away (17.869772 N, -77.749931 W).

Appendix B. Drafted Stratigraphic Columns

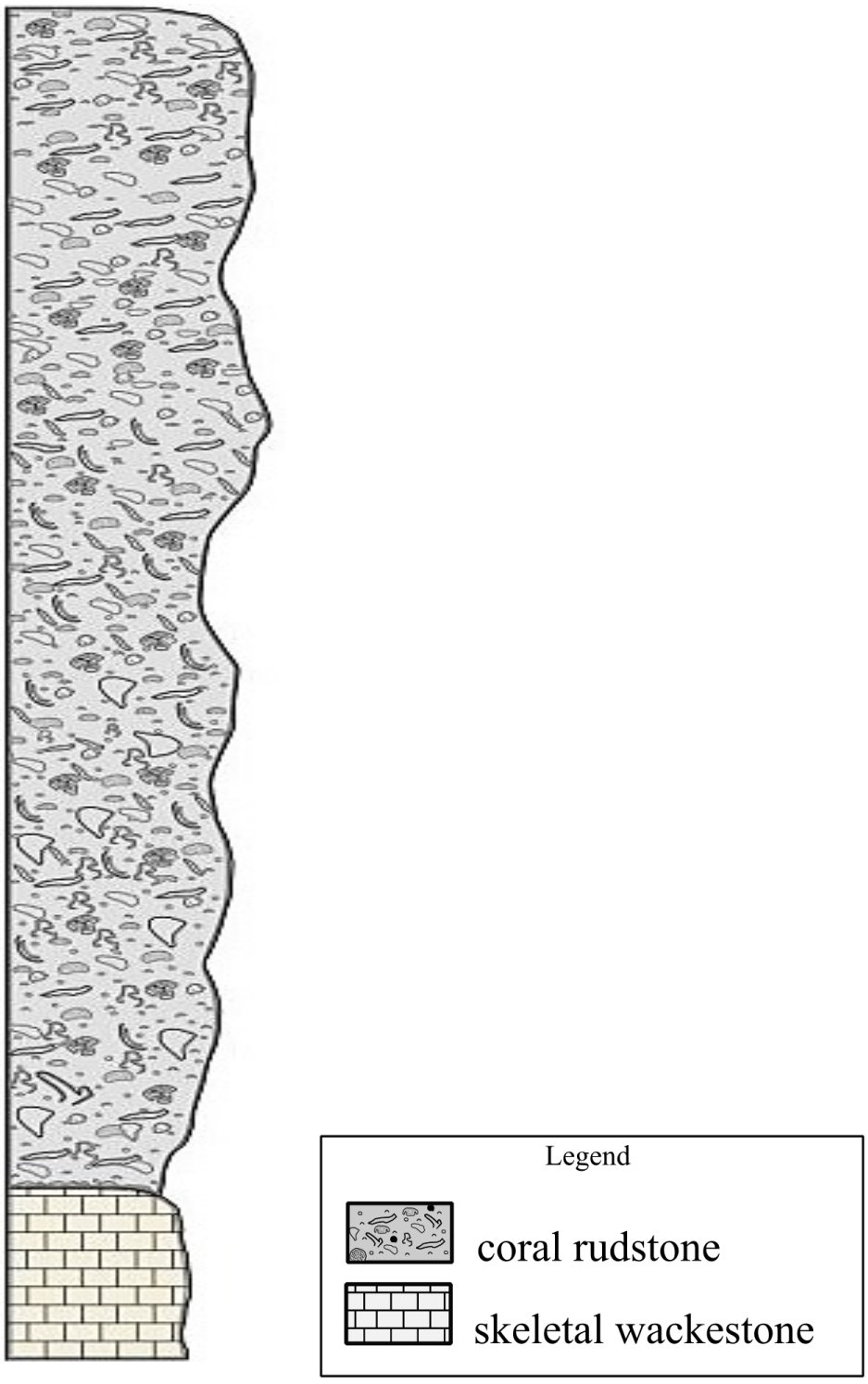

Appendix B-1. Generalized Stratigraphic Column of Section BB-1.

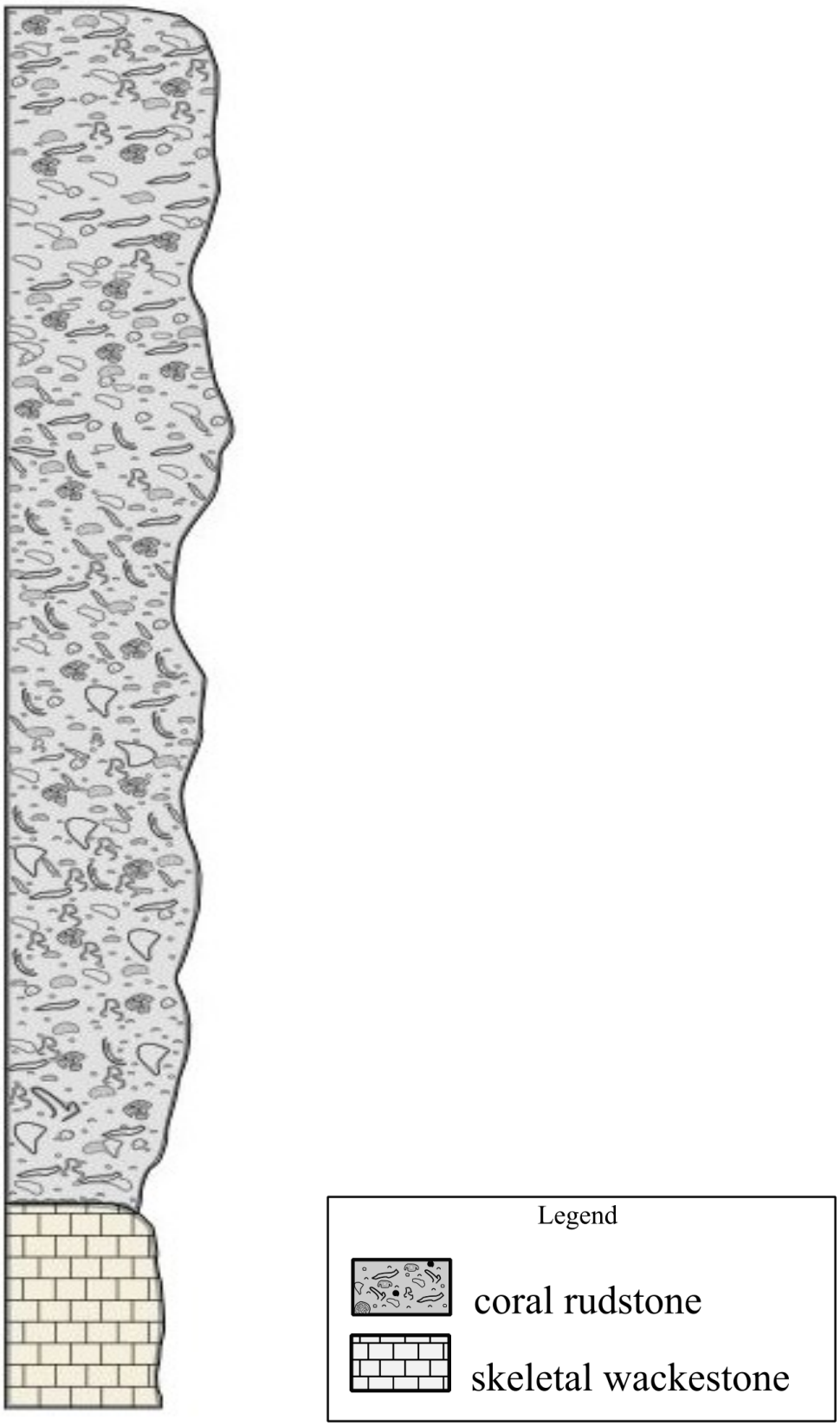

Appendix B-2. Generalized Stratigraphic Column of Section BB-2.

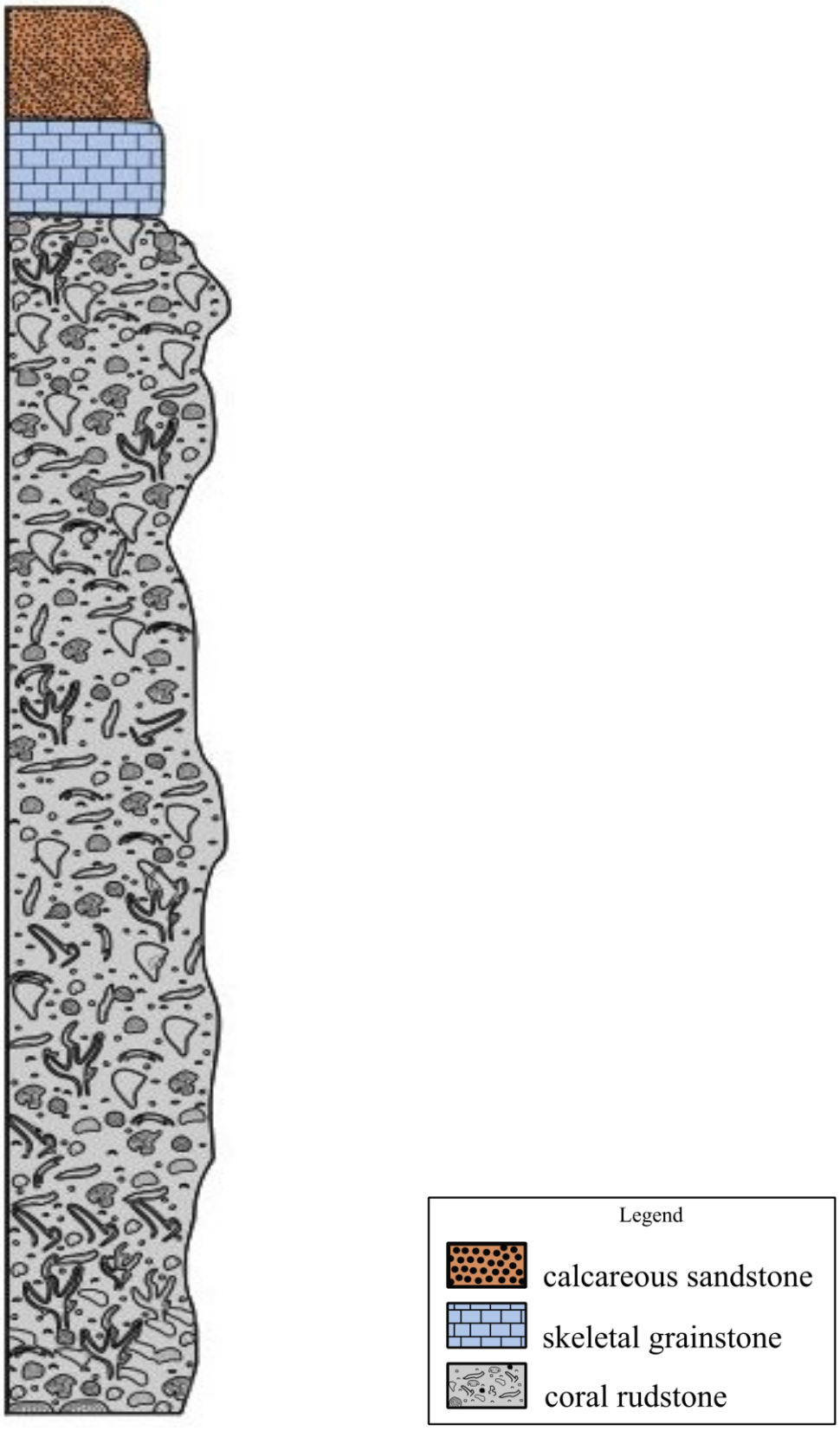

Appendix B-3. Generalized Stratigraphic Column of Section BB-3.

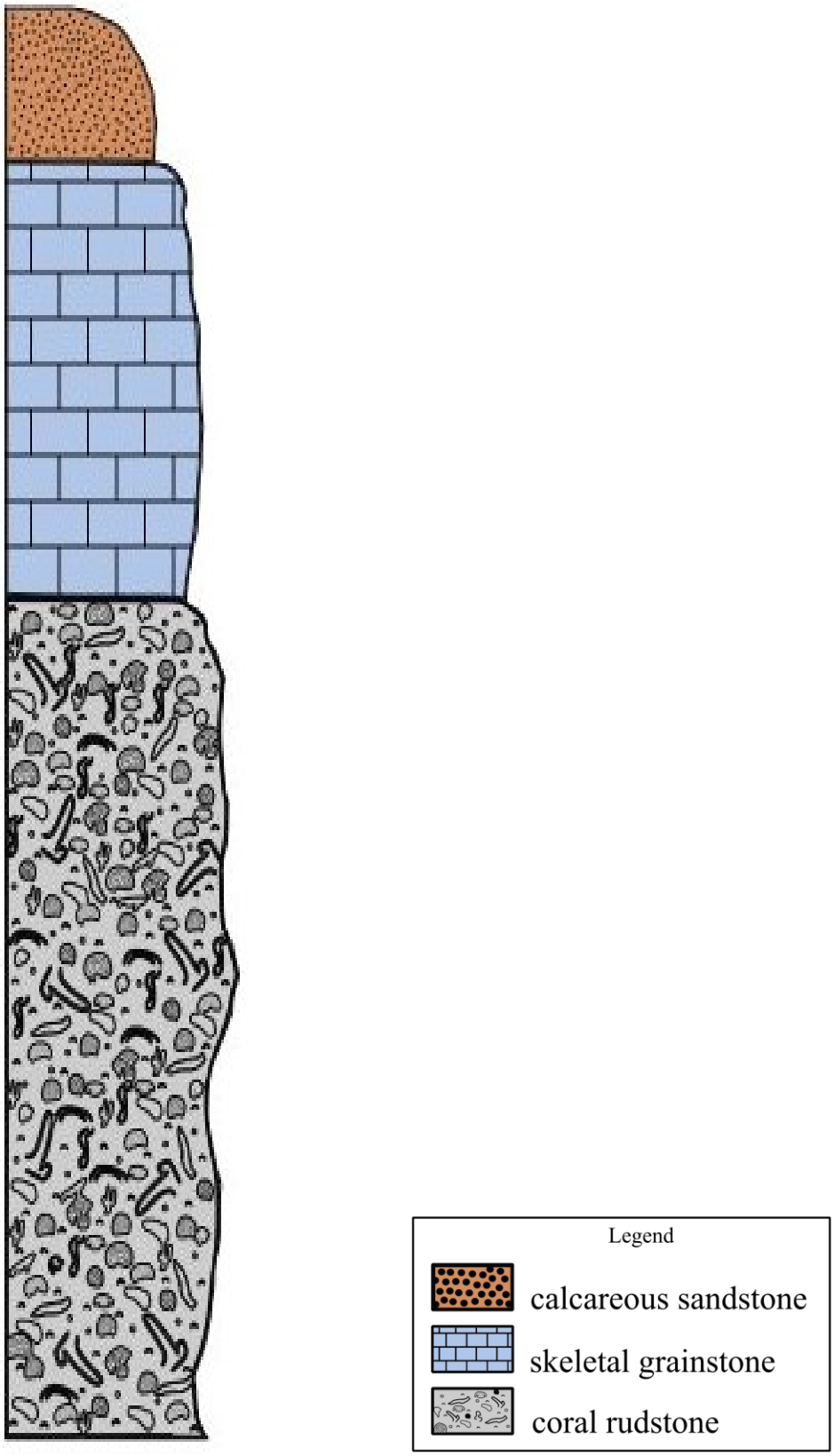

Appendix B-4. Generalized Stratigraphic Column of Section BB-4.

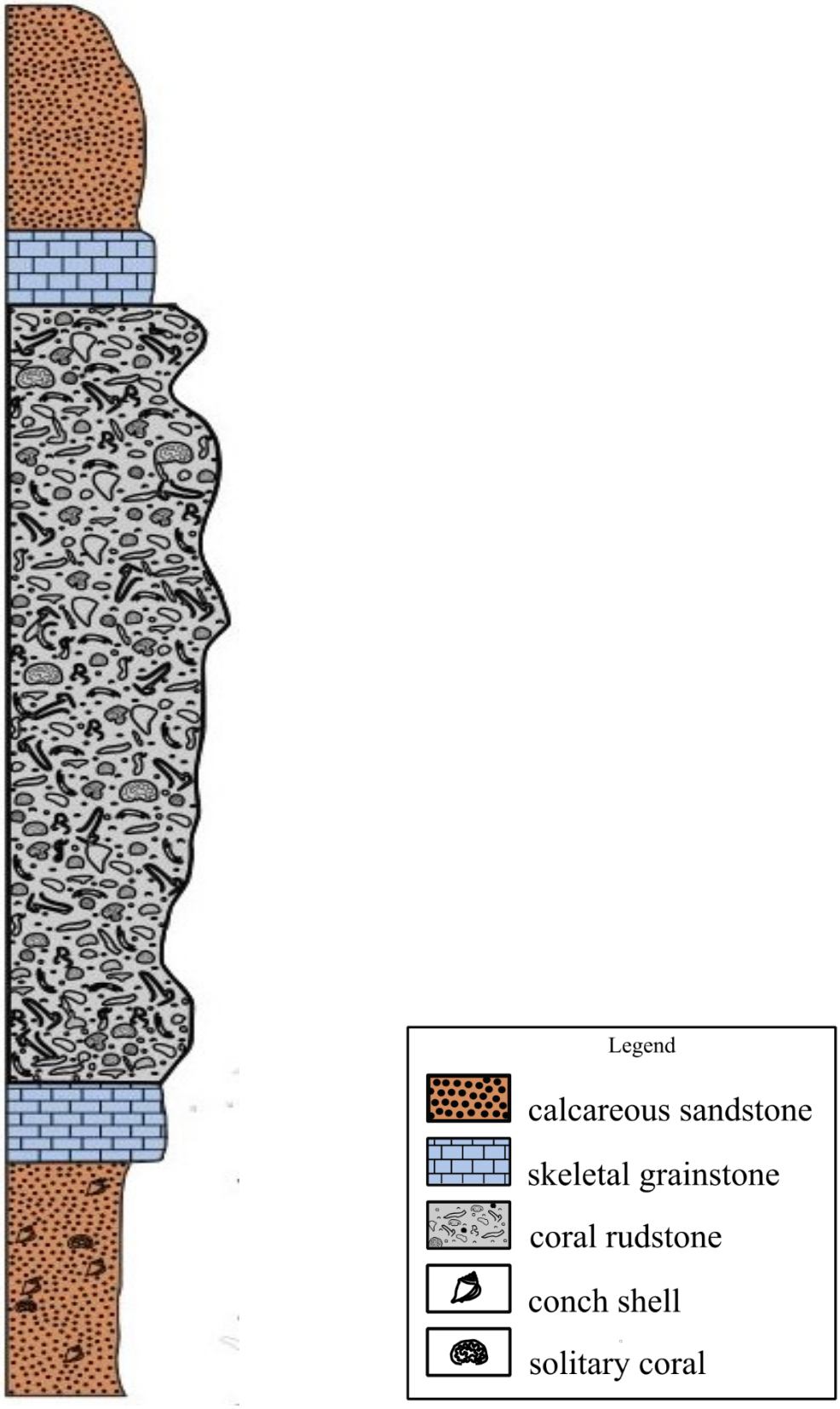

Appendix B-5. Generalized Stratigraphic Column of Section BB-5.

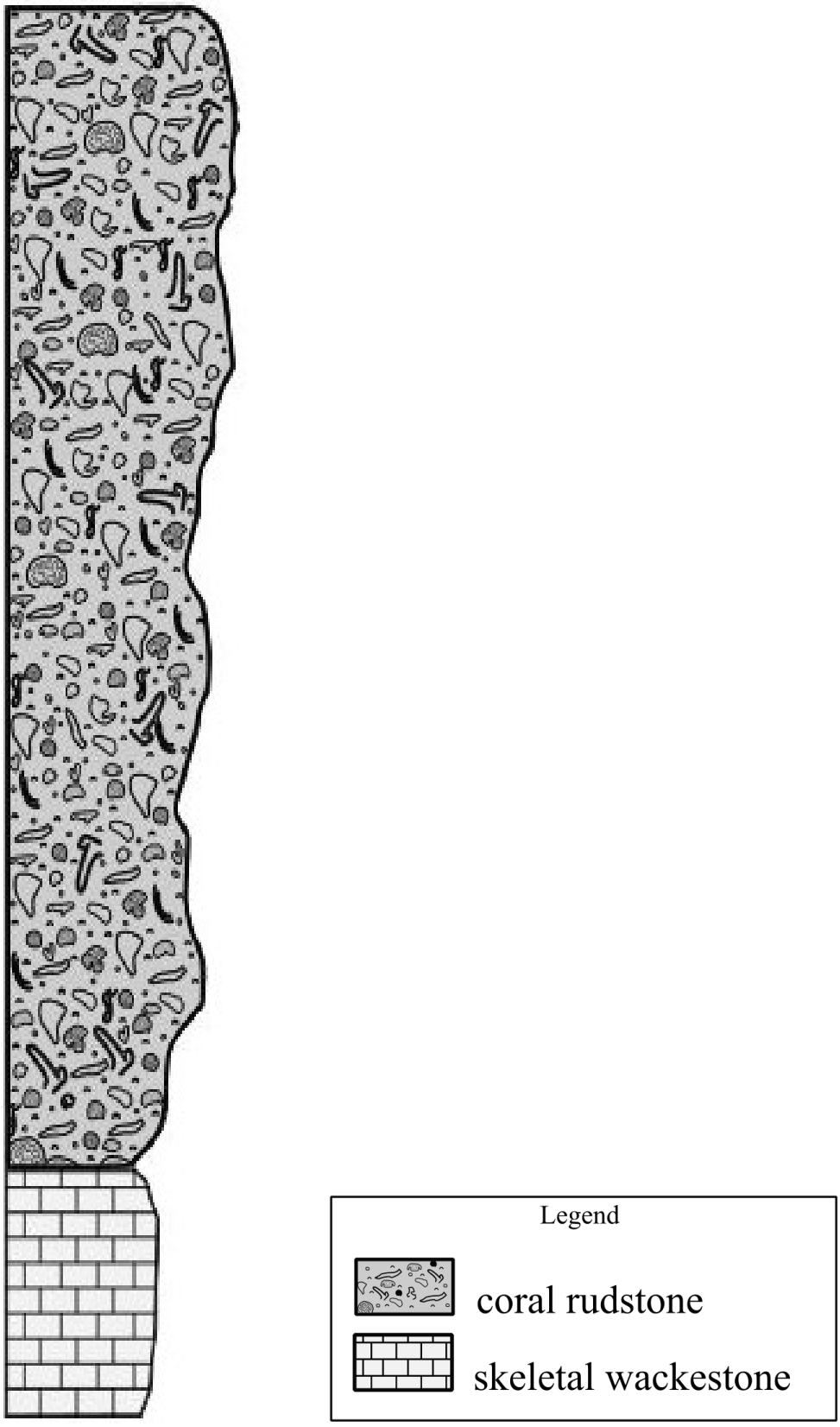

Appendix B-6. Generalized Stratigraphic Column of Section BB-6.

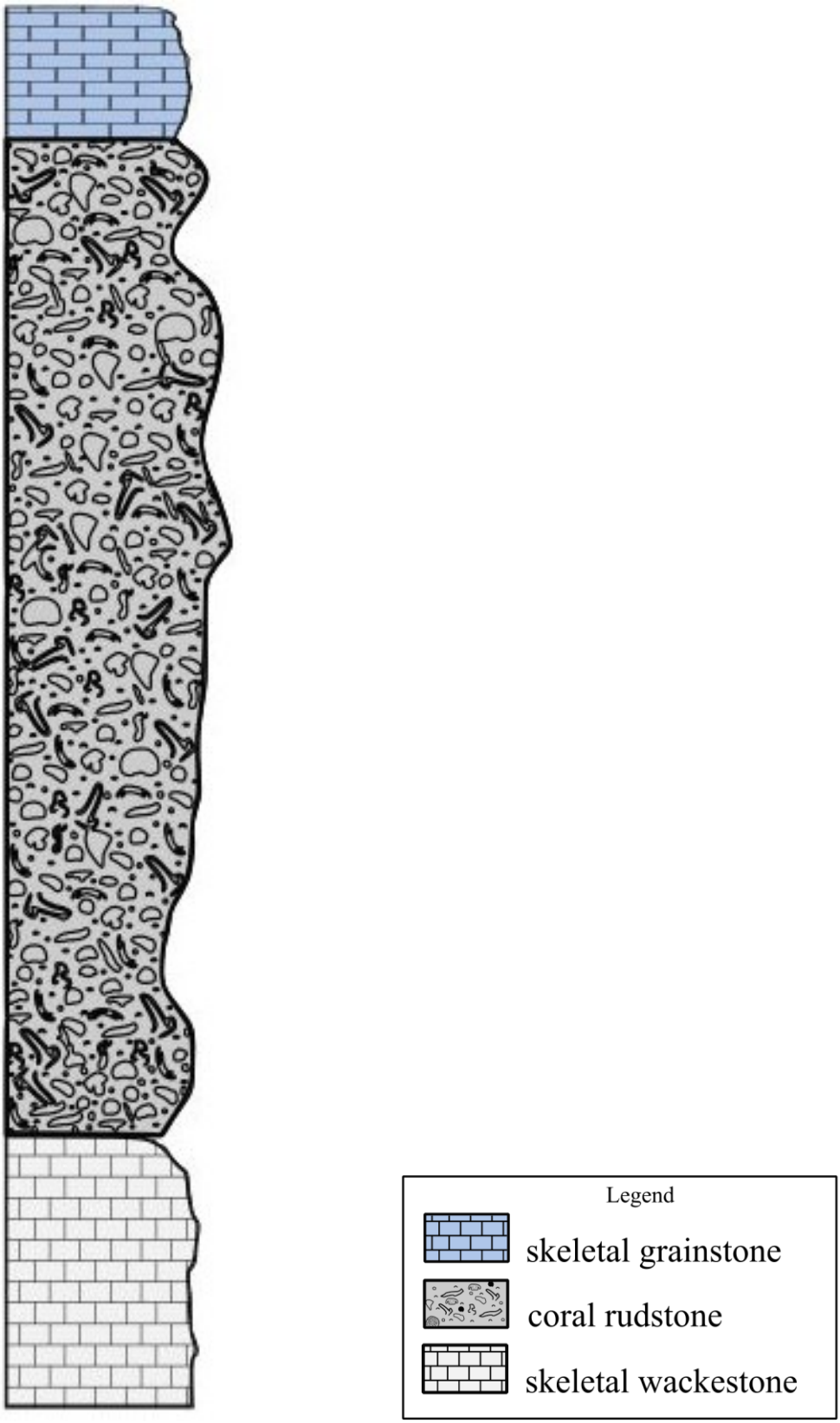

Appendix B-7. Generalized Stratigraphic Column of Section BB-7.

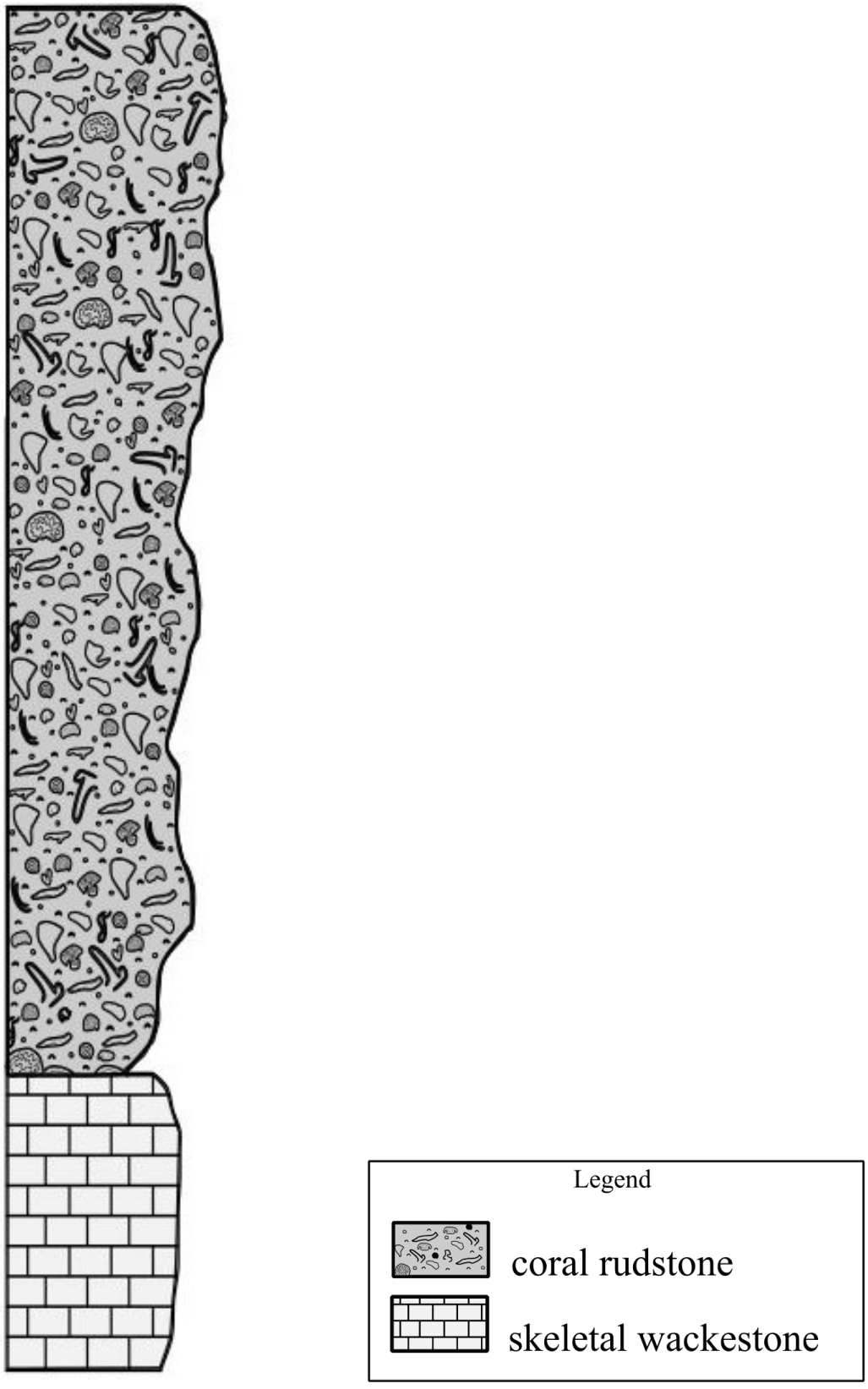

Appendix B-8. Generalized Stratigraphic Column of Section BSP-1.

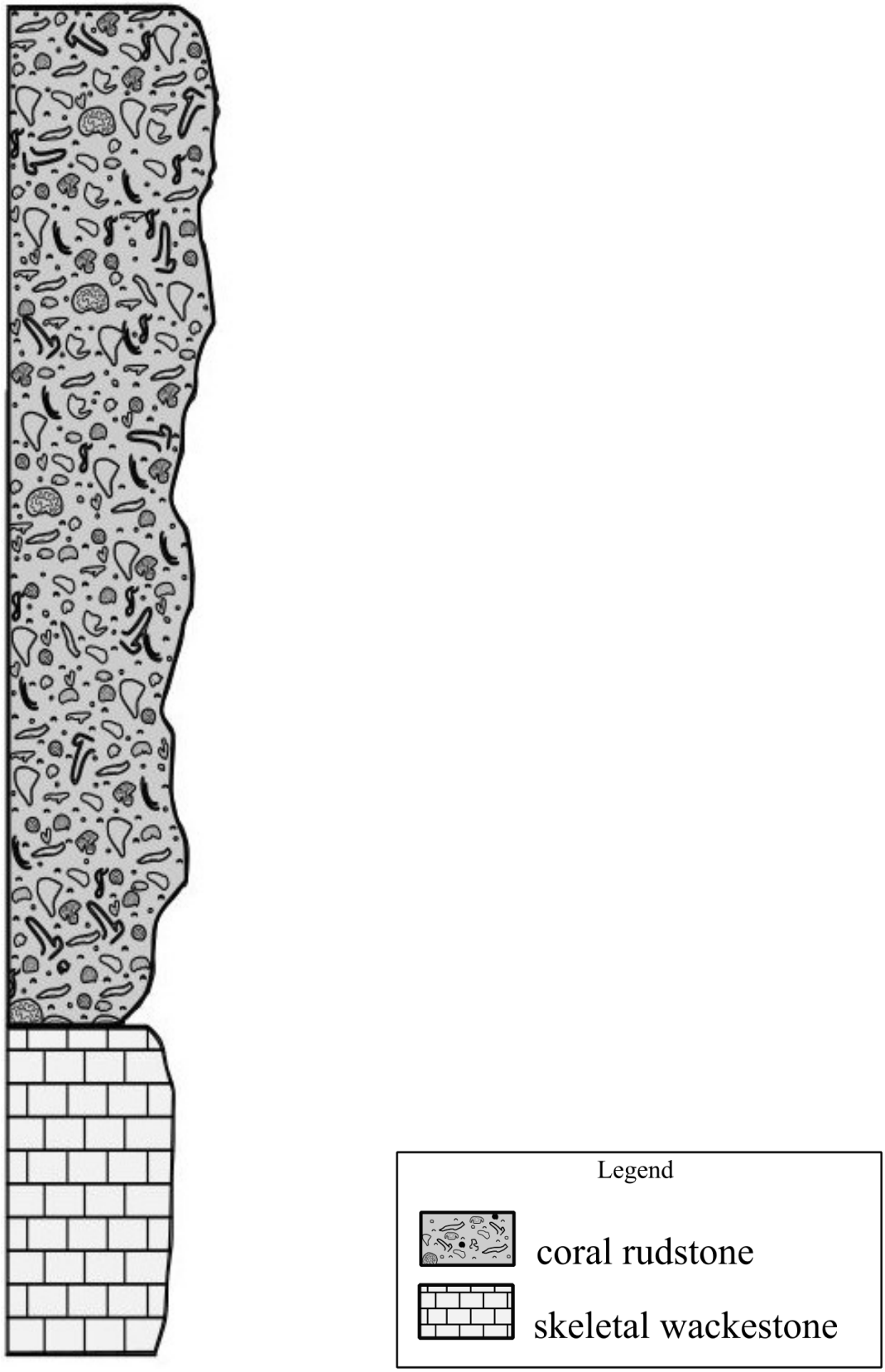

Appendix B-9. Generalized Stratigraphic Column of Section BSP-2.

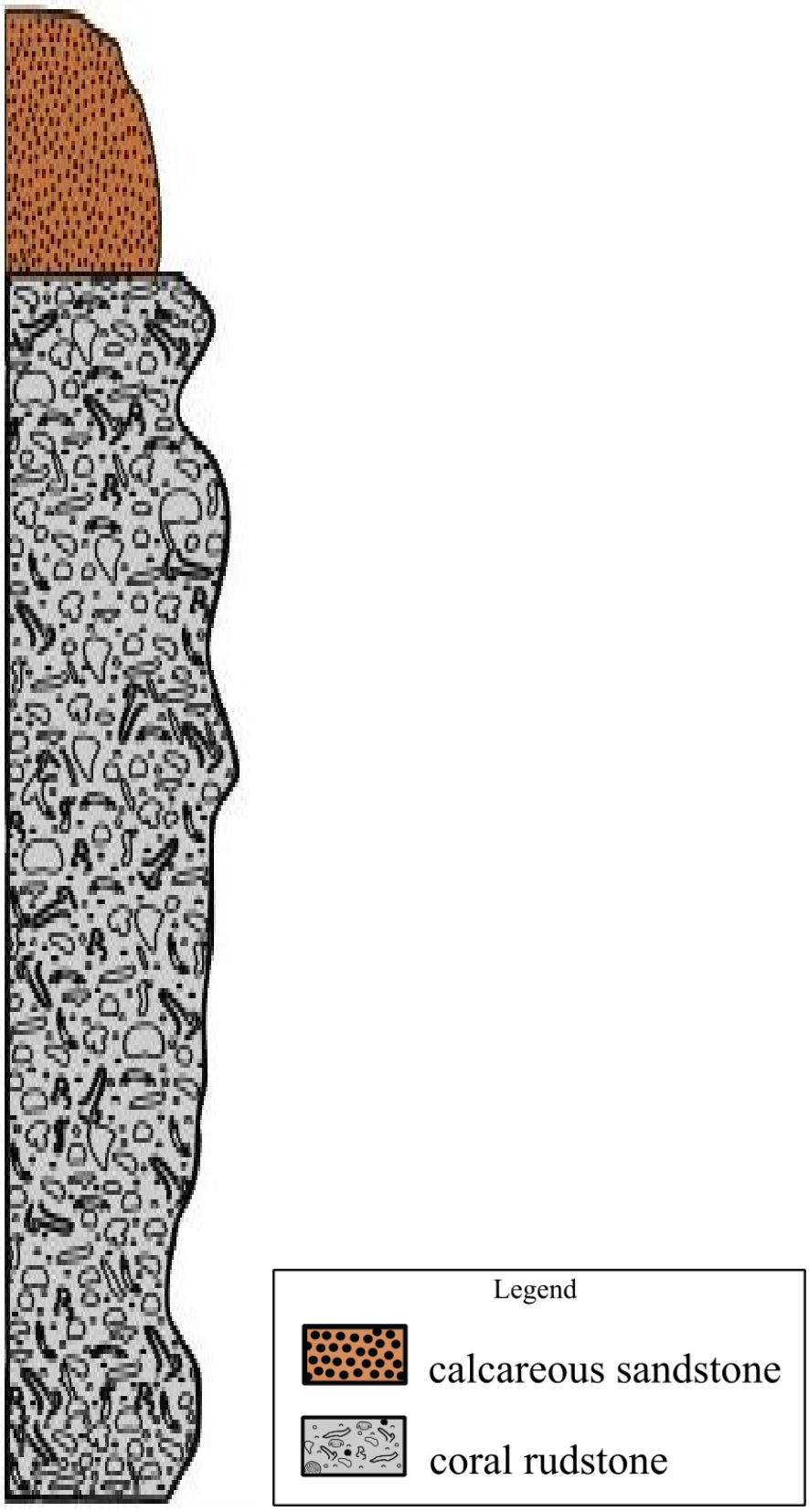

Appendix B-10. Generalized Stratigraphic Column of Section FCB-1.

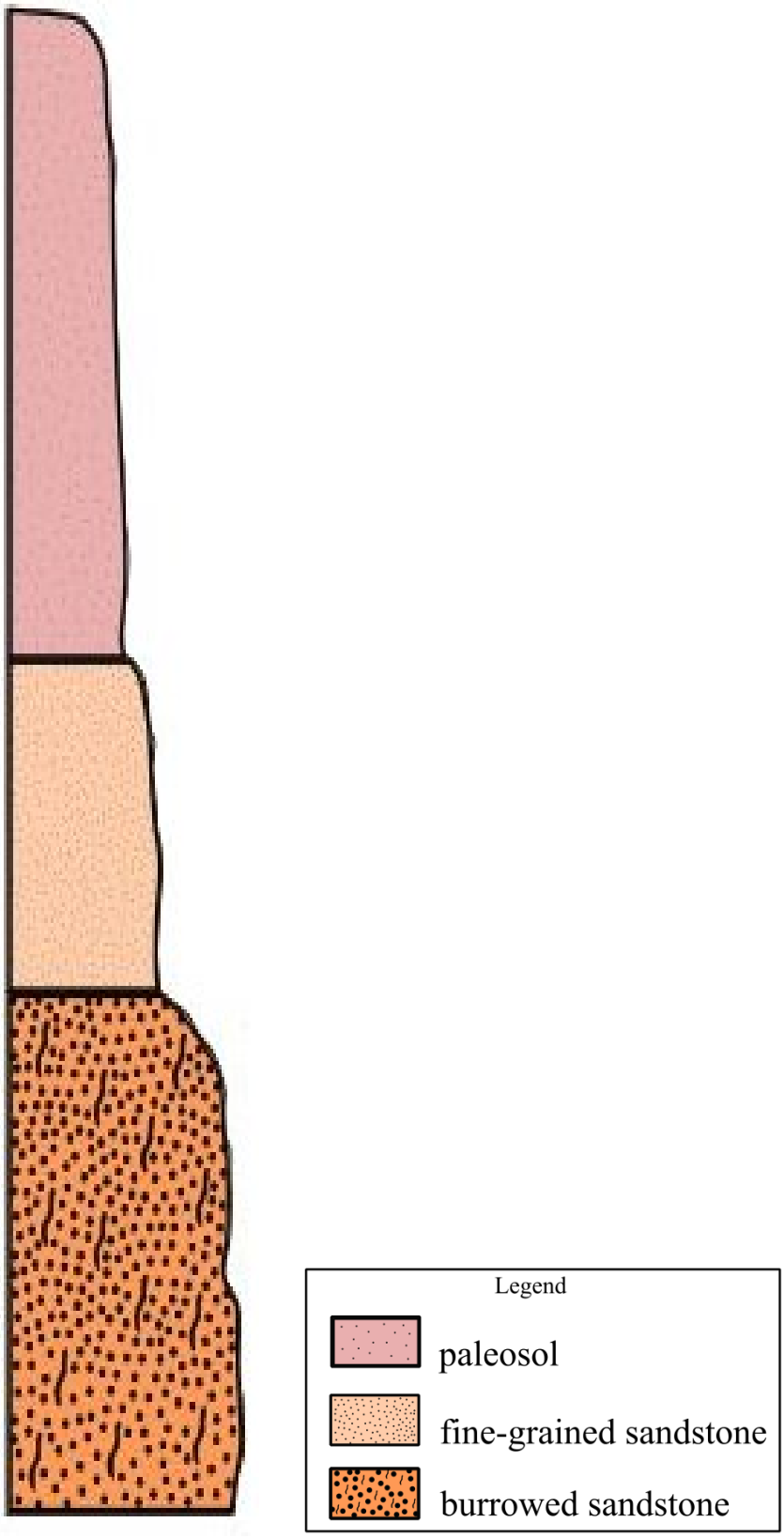

Appendix B-11. Generalized Stratigraphic Column of Section FCB-2.

Appendix C. Photo Catalog of Identified Fauna

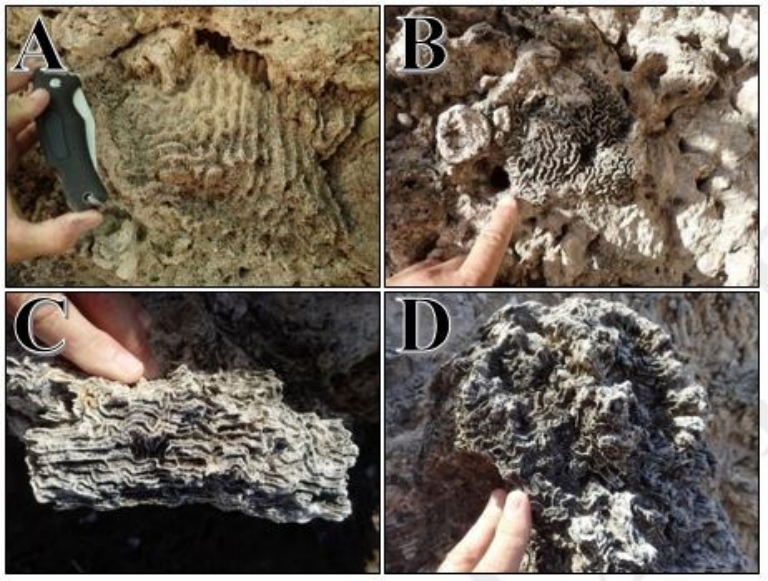

Appendix C-1. Identified *Diploria* spp. coral fauna. A) *Diploria labyrinthiformis* B) *Diploria labyrinthiformis* C) *Diploria labyrinthiformis* D) *Diploria* spp.

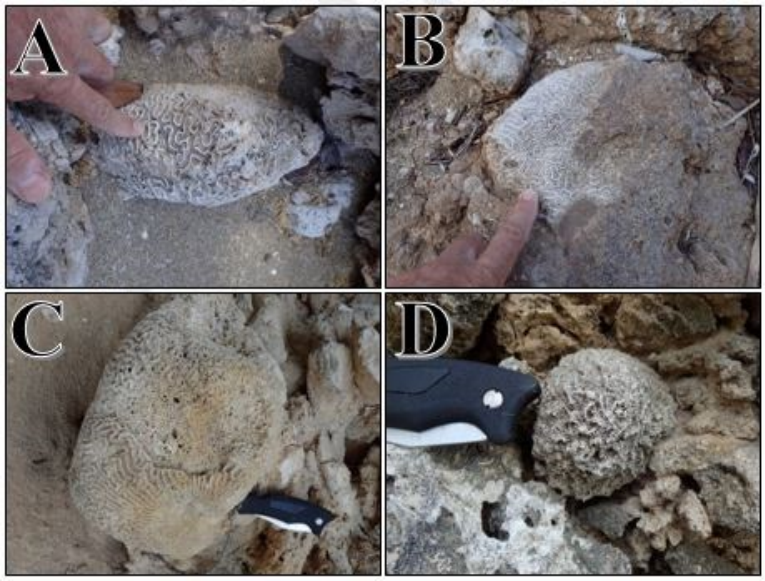

Appendix C-2. Identified *Diploria* spp. coral fauna. A) *Diploria strigosa* B) *Diploria strigosa* C) *Diploria labyrinthiformis* D) *Diploria* spp.

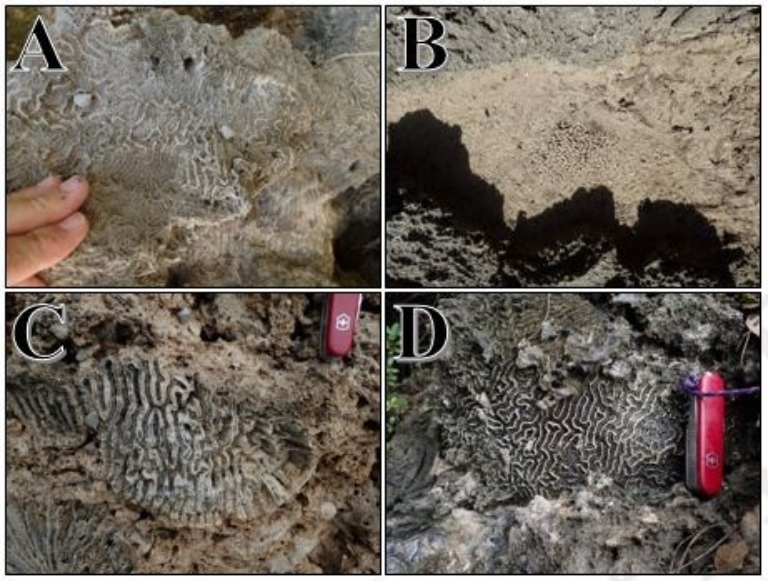

Appendix C-3. Identified *Diploria* spp. coral fauna. A) *Diploria strigosa* B) *Diploria strigosa* C) *Diploria strigosa* D) *Diploria labyrinthiformis*.

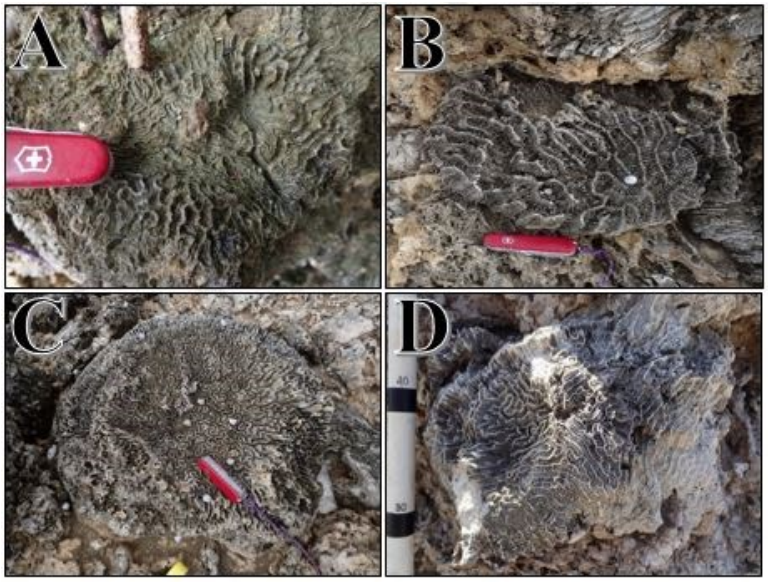

Appendix C-4. Identified *Diploria* spp. coral fauna. A) *Diploria strigosa* B) *Diploria* spp. C) *Diploria strigosa* D) *Diploria labyrinthiformis*.

Appendix C-5. Identified *Diploria* spp. coral fauna. A) *Diploria* spp. B) *Diploria* spp. C) *Diploria labrinthiformis* D) *Diploria* spp.

Appendix C-6. Identified *Diploria* spp. coral fauna. A) *Diploria* spp. B) *Diploria strigosa* C) *Diploria strigosa* D) *Diploria spp.*

Appendix C-7. Identified *Acropora* spp. coral fauna. A) *Acropora palmata* B) *Acropora cervicornis* C) *Acropora palmata* D) *Acropora palmata*.

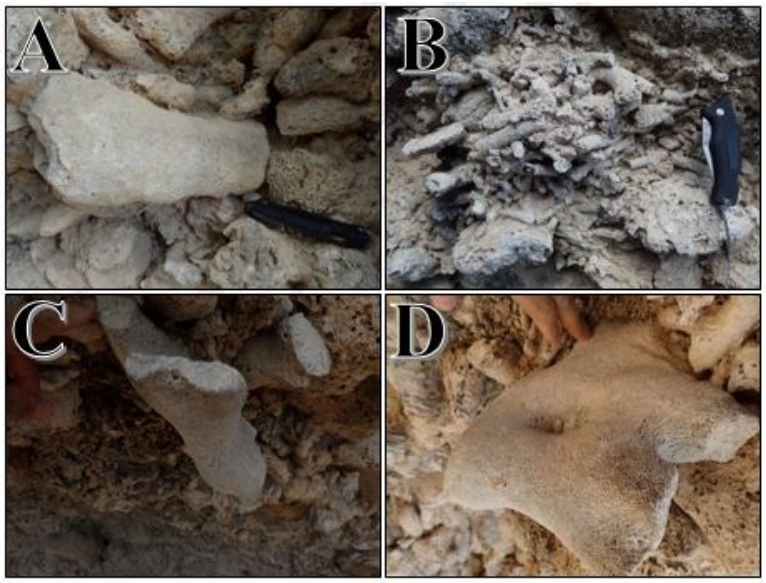

Appendix C-8. Identified *Acropora* spp. coral fauna. A) *Acropora palmata* B) *Acropora cervicornis* C) *Acopora palmata* D) *Acropora palmata*.

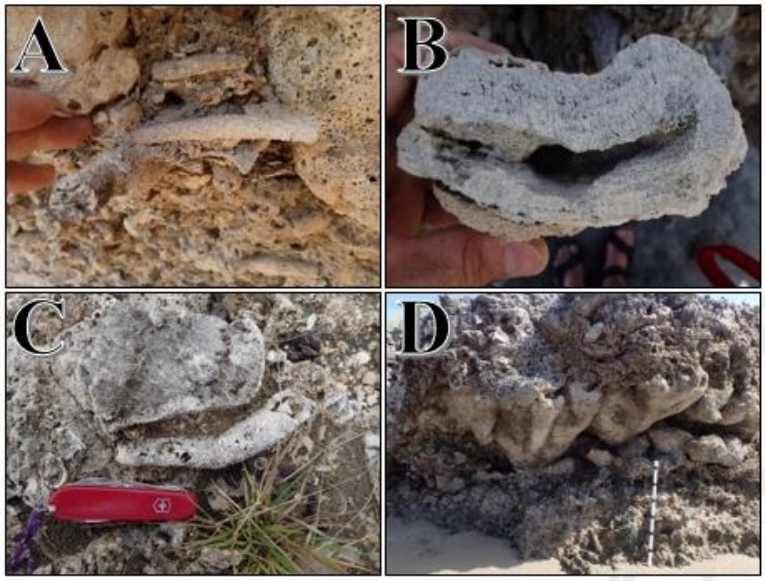

Appendix C-9. Identified *Acropora* spp. coral fauna. A) *Acropora cervicornis* B) *Acropora palmata* C) *Acropora cervicornis* D) *in situ Acropora palmata*.

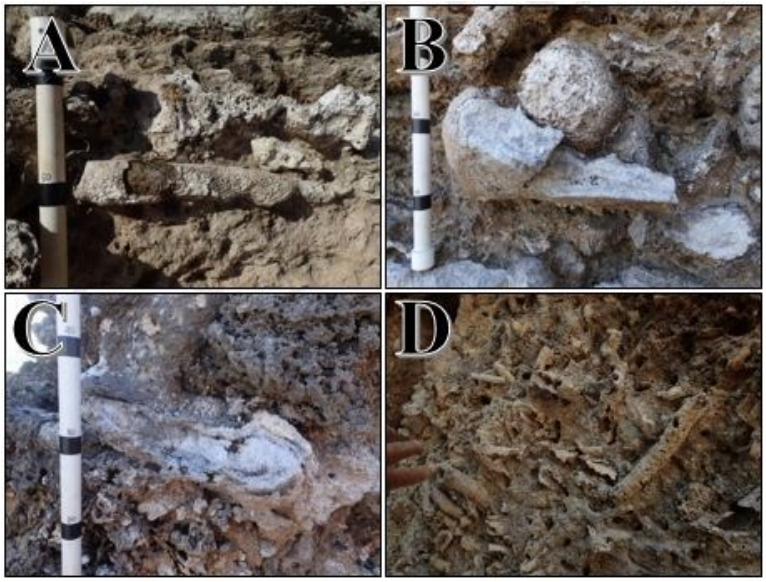

Appendix C-10. Identified *Acropora* spp. coral fauna. A) *Acropora cervicornis* B) *Acropora palmata* C) *Acropora palmata* D) *Acropora cervicornis*.

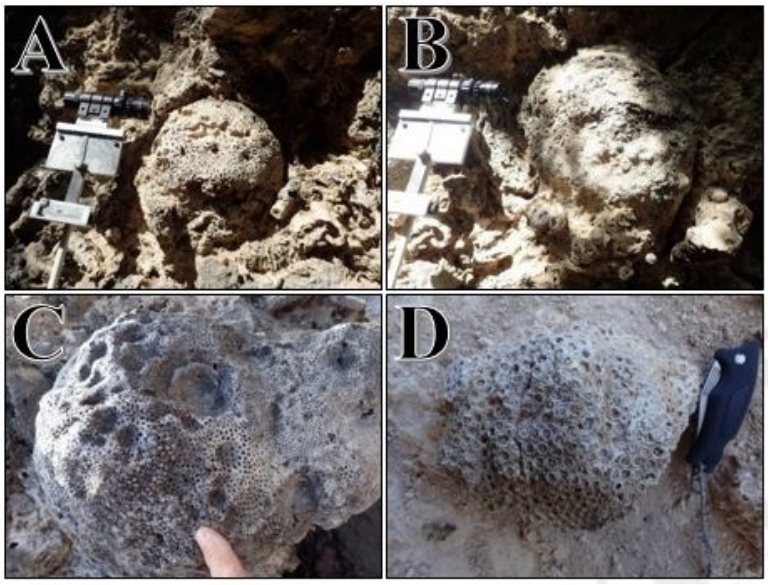

Appendix C-11. Identified *Montastrea* spp. coral fauna. A) *Montastrea annularis* B) *Montastrea cavernosa* C) *Montastrea* spp. D) *Montastrea cavernosa*.

Appendix C-12. Identified *Montastrea* spp. coral fauna. A) *Montastrea annularis* B) *Montastrea annularis* C) *Montastrea* spp. D) *Montastrea cavernosa*.

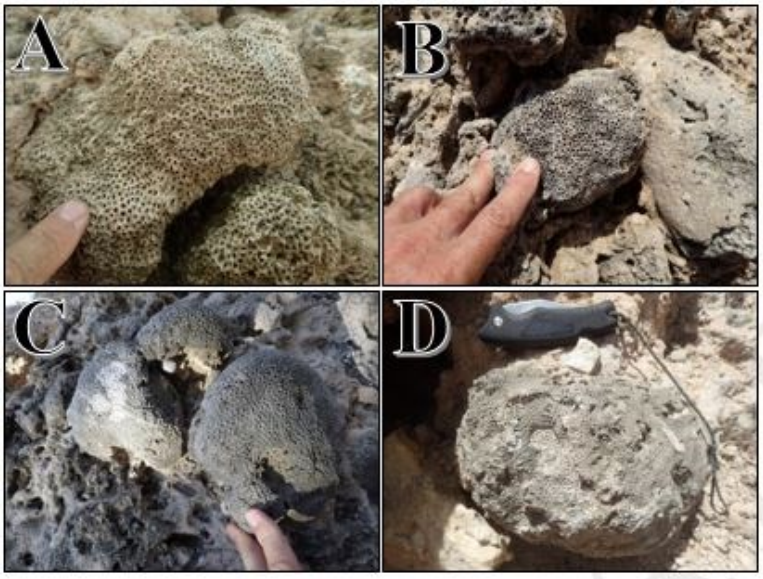

Appendix C-13. Identified *Porites* spp. and *Sidastrea* spp. coral fauna A) *Porites astreoides* B) *Porites astreoides* C) *Sidastrea siderea* D) *Sidastrea siderea*.

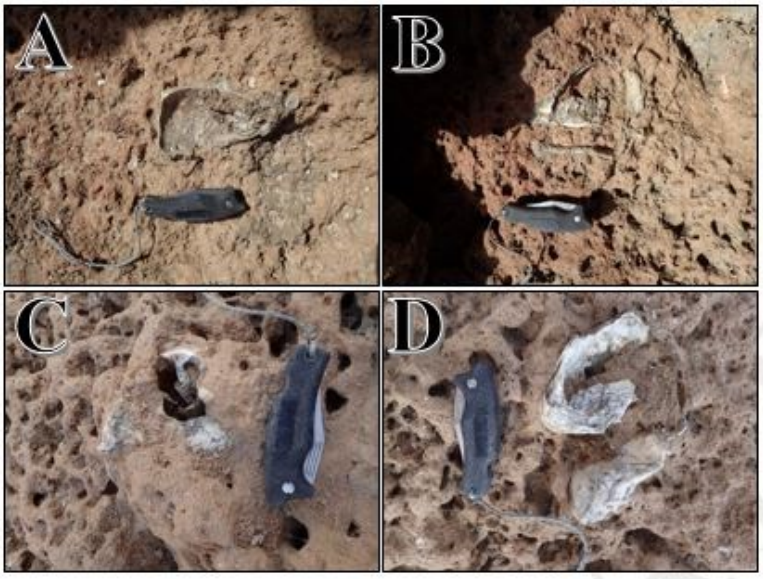

Appendix C-14. A) Queen Conch shell B) Queen Conch shell C) Queen Conch shell D) Queen Conch shell.

Appendix C-15. A) Queen Conch shell B) Queen Conch shell C) Queen Conch Shell D) Queen Conch shell.

Appendix D. Gamma-Ray Data

BB-1 m	BB-1 CPS	BB-2 m	BB-2 CPS	BB-3 m	BB-3 CPS	FCB-1 m	FCB-1 CPS	FCB-2 m	FCB-2 CPS
2.0	34.2	6.6	34.5	6.9	23.5	4.1	45.5	4.7	33.3
1.9	38.4	6.5	33.0	6.8	25.5	4.0	26.1	4.6	35.8
1.8	36.1	6.4	36.9	6.7	24.6	3.9	28.4	4.5	33.3
1.7	34.3	6.3	34.8	6.6	22.6	3.8	29.5	4.4	32.8
1.6	34.5	6.2	32.7	6.5	26.6	3.7	29.2	4.3	30.9
1.5	37.4	6.1	35.0	6.4	25.1	3.6	29.7	4.2	31.9
1.4	39.3	6.0	30.2	6.3	26.2	3.5	27.7	4.1	33.8
1.3	40.4	5.9	32.3	6.2	26.3	3.4	28.7	4.0	33.2
1.2	42.0	5.8	33.9	6.1	27.1	3.3	26.8	3.9	29.3
1.1	41.7	5.7	36.7	6.0	28.5	3.2	29.7	3.8	32.9
1.0	40.3	5.6	38.1	5.9	31.8	3.1	24.5	3.7	Cover
0.9	30.9	5.5	33.9	5.8	33.5	3.0	27.1	3.6	Cover
0.8	30.7	5.4	37.3	5.7	32.8	2.9	25.8	3.5	Cover
0.7	28.5	5.3	39.0	5.6	33.3	2.8	25.3	3.4	Cover
0.6	27.9	5.2	40.0	5.5	36.1	2.7	22.4	3.3	Cover
0.5	26.1	5.1	40.3	5.4	34.3	2.6	24.8	3.2	Cover
0.4	27.2	5.0	41.4	5.3	42.2	2.5	22.3	3.1	Cover
0.3	28.8	4.9	40.2	5.2	38.6	2.4	24.7	3.0	Cover
0.2	26.6	4.8	38.3	5.1	43.4	2.3	25.9	2.9	Cover
0.1	28.4	4.7	42.0	5.0	42.1	2.2	27.7	2.8	Cover
0.0	26.0	4.6	47.6	4.9	43.6	2.1	25.1	2.7	31.5
		4.5	39.8	4.8	44.8	2.0	26.9	2.6	28.5
		4.4	39.0	4.7	36.0	1.9	24.9	2.5	30.1
		4.3	42.4	4.6	39.0	1.8	24.8	2.4	33.0
		4.2	40.4	4.5	35.3	1.7	29.8	2.3	33.1
		4.1	45.8	4.4	34.8	1.6	27.3	2.2	39.2
		4.0	47.8	4.3	39.4	1.5	26.1	2.1	30.4
		3.9	39.9	4.2	41.3	1.4	26.5	2.0	28.1
		3.8	40.7	4.1	37.9	1.3	31.6	1.9	33.1
		3.7	45.7	4.0	37.0	1.2	28.8	1.8	29.0
		3.6	37.2	3.9	41.2	1.1	29.1	1.7	27.3
		3.5	40.3	3.8	42.1	1.0	28.3	1.6	26.2
		3.4	38.8	3.7	37.0	0.9	25.4	1.5	27.4
		3.3	36.1	3.6	40.7	0.8	25.1	1.4	28.6
		3.2	36.9	3.5	37.9	0.7	23.9	1.3	26.7
		3.1	39.8	3.4	33.7	0.6	25.4	1.2	29.1
		3.0	36.6	3.3	38.0	0.5	30.1	1.1	26.4
		2.9	39.2	3.2	37.1	0.4	29.5	1.0	29.2
		2.8	41.8	3.1	38.7	0.3	28.6	0.9	28.8

BB-1 m	BB-1 CPS	BB-2 m	BB-2 CPS	BB-3 m	BB-3 CPS	FCB-1 m	FCB-1 CPS	FCB-2 m	FCB-2 CPS
		2.7	40.8	3.0	34.3	0.2	28.6	0.8	34.9
		2.6	43.5	2.9	34.9	0.1	29.3	0.7	27.3
		2.5	45.1	2.8	32.3	0.0	34.6	0.6	35.0
		2.4	52.0	2.7	39.1			0.5	32.6
		2.3	43.6	2.6	41.2			0.4	31.1
		2.2	37.8	2.5	38.3			0.3	33.8
		2.1	33.3	2.4	41.3			0.2	34.8
		2.0	34.2	2.3	45.2			0.1	32.5
		1.9	33.9	2.2	38.8			0.0	33.2
		1.8	33.6	2.1	41.6				
		1.7	43.2	2.0	39.3				
		1.6	44.3	1.9	48.7				
		1.5	41.0	1.8	49.8				
		1.4	41.6	1.7	50.4				
		1.3	41.6	1.6	46.6				
		1.2	38.2	1.5	47.4				
		1.1	34.5	1.4	42.0				
		1.0	35.7	1.3	39.7				
		0.9	36.2	1.2	37.1				
		0.8	31.4	1.1	45.3				
		0.7	34.7	1.0	39.8				
		0.6	36.5	0.9	47.6				
		0.5	36.0	0.8	46.1				
		0.4	33.1	0.7	44.0				
		0.3	29.9	0.6	41.9				
		0.2	30.3	0.5	42.1				
		0.1	34.7	0.4	39.3				
		0.0	33.7	0.3	41.5				
				0.2	42.1				
				0.1	40.3				
				0.0	45.3				

Appendix E. Gamma-Ray Profiles

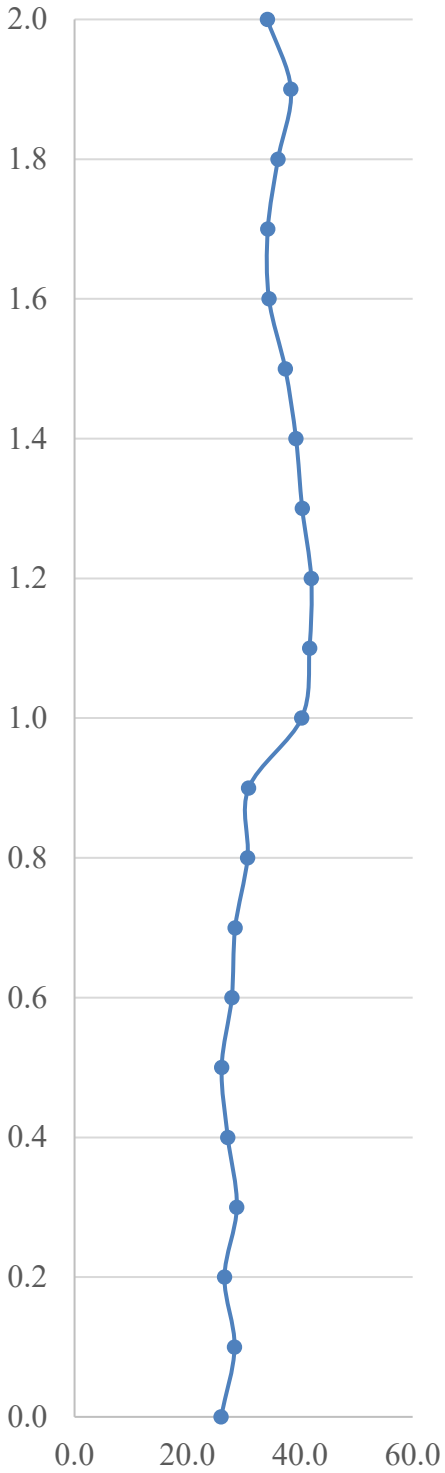

Appendix E-1. Gamma-ray profile from section BB-1.

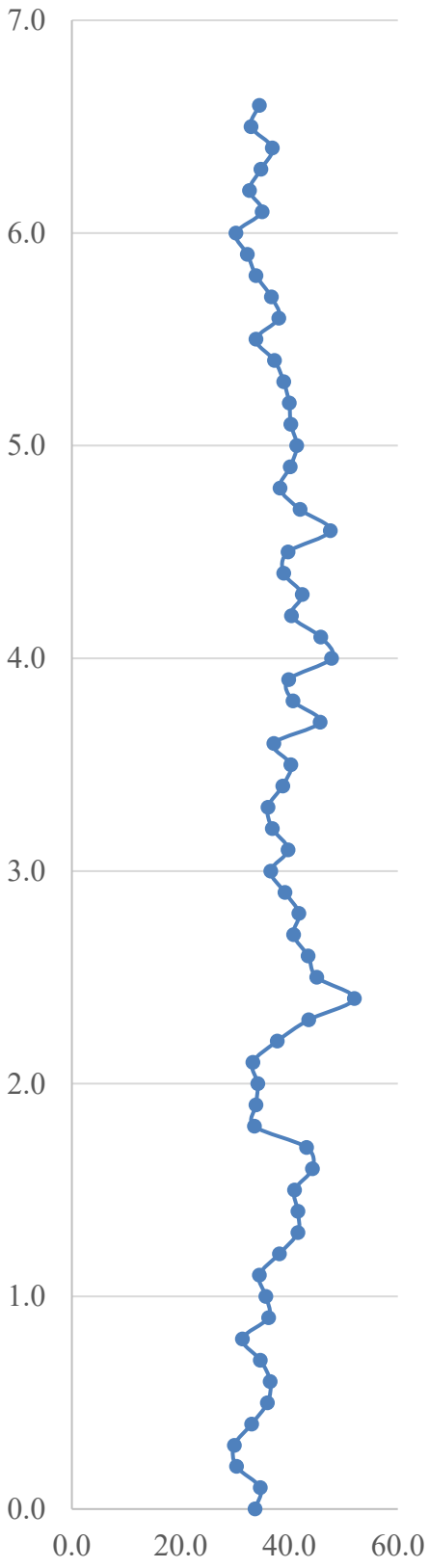

Appendix E-2. Gamma-ray profile from section BB-2.

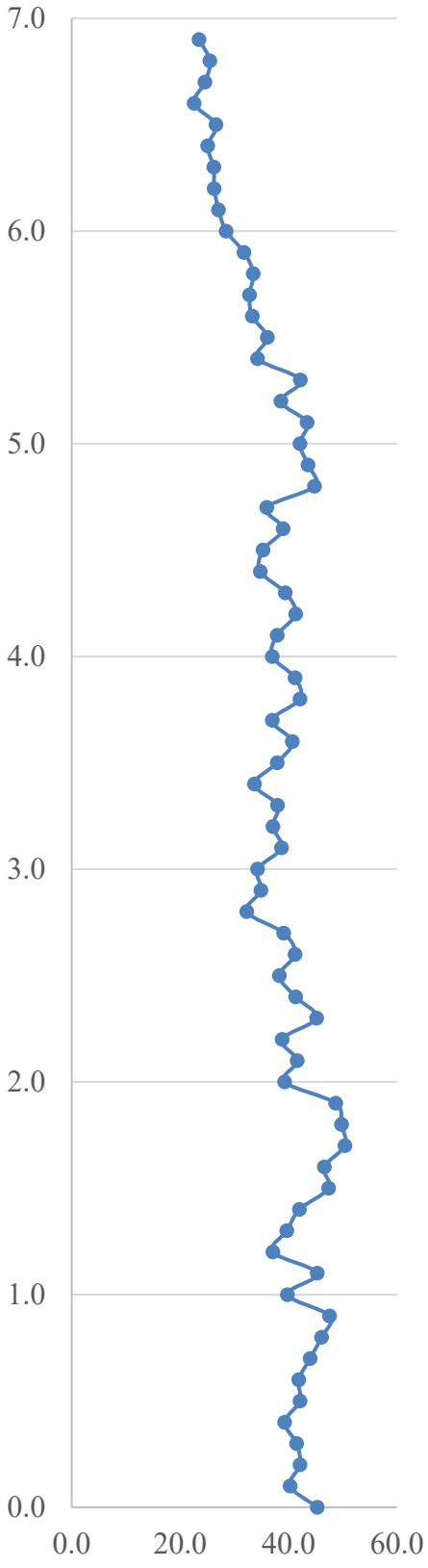

Appendix E-3. Gamma-ray profile from section BB-3.

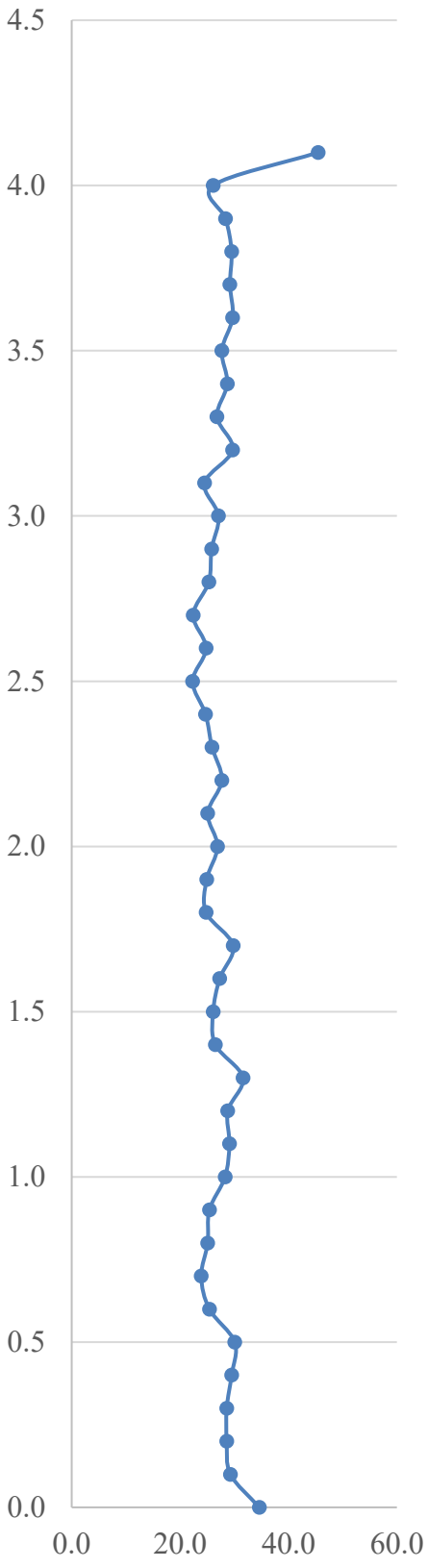

Appendix E-4. Gamma-ray profile from section FCB-1.

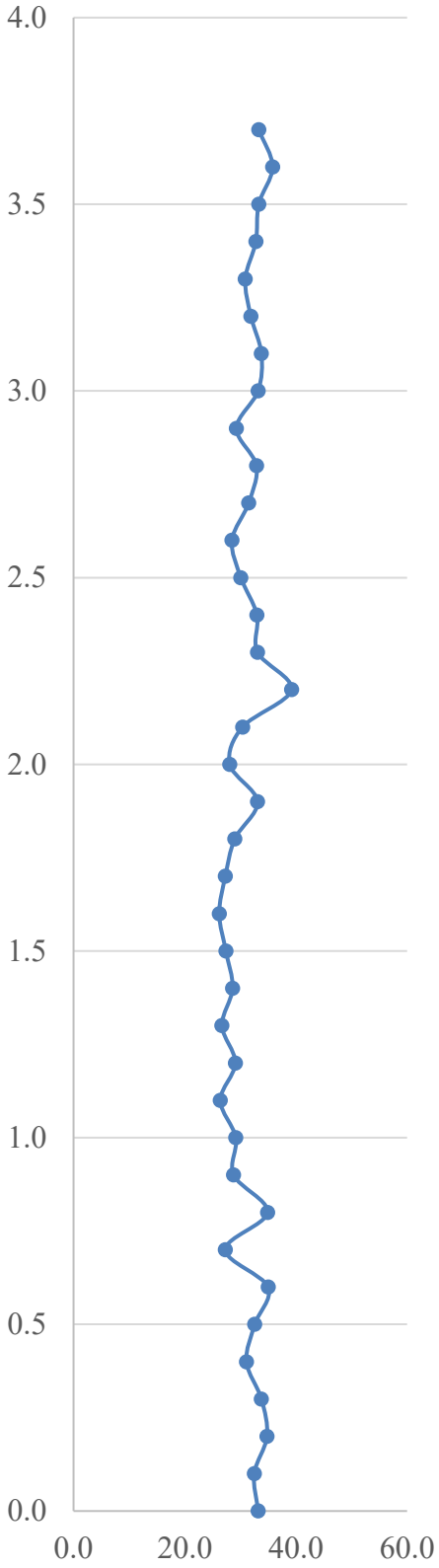

Appendix E-5. Gamma-ray profile from section FCB-2.